Halogen Bonding and Pharmaceutical Cocrystals: The Case of a Widely Used Preservative

UNIVERSITÀ DEGLI STUDI DI TORINO

Halogen bonding and pharmaceutical cocrystals:

The case of a widely used preservative

Michele Baldrighi,[†] Gabriella Cavallo,[†] Michele R. Chierotti,[‡] Roberto Gobetto,[‡] Pierangelo Metrangolo,[†,#] Tullio Pilati,[†] Giuseppe Resnati,*[†,#] and Giancarlo Terraneo[†,#]*

[†]NFMLab, Department of Chemistry, Materials, and Chemical Engineering ‘‘Giulio Natta’’, Politecnico di Milano, Via L. Mancinelli 7, 20131 Milan, Italy;

[‡]Department of Chemistry, University of Torino, V. P. Giuria 7, 10125 Turin, Italy;

[#]Center for Nano Science and Technology@Polimi, Istituto Italiano di Tecnologia, Via Pascoli 70/3, 20133 Milan, Italy.

KEYWORDS: Pharmaceutical cocrystals, halogen bonding, 3-iodo-2-propynyl-*N*-butylcarbamate (IPBC), crystal engineering, solid state NMR, X-ray crystal structure.

RECEIVED DATE (to be automatically inserted after your manuscript is accepted if required according to the journal that you are submitting your paper to)

ABSTRACT: 3-Iodo-2-propynyl-*N*-butylcarbamate (**IPBC**) is an iodinated antimicrobial product used globally as a preservative, fungicide, and algaecide. **IPBC** is difficult to obtain in pure form as well as to handle in industrial products because it tends to be sticky and clumpy. Here, we describe the preparation of four pharmaceutical cocrystals involving **IPBC**. The obtained cocrystals have been characterized by X-ray diffraction, solution and solid-state NMR, IR and DSC analyses. In all the described cases the halogen bond (XB) is the key interaction responsible for the self-assembly of the pharmaceutical cocrystals thanks to the involvement of the 1-iodoalkyne moiety of **IPBC**, which functions as a very reliable XB-donor, with both neutral and anionic XB-acceptors. Most of the obtained cocrystals have improved properties with respect to the source API, in terms, *e.g.*, of thermal stability. The cocrystal involving the GRAS excipient $CaCl_2$, has superior powder flow characteristics compared to the pure **IPBC**, representing a promising solution to the handling issues related to the manufacturing of products containing **IPBC**.

INTRODUCTION

In the last decades both academic groups and pharmaceutical companies have shown great interest in the application of crystal engineering principles to the control and tuning of the physical and chemical properties of solid-state active pharmaceutical ingredients (APIs). In particular, pharmaceutical cocrystals, *i.e.* the association in the crystal lattice of an API and a cocrystal former (CCF), have opened the opportunity for engineering solid-state forms designed to have tailored properties to enhance drug product bioavailability and stability, as well as to enhance processability of the solid material inputs in drug product manufacture.[1] For this reason, a growing number of scientific papers and patents dealing with multi-component crystals of APIs has recently appeared both in the general and specialized literature.[2]

According to a recent recommendation by FDA[3], the association between an API and a CCF should be classified as dissociable "API-excipient" molecular complex (with the CCF being the excipient) where the molecular association of API and its excipient(s) occurs within the crystal lattice. Therefore, API-CCF recognition and self-assembly are *de facto* supramolecular phenomena, which are typically driven by noncovalent interactions, among which hydrogen bonding (HB) plays the major role.[4] Due to the many functional groups present in their structure, APIs typically have a multifaceted profile in crystal engineering and embody a particularly great challenge when design and preparation of specific multi-component crystals is pursued. For this purpose, also the co-existence of several complementary H-bonds has been extensively exploited, and various binary and ternary pharmaceutical cocrystals have been described with improved properties compared to the pure, original APIs.[5]

The incorporation of halogen atoms into a drug candidate molecule has largely been used in drug discovery for two main reasons: - to develop analogues that are usually more lipophilic and

consequently more likely to cross the lipid membranes of body's tissues; - to slow down drug catabolism and thus to increase drug's activity (obstructive halogenations). By some estimates, 50% of compounds in high-throughput drug screening are halogenated, as well as are more that 23% of approved FDA drugs.[6] With the objective of obtaining the first examples of pharmaceutical cocrystals where halogen atoms play a key-role in driving the formation of the API-CCF adduct, we describe herein the synthesis and characterization of a series of cocrystals of 3-iodo-2-propynyl-*N*-butylcarbamate (**IPBC**), an iodinated antimicrobial product globally used as preservative, fungicide, and algaecide. Solution and solid-state NMR (SSNMR) as well as IR spectroscopic investigations, X-ray structural determinations, and calorimetry analyses demonstrate the remarkable ability of the iodo-alkyne moiety of **IPBC** to be involved in the formation of strong halogen bonds, with both neutral and ionic electron-donors, resulting in pharmaceutical cocrystals of **IPBC** (Scheme 1), which have improved processability profiles.

Scheme 1. Molecular structures of **IPBC** with carbon atom labeling numbers, used CCFs, and obtained halogen-bonded adducts.

RESULTS AND DISCUSSION

Synthetic Strategy. Halogen bonding (XB) [7] is the strong, specific, and directional interaction occurring between an electrophilic region (σ-hole)[8] on a covalently-bound halogen atom X (XB-donor site) and a nucleophilic region on a neutral molecule or an anion (XB-acceptor site).[9] In the last decade XB has been widely employed for the construction of numerous supramolecular systems with applications in fields as diverse as solid-state synthesis, non-linear optics,

photoresponsive polymers, liquid crystals, and anion recognition, among others.[10] However, only recently it has emerged clearly that XB can successfully be exploited to enhance affinity and modulate selectivity of ligand-protein binding. This may open totally new perspectives in lead discovery and drug design.[11]

All the halogen atoms may, in principle, function as XB-donor sites, with the strength of the interaction that increases with the polarizability of the halogen atom and, usually, increases with the electron-withdrawing ability of the moiety the halogen atom is covalently bound to. For C-bound halogen atoms, their XB-donor ability increases on going from haloalkanes to haloalkenes and haloalkynes ($X\text{-}Csp^3 < X\text{-}Csp^2 < X\text{-}Csp$). We thus identified 1-iodoalkyne derivatives[12] as ideal candidates to test the potential of XB in the formation of pharmaceutical cocrystals.

With this hypothesis in mind we selected **IPBC** as the API since its use as a broad-based biocide has become paramount in many different products including paints, coatings, metal-working fluids, wood protection, and healthcare products, as well as cosmetics.[13] However, this compound shows a low melting point (64-68 °C) and decomposes when heated above 85 °C. Moreover, **IPBC** has a very low solubility in water and is difficult to obtain in pure form as well as to handle in industrial products such as polymers and plastics, because it tends to be sticky and clumpy. Some of these technological limitations of **IPBC** may be potentially overcome if a new solid-state form of **IPBC** is obtained, *e.g.* by involving it in the formation of a cocrystal with a suitable CCF.

The crystal structure of the pure **IPBC**[14] reveals the pivotal role of the carbamate and iodoalkyne groups in the organization of the molecules in the crystal lattice. The carbonyl oxygen acts as a bidentate electron-donor site and forms one H-bond with the N-H moiety (O···N distance 2.904(6) Å, C-O···N angle 140.9(3)°) and one XB with the C-I moiety (C-I···O distance

2.933(4) Å, C-I···O angle 175.4(2)°) (Figure 1). This C-I···O distance corresponds to a "normalized contact"[15] (Nc) of 0.84, and the C-I···O angle is in perfect agreement with the expected directionality of strong XB. Thus, the crystal structure of the pure **IPBC** gives solid grounds to its possible involvement in halogen-bonded cocrystals, which, nevertheless, have never been reported, yet.

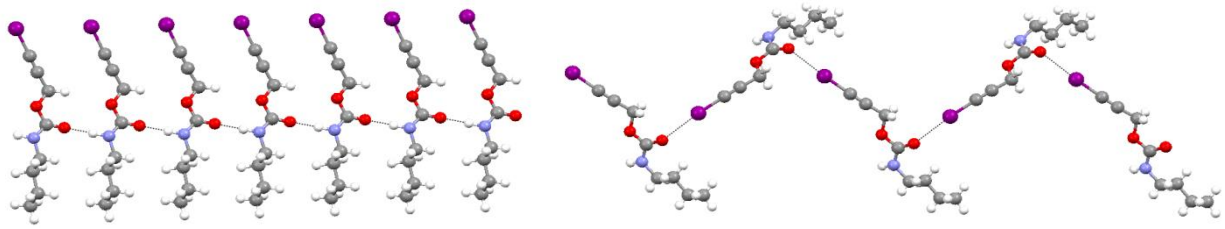

Figure 1. Ball and stick representation of hydrogen (left) and halogen-bonded (right) infinite chains present in the crystal packing of **IPBC**. Color code: Gray: carbon; red: oxygen; Blue: nitrogen; Purple: iodine; Hydrogen: white. HB and XB are pictured as black dotted lines.

As far as the CCFs are concerned, we selected two bipyridine derivatives, as neutral acceptors of XB (**BiPyEt** and **BiPy**), and two halide ions, as anionic acceptors of XB (**TBAI** and **$CaCl_2$**) (see Scheme 1). Our selection was guided by the fact that pyridyl N atoms and halide ions are the electron-donor sites most commonly involved in X-bonded adducts with iodoalkyne derivatives, as supported by our CSD search (see SI). We decided to use the pyridyl moiety as mimic of some typical GRAS CCFs such as pyridoxine (vitamin B6), niacin (nicotinic acid and its amide), while **TBAI** and **$CaCl_2$** where used as sources of halide ions, either organic or inorganic, which are highly represented in the FDA-GRAS CCF list. In particular, **$CaCl_2$** was selected as it is a GRAS excipient widely used for its dehydrating properties, and in the manufacturing of **IPBC**, it is desirable to produce **IPBC** with the lowest possible moisture content.

Crystalline adducts **1** and **2** were obtained on evaporation of solutions wherein the ratio between **IPBC** and **BiPyEt**, or **BiPy**, was 2:1. This ratio was adopted as the starting components were expected to work as monodentate XB-donor and bidentate XB-acceptors. ^{1}H NMR analyses of **1** and **2** obtained from these solutions revealed the expected 2:1 donor/acceptor ratio in the bulk crystalline solids. As far as the obtainment of the adducts **3** and **4** is concerned, they were obtained *via* solid-state reactions and the convenient ratios of starting compounds had to be identified *via* titration methods since it is well-known that halide ion coordination by XB-donors may involve from one to even four molecules.

Calorimetric and Vibrational Analysis. Cocrystal **1** melts at 82 °C and cocrystal **2** at 113 °C, both values are higher than the melting point of the pure **IPBC** and different from the two starting bipyridines (**IPBC,** 64-68 °C; **BiPyEt,** 112 °C; **BiPy,** 110°C). Adducts **1** and **2** both show single, well-defined melting endotherms, irrespective of the fact that they were obtained either using fast or slow crystallization methods from methanol solutions or through solid-state reactions where the two solid starting materials were co-grinded in a ball mill. This thermal behavior indicates that the starting materials are invariably interacting with each other at molecular level to form a well-defined crystalline species, rather than a generic physical mixture.

Differential scanning calorimetry (DSC) was also used to determine the preferred pairing ratio between **IPBC** and **TBAI** or **$CaCl_2$**. DSC analyses of mixtures where the **IPBC/TBAI** ratio was varied from 1:1 to 2:1 showed a first endotherm at 45 °C and a second one at 141 °C (melting point of the non-coordinated **TBAI**). When the ratio was increased to 4:1, the first endotherm remained nearly unchanged while a second one appeared at 66 °C (melting point of the excess **IPBC**). A single endothermic peak at 45 °C was, instead, observed with the 3:1 ratio suggesting this as the exact ratio of starting compounds in the adduct **3**. The same approach was adopted to

identify the preferred pairing ratio of **IPBC** and **$CaCl_2$** to give **4**. Only the adduct prepared with an **IPBC**:**$CaCl_2$** ratio of 4:1 showed one single endothermic peak at 85 °C. Very interestingly, this temperature is much higher than the melting point of the pure **IPBC** and is close to its decomposition temperature. Moreover, upon melting, no sign of decomposition was observed below the temperature of 120 °C (see Figure SI 3.2 in the SI). Similarly, no sign of decomposition has been observed below the temperature of 95 °C also for the adduct **3**.

IR spectroscopy was used to provide additional evidence of cocrystals' formation, since this technique is a fast, simple, very efficient, and widely used technique for this purpose. In general, the spectrum of a supramolecular adduct shows the bands of each starting components and the occurrence of an intermolecular interaction may be revealed by small changes, both in intensity and in position, that the absorptions of interacting functional groups, or close to interacting groups, disclose with respect to the pure starting components.

Usually the occurrence of XB results in red-shifts of diagnostic bands of the XB-donor and in blue-shifts of bands of the XB-acceptor. As expected, the IR spectrum of **1** shows several small variations in peaks belonging to both the starting modules, which are nicely consistent with the $N_{pyr}\cdots I$ XB occurrence. The symmetric ring stretching mode of **BiPyEt** at 990 cm^{-1} and of **BiPy** at 988 cm^{-1} are blue-shifted to 1001 cm^{-1} in **1** and to 994 cm^{-1} in **2**, respectively. Similar changes were observed for other pyridine rings involved in X-bonded cocrystals.[16] The $\nu_{Csp2\text{-}H}$ stretchings (above 3000 cm^{-1}) are less intense and at shorter wavelengths in **1** and **2** compared to **BiPyEt** and **BiPy**, respectively. These changes are consistent with an $n\rightarrow\sigma^*$ electron density donation from the pyridyl nitrogen to the iodine atom of the ethynyl moiety, resulting in an increased positive charge on the pyridine ring.

Some wavelength variations of bands associated with **IPBC**, the XB-donor, are also diagnostic of the XB presence in adducts **1-4**. For example, the triple bond stretching band is at 2198 cm^{-1} in the pure **IPBC** while is red-shifted in all the co-crystals: 2188 cm^{-1} in **1**, 2189 cm^{-1} in **2**, 2185 cm^{-1} in **3** and 2187 cm^{-1} in **4**, respectively. These shifts further confirm that the 1-iodoalkyne fragment of **1-4** is involved in the formation of halogen bonds.

As far as the bands associated with the carbamate moiety are concerned, the stretching band of the C=O bond in cocrystals **1** and **2** appears as a single peak and red shifted to 1691 cm^{-1} and 1683 cm^{-1}, respectively, consistent with a lower force constant as a consequence of the interaction with an electron acceptor moiety. Differently, in cocrystals **3** and **4** the presence of two bands in the ν(C=O) region suggests the existence of two C=O moieties with different interaction patterns. This is in agreement with the splitting of the ν(NH) band at 3341 cm^{-1} of the carbamate group in **IPBC** resulting in two bands at 3431 and 3308 cm^{-1} in **4**, which also suggests the presence of two N-H groups interacting with different intermolecular environments (all of the DSC graphs and IR spectra are reported in the SI).

NMR Studies in Solution. Previous studies have demonstrated that the ^{13}C signals of the iodinated carbons of iodoethynyl moieties undergo major low-field shifts on changing the solvent from chloroform to dimethylsulphoxide as a consequence of the XB occurring with the oxygen atoms of the solvent.[17] For this reason we decided to monitor the presence of X-bonded adducts in solutions of cocrystals **1-4** *via* the ^{13}C NMR technique.

The ≡*C*-I signals of 0.4 M deuterochloroform solutions of pure **IPBC** and cocrystals **1**, **2**, and **3** are at 3.68, 4.96, 4.48, and 8.07 ppm, respectively (Figure 2). On addition of incremental amounts of **BiPyEt** to a 0.4 M solution of **IPBC** in $CDCl_3$, the ≡*C*-I signal moved to 4.45, 4.71,

4.96, 5.31, and 5.56 ppm when the XB donor/acceptor ratio was 1:0.3, 1:0.4, 1:0.5, 1:0.6, and 1:0.7, respectively. **BiPy** and **TBAI** showed similar trends, shifts given by **TBAI** being larger than those of **BiPy** at all used ratios (the ≡*C*-I signal was at 4.18, 4.35, 4.48, 4.65, and 4.80 ppm for **BiPy** and 5.33, 6.69, 8.07, 9.30, and 10.42 ppm for **TBAI** when the used donor/acceptor ratios were as reported in the SI). The observed chemical shift change occurs as a consequence of the donation of electron density from the XB-acceptor to the iodoethynyl group and the greater shifts given by **3** with respect to **1** and **2** are consistent with the fact that anions function as better electron-donors than pyridines, and form stronger X-bonds than neutral lone-pair possessing heteroatoms. In all cases a single signal is observed, which is consistent with association equilibria occurring rapidly at R.T. at the NMR time scale.

The solubility of **4** and of **$CaCl_2$** in $CDCl_3$ was too low to allow for ^{13}C NMR spectra to be recorded and CD_3OD was thus used as solvent. In this solvent the pure **IPBC** has the iodoethynyl carbon at 6.25 ppm, namely at much higher frequencies than in chloroform solution due to the coordination of the iodine atom by the methanolic oxygen atom, an effective XB-acceptor. On the other hand, a 0.4 M solution of **4** showed the same signal at 6.82 ppm proving that the C-I···Cl^- XB is occurring even in such a competitive solvent.

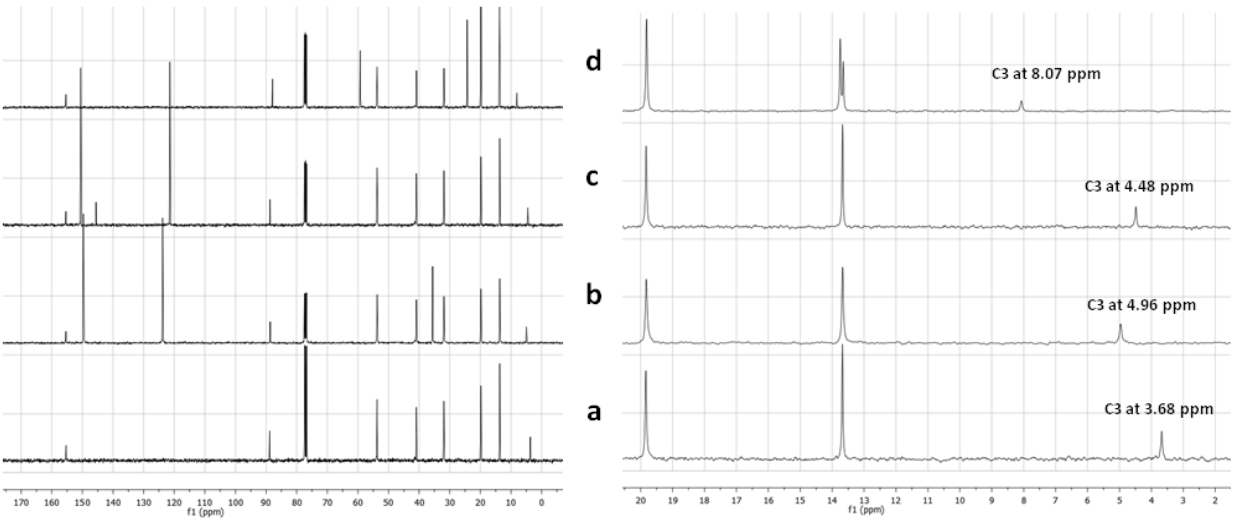

Figure 2. (Left) ^{13}C NMR spectra (180 – 0 ppm region) of 0.4 M $CDCl_3$ solutions of the pure **IPBC** (a) and cocrystals **1** (b), **2** (c), and **3** (d). (Right) Region between 1.5 - 20.5 ppm where the C3 signals are marked with their chemical shifts.

Single Crystal X-ray Analysis. The single crystal X-ray diffraction analysis of **1** confirmed that the **IPBC**/**BiPyEt** ratio in the cocrystal is 2:1. The basic motif in **1** is a trimeric unit where one **BiPyEt** molecule bridges two **IPBC** molecules through two highly linear and short I···N X-bonds (Figure 3). The asymmetric unit contains two slightly different trimeric systems wherein the C1-I1···N3 and C9-I2···N4 angles are 176.0(2)° and 174.1(2)°, respectively, while the I1···N3 and I2···N4 distances are 2.806(4) and 2.835(4) Å, respectively, and correspond to a "normalized contact"[15] of around 0.80. In addition, as in the crystal of pure **IPBC**, NH···O H-bonds involving the carbamate groups form two slightly different supramolecular ribbons wherein the N1···O2 and N2···O4 distances are 2.919(4) and 2.955(3) Å, respectively. In one ribbon, composed by trimeric units lying on the center of symmetry, the pyridyl rings are co-planar, while in the other

ribbon, composed by trimeric units staying on the *C2* axis, the pyridyl rings are almost perpendicular to each other.

The overall packing of **1** is a nice case wherein XB and HB cooperate orthogonally in building up a new cocrystal where the XB pins the CCF to the API molecule while leaving nearly unchanged the HB pattern observed in the pure API's structure.

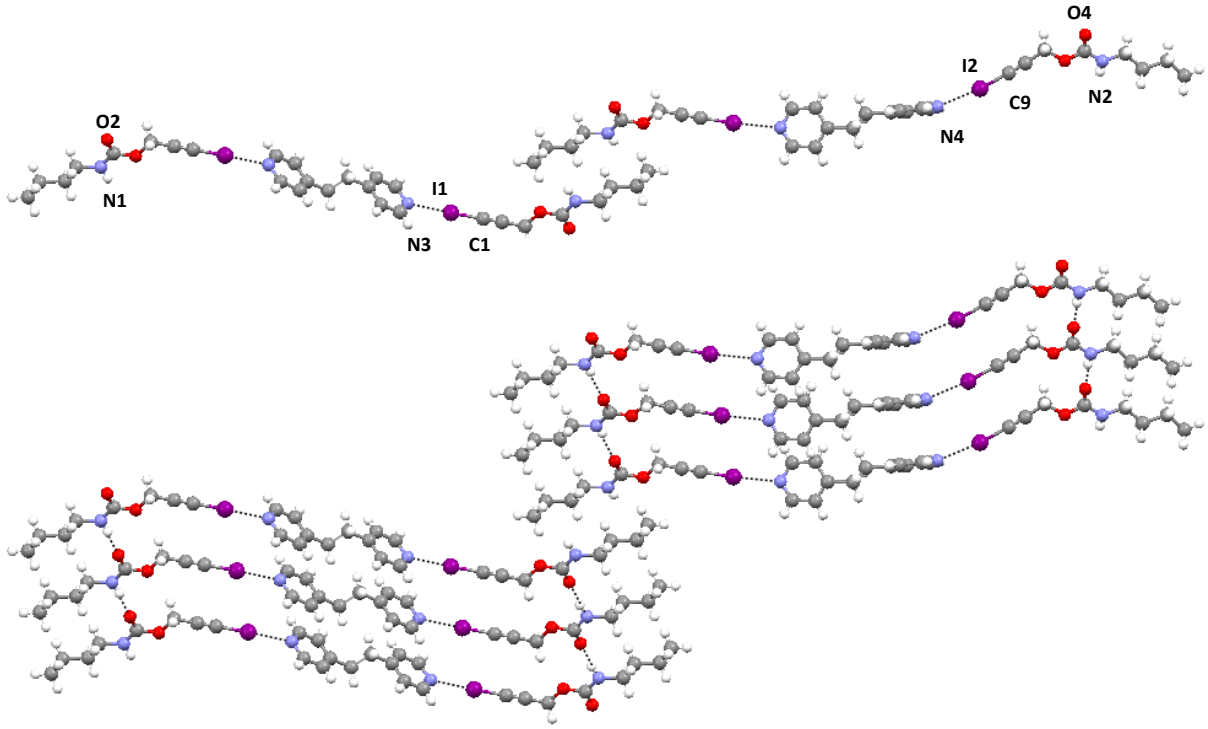

Figure 3. Top: The two X-bonded trimers of the asymmetric unit of **1**. Bottom: HB connects the two X-bonded trimers into two distinct ribbons (partial view). Color code as in Figure 1.

Finally, a weak H-bond (2.622(3) Å) between the carbonyl group and the *ortho* hydrogen atoms of the pyridine group contributes to the overall stabilization of the crystal lattice. The electron density transfer from the nitrogen atom to the electrophilic iodine makes the hydrogen

atoms in the *ortho* position quite acidic (as suggested by the IR) and particularly prone to interact with the electronic density on the carbonyl oxygen.

The crystal structure of **2**, formed upon self-assembly of **IPBC** and **BiPy**, gives a further proof of the reliability of the C≡C-I···N supramolecular synthon. The packing of **2** shares strong similarities with **1** (Figure 4). The fundamental motif is still a trimeric X-bonded unit composed by one **BiPy** molecule bridging two **IPBC** molecules after standard geometrical parameters (the C1-I1···N1 angle is 178.5(1)° and the I1···N1 distance is 2.816(4) Å, corresponding to a normalized contact of around 0.80). As in **1**, the supramolecular synthon N-H···O connects the trimers into infinite hydrogen-bonded ribbons, which develop along the *b*-axis (the N···O distance is 2.914(4) Å). Finally, the **BiPy** is further pinned in its position by weak HBs between its *ortho* and *meta* hydrogen atoms and the carbonyl oxygen atom of one **IPBC** molecule and the triple bond of another **IPBC** molecule.

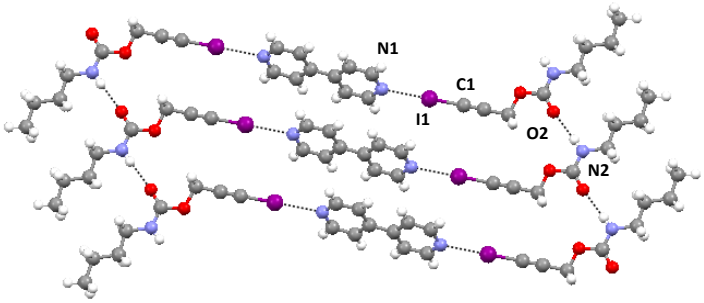

Figure 4. Partial view of the supramolecular ribbons formed *via* orthogonal XB and HB in **2**. Color code as in Figure 1.

Single crystals of **3** were grown by seeding a quasi-saturated CH_2Cl_2 solution of **IPBC** and **TBAI** (ratio 3:1) with the powder obtained by the ball-milling synthesis of **3** (see SI). X-ray analysis (Figure 5A) confirmed that the **IPBC**/**TBAI** ratio in **3** is 3:1, as predicted by DSC

experiments, and revealed the interplay of XB and HB occurring at the coordination sphere of the iodide ion. Iodide ion is functioning as tridentate XB-acceptor and occupies the vertex of an irregular trigonal pyramid (irregular tetrahedron, Figure 5A and 5C). Three edges of this tetrahedron are the three X-bonded **IPBC** molecules and the remaining three vertexes are the three methyl groups of the **IPBCs**. The X-bonds are almost linear, C17-I2···I1$^-$, C25-I3···I1$^-$, and C33-I4···I1$^-$ angles being 179.83(5)°, 172.70(5)°, and 174.84(5)°, respectively. The C≡C-I···I1$^-$ distances are I2···I1$^-$ 3.490(3) Å, I3···I1$^-$ 3.489(3) Å, and I4···I1$^-$ 3.843(3) Å (Nc = 0.84-0.93). The I2···I1$^-$···I4, I4···I1$^-$···I3, and I3···I1$^-$···I2 angles, which describe the iodide vertex, are 77.12(3)°, 77.20(3)° and 74.90(3)° respectively.

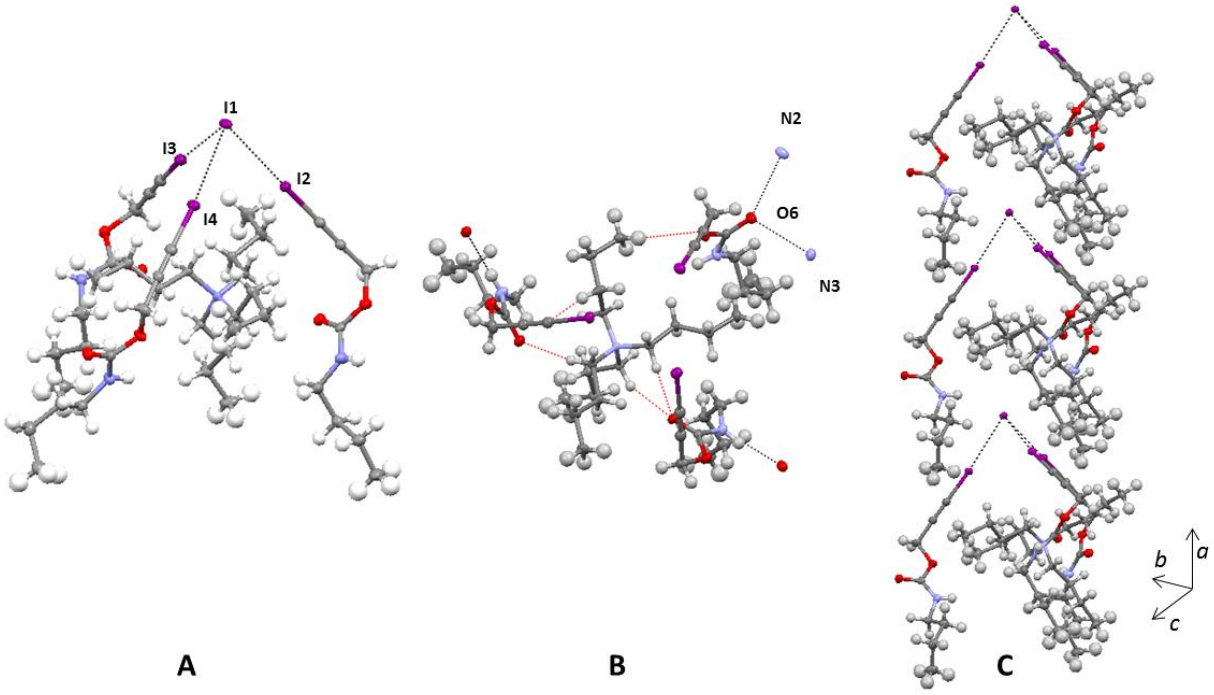

Figure 5. A: The X-bonded pyramidal motif composed by three **IPBC** molecules (pyramid sides) and one **TBAI** unit. B: Strong (black dotted lines) and weak H-bonds (red dotted lines) in **3**; the iodide ion has been deleted for the sake of clarity. C: Propagation of the halogen and

hydrogen-bonded pyramidal motifs along the *a*-axis. Both XB and HB are black dotted lines. Color code as in Figure 1.

Several H-bonds also appear in the crystal lattice of **3** (Figure 5B). The carbonyl group of one **IPBC** molecule is *exo*-oriented with respect to the inside of the pyramidal structure and forms two short H-bonds with two NH groups belonging to different and adjacent supramolecular pyramids ($O6_{x,y,z}\cdots N2_{x,0.5-y,0.5+z}$ 2.959(2) Å and $O6_{x,y,z}\cdots N3_{-x,1-y,2-z}$ 2.883(2) Å). Ammonium cations are pinned at the core of the pyramids and template them by a net of rather long H-bonds involving the carbonyl lone pairs and alkyne bond of **IPBC**. The ammonium cations also contribute to the piling of the pyramids along the *a*-axis (Figure 5C) *via* HB occurring between the acidic CH-N^+ hydrogens and the closest iodide ion ($I^-\cdots H_{1+x,y,z}$ 3.146(2) Å).

Unfortunately, it was not possible to obtain single crystals of the adduct **4**. For this reason we ball milled a mixture of **IPBC** and **$CaCl_2$** in 4:1 ratio obtaining a white microcrystalline powder, which was submitted to powder X-ray diffraction (PXRD) and SSNMR (see below) analyses. PXRD analyses of samples from ball mill experiments proved the absence of the characteristic peaks of starting compounds **IPBC** and **$CaCl_2$** (Figure 6) and indicated their quantitative solid-state reaction to give rise to a new crystalline form where **IPBC** (API) and **$CaCl_2$** (CCF) are associated in the crystal lattice, *i.e.* a pharmaceutical cocrystal.

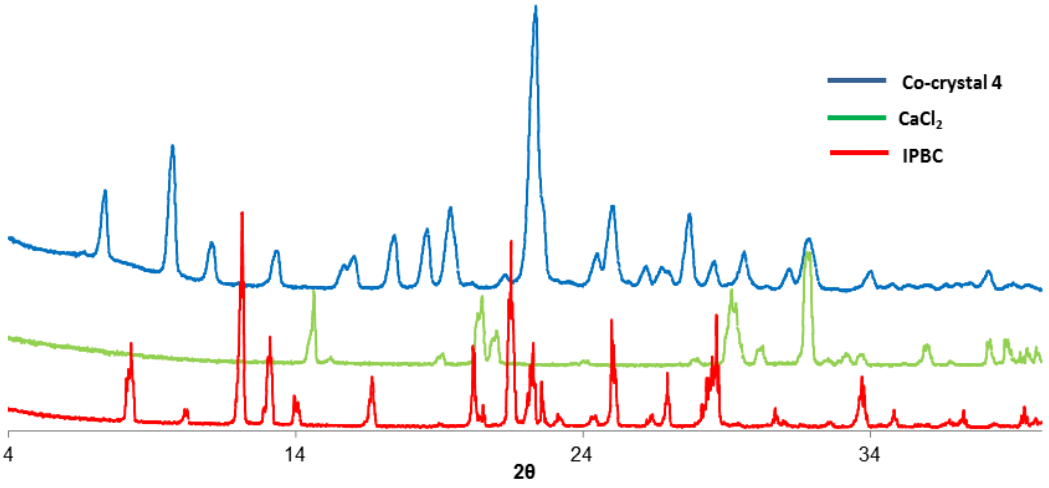

Figure 6. Experimental PXRD patterns of cocrystal **4** (blue line), **$CaCl_2$** (green line), and **IPBC** (red line).

Also cocrystals **1-3** were characterized by PXRD (see SI), and, similarly, their PXRD patterns showed the absence of characteristic peaks of the starting compounds **IPBC**, **BiPyEt, BiPy**, and **TBAI** and revealed the obtainment of three new pharmaceutical cocrystals of **IPBC**. Importantly, the obtained PXRD patterns were nicely matching with the simulated patterns coming from single crystal X-ray data (see SI), indicating that the structures obtained from single crystal X-ray analyses were representative of the bulk crystalline samples.

Solid-State NMR Analysis. While HB has been widely studied by means of SS NMR, this technique has only rarely been used for exploring XB.[18] However, as for HB, SSNMR techniques may provide important information concerning presence, environment, and strength of XB in solid adducts.[19] For this reason we undertook an accurate SSNMR study of the cocrystals **1-4** by means of various SSNMR techniques (^{1}H MAS and CRAMPS, ^{13}C and ^{15}N

CPMAS, and NQS spectral editing, see Experimental Section for acronyms and technical details). All of the ^{13}C and ^{15}N chemical shifts with assignments are reported in Table 1, while ^{13}C and ^{15}N CPMAS spectra are shown in Figures 7, respectively. For atom labeling we refer to the Scheme 1. Moreover, the analysis is focused mainly on atoms involved in XB or HB (C3, aromatic N, and amidic hydrogens) in order to compare the influence of the interactions on the chemical shifts.

The resonance splitting in the ^{13}C CPMAS spectra of cocrystals **1-3** nicely agrees with the number of independent molecules in the unit cell observed in the single crystal structures of **1-3**. On the other hand, the ^{13}C CPMAS spectrum of **4**, whose structure could not be solved by single crystal XRD analysis, gave important information about the presence of two independent **IPBC** molecules in the unit cell, as deducted from the two sets of signals observed.[20]

All of the ^{13}C CPMAS/NQS spectra (Figures 7 and 8) of cocrystals **1-4** are characterized by a high frequency shift of the C3 signal,[21] with respect to that of the pure **IPBC**, of about 7-10 ppm. Interestingly, larger shifts are observed for the samples **1** and **2**, featuring I···N interactions, than for **3** and **4**, which are characterized by I···X^- X-bonds (I^- or Cl^-, respectively). However, these shifts cannot directly be correlated to considerations on XB-strength in these systems, because of the very different crystalline environments around the C≡C-I moiety in cocrystals **1-3**.

Concerning the ^{15}N analysis, the pyridyl nitrogen atom signals of **1** and **2** in the ^{15}N CPMAS spectra undergo a low-frequency shift (8-14 ppm) with respect to those of the pure reagents (**BiPyEt** and **BiPy**) upon formation of the N···I interactions. This phenomenon, common also to HB, has already been reported for other X-bonded systems even though the shift direction depends on type of nitrogen and other factors.[22] On the other hand, the small shift (2.5 ppm)

observed for the N^+ signal in **3** with respect to the pure **TBAI** agrees with the small molecular rearrangement with lack of HB and formation of XB that occurs upon co-crystallization.

Concerning NH resonances of **IPBC**, signals around 57-61 ppm indicate the presence of N-H···O interactions, while signals around 68-71 ppm correspond to free NH groups (see Figure SI 6.1 in SI). Thus, from the ^{15}N chemical shifts, we can suggest that in cocrystal **4**, one independent molecule is characterized by an NH involved in an N-H···O HB while in the other the NH is free. This experimental evidence nicely matches with structural information obtained from IR data.

All ^1H MAS and CRAMPS spectra but that of the cocrystal **3**, which melted in the rotor during the acquisition, are reported in Figure 8 Right. All cocrystals[23] are characterized by weak HB interactions as highlighted by the chemical shift of the H-bonded protons (around 7.0-8.5 ppm) in agreement with long X-ray N-O distances (around 2.9 Å, see above). However, in the adducts **1**, **2**, and **4** the N-H···O interactions are slightly stronger than in the pure **IPBC** (δ_{1H} around 8.3-8.5 in the formers and around 7.0 in the latter).

Table 1. ^{13}C and ^{15}N chemical shifts with assignments for pure reagents (**IPBC**, **BiPyEt**, **BiPy**, and **TBAI**) and cocrystals **1**-**4**. NQS experiments were fundamental for unambiguously assigning chemical shifts of overlapped C3 resonances.

	Atom	Note	Pure reagent	**1**	**2**	**3**	**4**
IPBC	C4	C=O	157.3	156.5/156.1[a]	156.3	157.2/156.2	157.7/155.4
	C2	C_q	87.6	87.0/85.6	86.3	87.8/87.5/85.5	87.3
	C1	CH_2	55.9	55.4	55.9	54.9/54.0/53.6	55.2/54.7
	C5	CH_2	42.7	44.0	43.6	41.8/41.4	43.8/43.3

	C6	CH_2	33.9	35.5/32.5	32.1	32.7/32.3	34.1/32.2
	C7	CH_2	22.4	22.7	22.4	22.4/22.2	22.1/21.9
	C8	CH_3	16.2/15.8	16.1	15.8	16.3/15.6	16.5/15.8
	C3	C_q	12.2[b]	20.3[b]	22.0[b]	19.3/20.9/ 22.3	19.3[b]
	N	NH	64.6	61.6/60.0	61.7	68.6/57.7	70.1/61.6
BiPyEt		CH_2	38.4	36.3	-	-	
		CH	151.0/124.8	149.9/125.4/ 123.7	-	-	
		C_q	151.0	151.2/149.9	-	-	
		N	288.5	272.9/272.1	-	-	
BiPy		CH	146.8/123.1/121.4	-	150.5/119.3[c]	-	
		C_q	149.3/148.2	-	142.7	-	
		N	288.6	-	280.9	-	
TBAI	α	CH_2	61.3	-	-	59.6[a]	
	β	CH_2	26.4	-	-	25.3/24.5[c]	
	γ	CH_2	21.3	-	-	21.2/20.9	
	δ	CH_2	15.2/15.0/14.2	-	-	15.0/14.5	
		N^+	43.9	-	-	41.4	

[a] multiplet or broadening due to a 2nd-order effect of dipolar coupling to the quadrupolar nitrogen-14 nucleus; [b] broadening due to a 2nd-order effect of dipolar coupling to the quadrupolar iodine-27 nucleus; [c] broadening due to static or dynamic disorder.

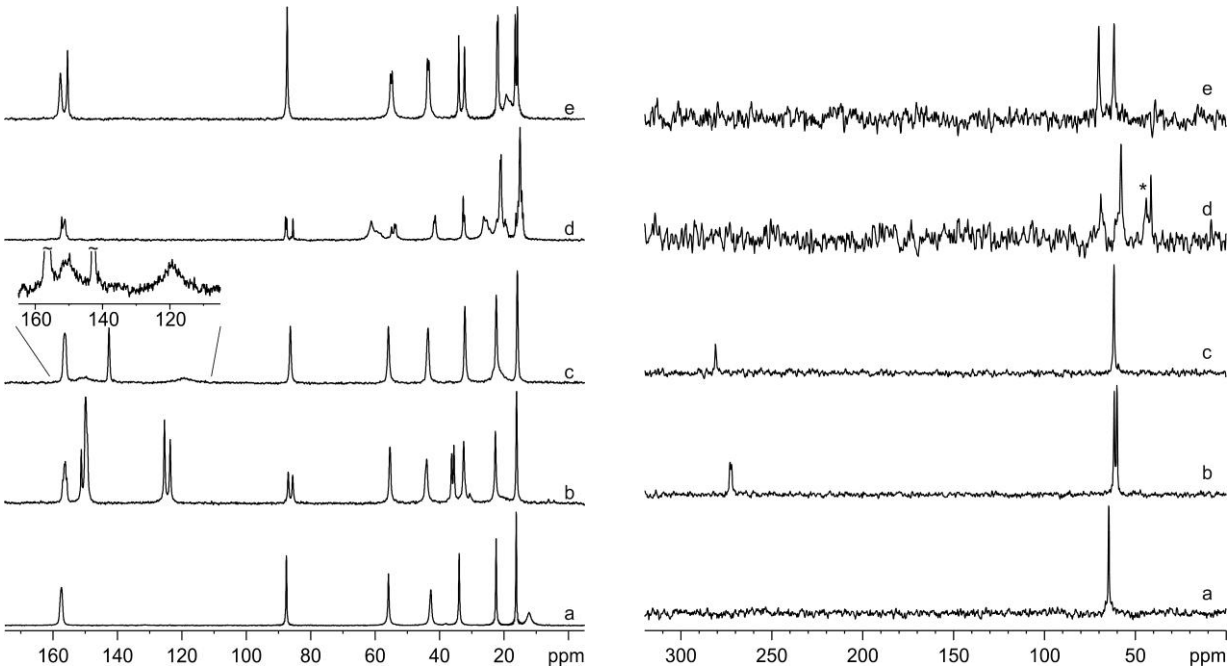

Figure 7. Left: ^{13}C (100 MHz) CPMAS spectra of the pure **IPBC** (a), **1** (b), **2** (c), **3** (d), and **4** (e) recorded at 12 kHz with a contact time of 7 ms. The cocrystal **2** clearly shows rotation of the **BiPy** moiety around the N-N axis as observed from the broadening of the aromatic carbon atoms, which are averaged by two (see inset in spectrum c). Right: ^{15}N (40 MHz) CPMAS spectra of the pure **IPBC** (a), **1** (b), **2** (c), **3** (d), and **4** (e) recorded at 9 kHz. The asterisk indicates the presence of the free **TBAI** due to the partial melting of **3** in the rotor.

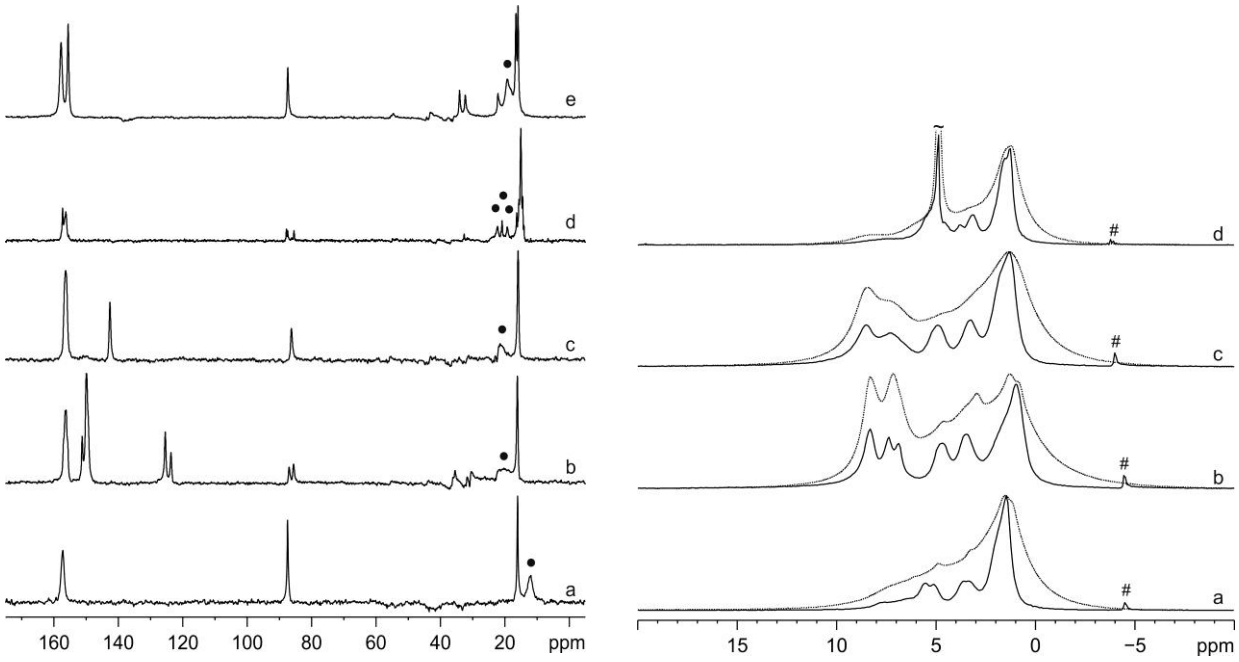

Figure 8. Left: ^{13}C (100 MHz) NQS spectra of the pure **IPBC** (a), **1** (b), **2** (c), **3** (d), and **4** (e) recorded at 12 kHz with a contact time of 7 ms. C3 signals are marked with black circles. Right: ^{1}H (400 MHz) MAS (dotted lines) and CRAMPS (solid lines) spectra of the pure **IPBC** (a), **1** (b), **2** (c), and **4** (d) recorded at 32 (MAS) and 12.5 (CRAMPS) kHz. Carrier frequency in CRAMPS spectra are marked with hashes.

Powder flow properties measurements. Manufacturing of pure **IPBC** in industrial products faces drawbacks. **IPBC** is difficult to handle as it tends to be clumpy and sticky. This implies that it cannot be fed easily from the blending equipment, or the automatic feeding device, that are commonly used in industrial plants where powdered materials are processed.[24] Due to the high cohesiveness of its powders, **IPBC** tends to aggregate even after a pulverization procedure and further limitations of its industrial employment arise when a good dispersion of the material is

required. This behavior forces the implementation of a physical break up step of its clumps during some industrial processes. Even with this procedure it becomes difficult to predetermine its degree of clinging to the walls of the mixing vessel resulting in hazardous clean-up procedure and enhanced manufacturing costs.

One method to estimate the flowing properties of granular materials is to measure the "angle of repose" of powders,[25] which is the steepest angle of descent of the slope relative to the horizontal plane when material on the slope face is on the verge of the sliding. The value of the angle of repose is the outcome of the balance between two forces, gravity and interparticulate cohesion. The smaller the value of the angle of repose, the higher is the free-flow characteristic of the granular material.

In general, the change of the cohesive properties of powders and the obtainment of materials with better powder flow properties are advantages that cocrystals may provide . The cocrystal **4** was selected to check possible improvements in powder flow properties as its CCF, being included in the GRAS list, seems particularly apt for industrial applications. Moreover, the brittleness of its powders provides a first indication about the possible good flow properties of the material.

Powders of **IPBC** and the cocrystal **4** were let flow from a funnel at a fixed height on a flat surface, and the angle of repose of the formed cone was measured (see Experimental Section and SI). As expected, the very high cohesiveness of the pure **IPBC** prevented a regular cone of powders to be obtained, the final formed figures resembling irregular piles shaped similar to the funnel's tube termination (Figure 9A and 9C). On the contrary, cocrystal **4** showed very good flow properties (Figure 9B and 9D): symmetrical cones of cocrystal powder were easily formed with angles of repose spanning from 13° to 20° depending on the height of the funnel from the

base. These values for cocrystal **4** are classified by European Pharmacopeia[25a] as "excellent" and indicate a free-flowing powder that is particularly suitable for automated industrial handling.

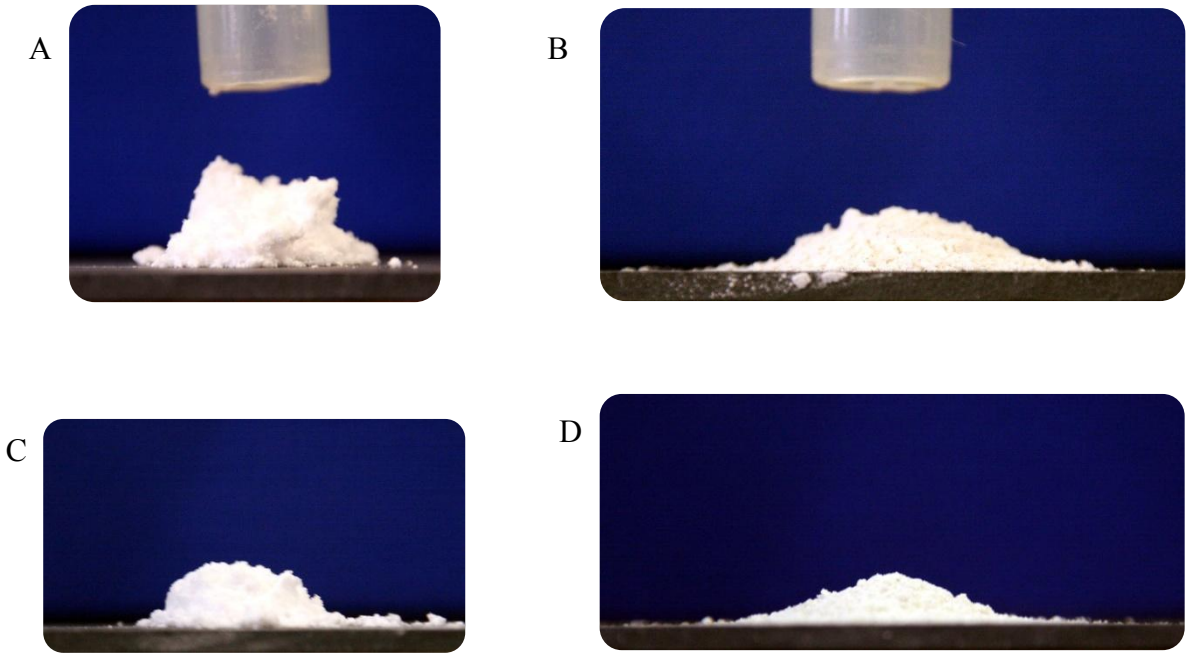

Figure 9. Pictures of cones of **IPBC** (A, C) and cocrystal **4** (B, D) powders, taken after flowing the powders through the funnel from 25 mm (A, B) and 50 mm (C, D) heights. The cylindrical shape of IPBC cones indicates clearly the high cohesion of the powders, while the flat cone shape of the cocrystal **4** indicates improved powder flow properties.

CONCLUSIONS

In summary, herein we have described the synthesis of four pharmaceutical cocrystals, **1-4**,[26] of 3-iodo-2-propynyl-*N*-butylcarbamate (**IPBC**), an iodinated antimicrobial product used globally as a preservative, fungicide, and algaecide. The results described in this article represent

the first applications of the use of XB for the obtainment of pharmaceutical cocrystals of a halogenated API.

In the described cases, the 1-iodoalkyne moiety has been proven to be a very reliable XB-donor group that forms very stable cocrystals with both neutral and anionic XB-acceptors. The obtained cocrystals have been fully characterized with various techniques (single crystal and powder X-ray, solution and solid-state NMR, IR and DSC), which have all shown that XB is the key interaction responsible for the self-assembly of the reported pharmaceutical cocrystals. Importantly, in the reported cocrystals, XB does not interfere with the HB pattern of the carbamate moiety of **IPBC**, which remains very much intact. This is important because of the complexity of chemical structures of APIs, which embody a particularly great challenge when design and preparation of specific multi-component crystals are pursued. We have shown here that XB and HB can successfully be combined in an orthogonal manner in order to obtain new cocrystals of halogenated APIs. The strategy reported here is, in principle, applicable to any APIs featuring the iodoalkyne moiety.

Halogen atoms are fairly present in FDA-approved drug molecules, the results reported in this paper may pave the way towards the extensive use of XB to contribute to improved drug product performance (*e.g.*, solubility, dissolution). Most of the cocrystals described in this paper have shown improved properties with respect to the source API, in terms, *e.g.* of powder flow properties and thermal stability. The cocrystal **4**, in particular, involving a GRAS cocrystal former widely used as dehydrating excipient, has serious possibilities of technological exploitation.[26] The measurement of the angle of repose of its powders have confirmed that cocrystal **4** has superior free-flow characteristics compared to the pure **IPBC**. The exploitation of

cocrystal **4** in biocide formulations is under current investigation in our laboratory and will be reported elsewhere.

EXPERIMENTAL SECTION

General. Starting materials were purchased from Sigma-Aldrich and used without further purification. Single crystals of adducts **1** and **2** were obtained *via* slow evaporation of methanol from concentrated solution of appropriate amounts of starting materials. Formed crystals were separated before the complete evaporation of the solvent occurred. Solid-state syntheses were performed using a Retsch MM 400 ball mill with 5.0 mL vessels. Single crystals of adduct **3** were obtained by seeding a quasi-saturated CH_2Cl_2 solution of IPBC and TBAI with the powder obtained by the ball-milling synthesis.

Single-Crystal X-ray Data Collection and Structure Determinations. Crystals suitable for X-ray crystallography were selected using an optical microscope. X-ray diffraction data were collected on a Bruker-AXS KAPPA-APEX II CCD diffractometer using Mo-Kα radiation (λ = 0.71073 Å). Data integration and reduction were performed using SaintPlus 6.01. Absorption correction was performed with a mult-scan method implemented in SADABS.[27] Space groups were determined using XPREP implemented in APEX II suite. Structures were solved using SHELXS-97 (direct methods) and refined using SHELXL-97[28] (full-matrix least-squares on F^2) contained in APEX II and WinGX v1.80.01[29] software packages. All non-hydrogen atoms were refined anisotropically. Hydrogen atoms were placed in geometrically calculated positions and included in the refinement process using a riding model with isotropic thermal parameters (Table 1).The molecular diagrams were generated using Mercury 3.0[30]. CIF files containing

crystallographic data can be obtained free of charge from Cambridge Crystallographic Data Centre *via* www.ccdc.cam.ac.uk/data_request/cif.

Table 2. Single crystal X-ray data and structure refinement parameters for cocrystals **1**-**3**.

	1	**2**	**3**
Chemical Formula	$2(C_8H_{12}INO_2)$, $C_{12}H_{12}N_2$	$C_8H_{12}INO_2$, $0.5(C_{10}H_8N_2)$	$3(C_8H_{12}NO_2I)$, $C_{16}H_{36}N^+I^-$
Formula weight	746.41	359.18	1212.62
Temperature K	297(2)	296(2)	103(2)
Crystal system	Monoclinc	Monoclinc	Monoclinc
Space group	*P2/c*	*C2/c*	*P 21/c*
***a* (Å)**	30.666(3)	28.683(2)	10.7688(9)
***b* (Å)**	4.9869(4)	4.9270(4)	20.204(2)
***c* (Å)**	21.068(2)	21.429(2)	23.735(2)
α(°)	90.00	90.00	90.00
β (°)	92.115(6)	99.92(2)	94.778(2)
γ(°)	90.00	90.00	90.00
Volume (Å^3)	3219.7(5)	2983.1(4)	5146.1(8)
Z	4	8	4
Density (gcm^{-3})	1.540	1.599	1.565
μ (mm^{-1})	1.989	2.144	2.464
***F* (000)**	1480	1416	2400
ABS T_{min}, T_{max}	0.5937, 0.7461	0.4444, 0.5410	0.3716, 0.4478
$\theta_{min, max}$ (°)	0.66 - 27.50	1.44 - 28.86	2.15, 34.45

$h_{min, max}$	-39, 39	-38, 38	-16, 15
$k_{min, max}$	-6, 6	-6, 6	-30, 31
$l_{min, max}$	-27, 27	-28, 29	-36, 37
No. of reflections.	7414	3916	19710
No. unique reflections.	4592	2785	16146
No of parameter	353	227	703
$R_{\_all}$, $R_{\_obs}$	0.0761, 0.0383	0.0475, 0.0302	0.0356, 0.0228
$wR2_{\_all}$, $wR2_{\_obs}$	0.1234, 0.0952	0.0859, 0.0718	0.0499, 0.0448
$\Delta\rho_{max, min}$ (eÅ^{-3})	-0.405, 0.714	-0.395, 0.668	-0.518, 0.901
G.o.F	1.077	1.043	1.050
CCDC No.	891325	891326	891327

Powder X-ray Diffraction (PXRD) Analysis. A Bruker AXS D8 powder diffractometer was used for all PXRD measurements with experimental parameters as follows: Cu-Kα radiation (λ = 1.54056Å), scanning interval: 5-40° 2θ. Step size 0.016°, exposure time 1.5 s per step. Experimental PXRD patterns and simulated PXRD patterns from single crystal data were compared to confirm the composition of bulk materials.

Differential Scanning Calorimetry (DSC) Analysis. Thermal analysis was performed on a Mettler Toledo DSC 823e differential scanning calorimeter. Aluminum crucibles were used for all samples, and the instrument was calibrated using indium as standard. For reference, an empty crucible was used. The thermal analysis was performed from 25 °C to 250 °C at a rate of 10 °C/min.

Infrared Spectroscopy (IR) Analysis. The IR characterization of samples was performed on a Nicolet Nexus FTIR spectrometer equipped with Smart Endurance ATR-device. Spectra were

measured over the range of 4000-550 cm^{-1} and analyzed using Omnic software v 6.2. Peak values are given in wavenumbers and rounded to 1 cm^{-1} upon automatic assignment. The peak intensity is described as: strong (s); medium (m), weak (w) and broad (b).

Elemental analysis (EA). Elemental analysis (*CHN*) were performed by Perkin Elemer Precisely, Series II (2004).

Cocrystallization *via* solvent evaporation.

3-Iodo-2-propynyl-*N*-butylcarbamate · 1,2-bis(4-pyridyl)ethane (2(IPBC)·BiPyEt, **1).** A solution of 1,2-bis(4-pyridyl)ethane (**BiPyEt**, 5 mg, 0.027 mmol) in methanol (0.5 mL) was added to a solution of 3-iodo-2-propynyl-*N*-butylcarbamate (**IPBC**, 15.2 mg, 0.054 mmol) in the same solvent (0.5 mL). Slow isothermal evaporation of the solvent afforded colorless crystals of **2(IPBC)·BiPyEt** (**1**) after 2 days. M.p. = 82 °C. Grinding was performed using a 2:1 ratio, respectively.

(ATR)-FTIR ν: 3321 (s), 2961 (m), 2937 (m), 2873 (w), 2188 (w), 1691 (s), 1602 (m), 1532 (s), 1417 (m), 1347 (m), 1279 (s), 1240 (s), 1123 (m), 1046 (s), 1001 (m), 963 (w), 809 (m), 777 (m), 630 (s) cm^{-1}.

EA *(CHN)* Calculated C: 45.06%, H: 4.86% and N: 7.51%. Found: C: 45.09%, H: 4.88% and N: 7.53%.

3-Iodo-2-propynyl-*N*-butylcarbamate · 4,4'-bipyridine (2(IPBC)·BiPy, **2).** A solution of 4,4'-bipyridine (**BiPy**, 7.5 mg, 0.048 mmol) in methanol (0.3 mL) was added to a solution of 3-iodo-2-propynyl-*N*-butylcarbamate (**IPBC**, 27 mg, 0.096 mmol) in the same solvent (0.7 mL).

Slow isothermal evaporation of the solvent afforded colorless crystals of **2(IPBC)·BiPy** (**2**) after 2.5 days. M.p. = 113 °C. Grinding was performed using a 2:1 ratio, respectively.

(ATR)-FTIR ν: 3325 (s), 2963 (m), 2934 (m), 2872 (m), 2189 (w), 1683 (s), 1592 (m), 1535 (m), 1403 (m), 1346 (w), 1280 (m), 1244 (m), 1213 (w), 1125 (m), 1045 (m), 994 (w), 957 (w), 806 (s), 614 (s) cm^{-1}.

EA *(CHN)* Calculated C: 43.47%, H: 4.49% and N: 7.80%. Found: C: 43.43%, H: 4.46% and N: 7.82%.

Cocrystallization *via* grinding and seeding.

3-Iodo-2-propynyl-*N*-butylcarbamate · tetra-*n*-butylammonium iodide (3(IPBC)·TBAI, 3). 3-Iodo-2-propynyl-*N*-butylcarbamate (**IPBC**, 113.8 mg, 0.405mmol) and tetra-*n*-butylammonium iodide (**TBAI**, 50 mg, 0.135mmol) were ground in a high-speed ball milling apparatus for 30 min at 30 Hz. The resulting microcrystalline powder was analyzed by FT-IR, DSC, and X-ray powder diffraction. M.p. = 45°C. Single crystals of **3** were obtained *via* seeding a quasi-saturated dichloromethane solution of the **IPBC** and **TBAI** in 3:1 ratio with the finely milled powder coming from the solid-state reaction; then the solvent was slowly evaporated at room temperature.

(ATR)-FTIR ν: 3324 (s), 2957 (m), 2931 (m), 2872 (m), 2185 (w), 1718 (s), 1688 (s), 1532 (s), 1471 (m), 1377 (w), 1363 (w), 1246 (s), 1135 (s), 1052 (s), 1026 (s), 989 (m), 881 (w), 775 (w), 735 (m), 608 (m) cm^{-1}.

EA *(CHN)* Calculated C: 39.62%, H: 5.98% and N: 4.62%. Found: C: 39.55%, H: 5.95% and N: 4.59%.

3-Iodo-2-propynyl-*N*-butylcarbamate · calcium chloride (4(IPBC)·$CaCl_2$, 4). 3-Iodo-2-propynyl-*N*-butylcarbamate (**IPBC**, 348 mg, 1.24 mmol) and calcium chloride (34 mg, 0.31 mmol) were ground in a high-speed ball milling apparatus for 15 min at 30 Hz. The resulting microcrystalline powder **4** was analyzed by FT-IR, DSC, and X-ray powder diffraction. M.p. = 85°C.

(ATR)-FTIR ν: 3431 (m), 3308 (m), 2955 (m), 2871 (w), 2187 (w), 1730 (s), 1682 (s), 1558 (s), 1522 (s), 1413 (w), 1368 (w), 1279 (m), 1241 (s), 1143 (m), 1109 (m), 1025 (s), 988 (m), 945 (m), 775 (m), 609 (m) cm^{-1}.

EA *(CHN)* Calculated **4(IPBC)·$CaCl_2$·$3H_2O$:** C: 29.81%, H: 4.22% and N: 4.35%. Found: C: 29.93%, H: 4.24% and N: 4.37%.

Solution NMR (^{13}C NMR) Analysis. ^{13}C NMR spectra were recorded at 300 K on a Bruker AV400 spectrometer. Experiments were carried out in $CDCl_3$ and methanol-d_4.

3-Iodo-2-propynyl-*N*-butylcarbamate (**IPBC**) and adducts **1-3** were dissolved in $CDCl_3$. A 0.4 M concentration with respect to **IPBC** was used in all the experiments. Incremental amounts of XB-acceptor have been added in order to evaluate the chemical shift variation of the carbon bound to iodine (Scheme 1). ^{13}C chemical shifts of 3-iodo-2-propynyl-*N*-butylcarbamate are reported below. ^{13}C NMR spectrum of cocrystal **4** was recorded in methanol-d_4.

3-Iodo-2-propynyl-*N*-butylcarbamate (IPBC, 0.4 M**).** (101 MHz, $CDCl_3$) δ: 155.34 (C4), 88.82 (C2), 53.75 (C1), 40.91 (C5), 31.91 (C6), 19.84 (C7), 13.68 (C8), 3.68 (C3) ppm.

2(3-Iodo-2-propynyl-*N*-butylcarbamate) · 1,2-bis(4-pyridyl)ethane (**1**, 0.4 M, 0.3 eq of **BiPyEt**), δ (101 MHz, $CDCl_3$): 155.38, 88.73, 53.72, 40.89, 31.90, 19.83, 13.67, 4.45 (C3) ppm.

1 (0.4 M, 0.4 eq of **BiPyEt**), δ (101 MHz, $CDCl_3$): 155.40, 88.70, 53.71, 40.88, 35.61, 31.89, 19.83, 13.67, 4.71 (C3) ppm. **1** (0.4 M, 0.5 eq of **BiPyEt**), δ (101 MHz, $CDCl_3$): 155.41, 88.67, 53.70, 40.87, 35.61, 31.89, 19.82, 13.67, 4.96 (C3) ppm. **1** (0.4 M, 0.6 eq of **BiPyEt**), δ (101 MHz, $CDCl_3$): 155.43, 88.62, 53.69, 41.45, 40.86, 35.59, 31.88, 19.82, 13.67, 5.31 (C3) ppm. **1** (0.4 M, 0.7 eq of **BiPyEt**), δ (101 MHz, $CDCl_3$): 155.44, 88.59, 53.68, 40.85, 35.58, 31.87, 19.82, 13.67, 5.56 (C3) ppm.

2(3-iodo-2-propynyl-*N*-butylcarbamate) · 4,4'-bipyridine (**2**, 0.4 M, 0.3 eq of **BiPy**). δ (101 MHz, $CDCl_3$): 155.38, 88.76, 53.73, 40.89, 31.90, 19.83, 13.67, 4.18 (C3) ppm. **2** (0.4 M, 0.4 eq of **BiPy**), δ (101 MHz, $CDCl_3$): 155.39, 88.74, 53.73, 40.89, 31.89, 19.83, 13.67, 4.35 (C3) ppm. **2** (0.4 M, 0.5 eq of **BiPy**), δ (101 MHz, $CDCl_3$): 155.40, 88.73, 53.73, 40.88, 31.89, 19.83, 13.67, 4.48 (C3) ppm. **2** (0.4 M, 0.6 eq of **BiPy**), δ (101 MHz, $CDCl_3$): 155.41, 88.71, 53.72, 40.88, 31.88, 19.83, 13.67, 4.65 (C3) ppm. **2** (0.4 M, 0.7 eq of **BiPy**), δ (101 MHz, $CDCl_3$): 155.42,88.69, 53.71, 40.87, 31.88, 19.82, 13.67, 4.80 (C3) ppm.

3(3-Iodo-2-propynyl-*N*-butylcarbamate) · tetrabutylammoniumiodide (**3**, 0.4 M, 0.1 eq of **TBAI**), δ: (101 MHz, $CDCl_3$): 155.36, 88.47, 53.75, 40.89, 31.90, 19.83, 13.67, 5.33 (C3) ppm. **3** (0.4 M, 0.2 eq of **TBAI**), δ: (101 MHz, $CDCl_3$): 155.37, 88.19, 53.75, 40.87, 31.89, 19.83, 13.66, 6.69 (C3) ppm. **3** (0.4 M, 0.3 eq of **TBAI**), δ: (101 MHz, $CDCl_3$):155.39, 87.90, 53.74, 40.86, 31.88, 19.81, 13.65, 8.07 (C3) ppm. **3** (0.4 M, 0.4 eq of **TBAI**), δ: (101 MHz, $CDCl_3$): 155.39, 87.64, 53.73, 40.84, 31.87, 19.80, 13.65, 9.30 (C3) ppm. **3** (0.4 M, 0.5 eq of **TBAI**), δ: (101 MHz, $CDCl_3$): 155.40, 87.40, 53.72, 40.82, 31.86, 19.78, 13.64, 10.42 (C3) ppm.

3-Iodo-2-propynyl-*N*-butylcarbamate (**IPBC**, 0.4 M). δ (101 MHz, methanol-d_4): 156.56, 88.07, 53.08, 40.29, 31.59, 19.52, 12.74, 6.25 (C3) ppm.

4(3-Iodo-2-propynyl-*N*-butylcarbamate) · calcium chloride (**4**, 0.4 M). δ (101 MHz, methanol-d_4): 156.58, 87.99, 53.18, 40.34, 31.59, 19.55, 19.37, 12.98, 12.82, 6.82 (C3) ppm.

Solid-state NMR Analysis (SSNMR). SSNMR measurements were run on a Bruker AVANCE II 400 instrument operating at 400.23, 100.65 and 40.56 MHz for ^{1}H, ^{13}C and ^{15}N, respectively. ^{13}C and ^{15}N CPMAS (Cross-Polarization Magic-Angle-Spinning) spectra were recorded at room temperature at the spinning speed of 12 kHz. Cylindrical 4 mm o.d. zirconia rotors with sample volume of 80 μL were employed. A ramp cross-polarization pulse sequence was used with contact times of 7 (^{13}C) or 4 (^{15}N) ms, a ^{1}H 90° pulse of 3.30 μs, recycle delays of 5-7 s, and 256 (^{13}C) or 2048-14000 (^{15}N) transients. Non-quaternary-suppression experiments (NQS) were run with dephasing times of 25-35 μs. The two pulse phase modulation (TPPM) decoupling scheme was used with a frequency field of 75 kHz.

^{1}H MAS (Magic-Angle-Spinning) and ^{1}H CRAMPS (Combined Rotation And Multiple Pulse Sprectroscopy) experiments were performed on a 2.5 mm Bruker probe. The ^{1}H MAS spectra were acquired at the spinning speed of 32 kHz with the DEPTH sequence (π/2–π–π) for the suppression of the probe background signal. ^{1}H CRAMPS spectra were acquired using a windowed-PMLG (*w*PMLG5)[31] pulse sequence of dipolar decoupling at the spinning speed of 12.5 kHz with a ^{1}H 90° pulse lengths of 2.5 μs. The pulse width and the RF power were finely adjusted for best resolution.

^{1}H, ^{13}C and ^{15}N scales were calibrated with adamantane (^{1}H signal at 1.87 ppm), glycine (^{13}C methylene signal at 43.86 ppm) and $(NH_4)_2SO_4$ (^{15}N signal at δ=355.8 ppm with respect to CH_3NO_2) as external standards.

Powder flow property measurements. Experiments setup: 1.00 g of powders (**IPBC** or cocrystal **4**) and a plastic funnel with the bottom opening of 1 cm diameter were used. The powder was charged into the funnel, closing the lower opening of the funnel with a glass slide, then the slide was removed and the powder was let to flow from the funnel to a horizontal ceramic base. Two different funnel heights (25 mm and 50 mm) were used in order to compare the effect of this parameter on the cone shape. Pictures of the powder cone were taken in-line with the base of the cone using a reflex CCD camera. Height and diameter of the cone were measured by counting the pixels composing the height and the base of the digital picture. Angle of repose was calculated using the equation 1:

$$\tan(\alpha) = \frac{heigth}{0.5 \times diameter} \quad \text{eq.1}$$

Angle of reposes for cocrystal **4** are reported (see SI). The angle of repose for pure **IPBC** was not calculated since the high cohesion of powders prevented a conical shape from being obtained.

ASSOCIATED CONTENT

SI Supporting Information

CSD analysis, ATR-FTIR, DSC, crystallographic information (cif and check-cif) and PXRD results, solid state NMR studies and ^{1}H and ^{13}C NMR spectra in solution for **1-4**, angle of repose measurements. This material is available free of charge via the Internet at http://pubs.acs.org.

AUTHOR INFORMATION

Corresponding Authors

pierangelo.metrangolo@polimi.it; giuseppe.resnati@polimi.it

Notes

The authors declare no competing financial interest.

ACKNOWLEDGMENTS

G.C., P.M., G.R., and G.T. acknowledge Fondazione Cariplo (projects 2009-2550 and 2010-1351) for financial support. Massimiliano Accardo from FluorIT srl is acknowledged for useful discussions.

REFERENCES

(1) (a) Schultheiss, N.; Newman, Pharmaceutical Cocrystals and Their Physicochemical Properties. A. *Cryst. Growth Des*. **2009**, 9, 2950-2967. (b) Thayer, A. M. Form and Function. The Choice of Pharmaceutical Crystalline Form Can Be Used to Optimize Drug Properties, and Cocrystals Are Emerging as New Alternatives. *Chem. Eng. News* **2007**, *85*, 17-30. (c) Balgden,

N.; de Matas, M.; Gavan, P. T.; York, P. Crystal Engineering of Active Pharmaceutical Ingredients to Improve Solubility and Dissolution Rates. *Adv. Drug. Dev. Rev.* **2007**, 59, 617-630. (d) Hickey, M. B.; Peterson, M. L.; Scoppettuolo, L. A.; Morrisette, S. L.; Vetter, A.; Guzmán, H.; Remenar, J. F.; Zhang, Z.; Tawa, M. D.; Haley, S.; Zaworotko, M. J.; Almarsson, Ö. Performance Comparison of a Co-crystal of Carbamazepine with Marketed Product. *Eur. J. Pharm. Biopharm.* **2007**, *67*, 112-119. (e) Nehm, J. S.; Rodrìguez-Spong, B.; Rodrìguez-Hornedo, N. Phase Solubility Diagrams of Cocrystals Are Explained by Solubility Product and Solution Complexation. *Cryst. Growth Des.* **2006**, *6*, 592-600. (f) Trask, A. V.; Motherwell, W. D. S.; Jones, W. Pharmaceutical Cocrystallization: Engineering a Remedy for Caffeine Hydration. *Cryst. Growth Des*. **2005**, *5*, 1013-1021. (g) Childs, S. L.; Chyall, L. J.; Dunlap, J. T.; Smolenskaya, V. N.; Stahly, P. Crystal Engineering Approach to Forming Cocrystals of Amine Hydrochlorides with Organic Ocids. Molecular Complexes of Fluoxetine Hydrochloride with Benzoic, Succinic, and Fumaric Acids. *J. Am. Chem. Soc.* **2004**, *126*, 13335-13342. (h) Almarsson, Ö.; Zaworotko, M. J. Crystal Engineering of the Composition of Pharmaceutical Phases. Do Pharmaceutical Co-crystals Represent a New Path to Improved Medicines? *Chem. Commun.* **2004**, 1889-1896.

(2) (a) Brittain, H.G. Cocrystal Systems of Pharmaceutical Interest: 2010. *Cryst. Growth Des.* **2012**, *12*, 1046-1054. (b) Bica, K.; Rodríguez, H.; Gurau , G.; Cojocaru, A. O.; Riisager, A.; Fehrmann, R.; Rogers R. D. Pharmaceutically Active Ionic Liquids with Solids Handling, Enhanced Thermal Stability, and Fast Release. *Chem. Commun.* **2012**, *48*, 5422-5424 (c) Qiao, N.; Li, M.;Schlindwein, W.; Malek, N.; Davies, A.; Trappitt, G. Pharmaceutical Cocrystals: An Overview. *Int. J. Pharm.* **2011**, *419*, 1-11. (d) Khan, M.; Enkelmann, V.; Brunklaus, G. Crystal Engineering of Pharmaceutical Co-crystals: Application of Methyl Paraben as Molecular Hook.

J. Am. Chem. Soc. **2010**, *132*, 5254-5263. (e) Anderson, K. M.; Probert, M. R.; Whiteley, C. N.; Rowland, A. M.; Goeta, A. R.; Steed, J. W. Designing Co-Crystals of Pharmaceutically Relevant Compounds That Crystallize with Z ' > 1. *Cryst. Growth Des.* **2009**, *9*, 1082-1087. (f) Basavoju, S.; Bostrom, D.; Velaga, S. P. Indomethacin-Ssaccharin Cocrystal: Design, Synthesis and Preliminary Pharmaceutical Characterization. *Pharm. Res.* **2008**, *25*, 530-541. (g) Shan, N.; Zaworotko, M. J. The Role of Cocrystals in Pharmaceutical Science. *Drug Disc. Today* **2008**, *13*, 440-446. (h) Trask, A. V. An Overview of Pharmaceutical Cocrystals as Intellectual Property. *Mol. Pharm.* **2007**, *4*, 301-309. (i) Basavoju, S.; Bostrom, D.; Velaga, S. P. Pharmaceutical Cocrystal and Salts of Norfloxacin. *Cryst. Growth Des*. **2006**, 6, 2699-2708. (j) Vishweshwar, P.; McMahon, J. A.; Bis, J. A.; Zaworotko, M. J. Pharmaceutical Co-Crystals. *J. Pharm. Sci.* **2006**, *95*, 499-516.

(3) (a) Guidance for Industry Regulatory Classification of Pharmaceutical Co-Crystals, December 2011 http://www.fda.gov/Drugs/GuidanceComplianceRegulatoryInformation/Guidances/default.htm. (b) McNamara, D. P.; Childs, S. L.; Giordano, J.; Iarriccio, A.; Cassidy, J.; Shet, M. S.; Mannion, R.; O'Donnell, E.; Park, A. Use of a Glutaric Acid Cocrystal to Improve Oral Bioavailability of a Low Solubility API. *Pharm. Res.* **2006**, *23*, 1888-1897. (c) Trask, A. V.; Motherwel, S. W. D.; Jones, W. Physical Stability Enhancement of Theophylline via Cocrystallization. *Intern. J. of Pharm.* **2006**, *320*, 114-123.

(4) (a) Adaler, T. K.; Sankolli, R.; Dastidar, P. Homo- or Heterosynthon? A Crystallographic Study on a Series of New Cocrystals Derived from Pyrazinecarboxamide and Various Carboxylic Acids Equipped with Additional Hydrogen Bonding Sites. *Cryst. Growth Des.* **2012**, *12*, 2533-2542. (b) Gorman, E. M.; Samas, B.; Munson, E. J. Understanding the Dehydration of

Levofloxacin Hemihydrate *J. Pharm. Sci.* **2012**, *101*, 3319-3330. (c) Grobelny, P.; Mukherjee, A.; Desiraju, G. R. Drug-Drug Co-crystals: Temperature-Dependent Proton Mobility in the Molecular Complex of Isoniazid with 4-Aminosalicylic Acid Solids. *CrystEngComm* **2011**, *13*, 4358-4364. (d) Bica, K.; Shamshina, J.; Hough, W. L.; MacFarlane, D. R.; Rogers, R. D. Liquid Forms of Pharmaceutical Co-crystals: Exploring the Boundaries of Salt Formation. *Chem.Commun.* **2011**, *47*, 2267-2269. (e) Varughese, S.; Azim, Y.; Desiraju, G. R. Molecular Complexes of Alprazolam with Carboxylic Acids, Boric Acid, Boronic Acids, and Phenols. Evaluation of Supramolecular Heterosynthons Mediated by a Triazole Ring. *J. Pharm. Sci.* **2010**, *99*, 3743-3753. (f) Stanton, M.K.; Tufekeic, S.; Morgan, C.; Bak, A. Drug Substance and Former Structure Property Relationships in 15 Diverse Pharmaceutical Co-Crystals. *Cryst. Growth Des* **2009**, *9*, 1344-1352. (g) Bhatt, P. M.; Azim, Y.; Thakur, T. S.; Desiraju, G. R. Co-Crystals of the Anti-HIV Drugs Lamivudine and Zidovudine. *Cryst. Growth Des.* **2009**, *9*, 951-957. (h) Bucar, D.-K.; Henry, R. F.; Lou, X.; Borchardt, T. B.; Zhang, G. G. Z. A ‘‘Hidden’’ Co-crystal of Caffeine and Adipic Acid. *Chem.Commun.* **2007**, 525-527. (i) Babu, N. J.; Reddy, L. S.; Nangia A. Amide-N-Oxide Heterosynthon and Amide Dimer Homosynthon in Cocrystals of Carboxamide Drugs and Pyridine N-Oxides. *Mol. Pharm.* **2007**, *4*, 417-434. (j) Vishweshwar, P.; McMahon, J. A.; Peterson, M. L.; Hickey, M. B.; Shattock, T. R.; Zaworotko, M. J. Crystal Engineering of Pharmaceutical Co-crystals From Polymorphic Active Pharmaceutical Ingredients. *Chem. Commun.* **2005**, 4601-4603. (k) McMahon, J. A.; Bis, J. A.; Vishweshwar, P.; Shattock, T. R.; McLaughlin, O. L.; Zaworotko, M. J. Crystal Engineering of the Composition of Pharmaceutical Phases. 3. Primary Amide Supramolecular Heterosynthons and Their Role in the Design of Pharmaceutical Co-crystals. *Z. Kristallogr.* **2005**, *220*, 340-350. (l) Trask, A. V.; Motherwell, W. D. S.; Jones, W. Pharmaceutical Cocrystallization: Engineering a Remedy for

Caffeine Hydration. *Cryst. Growth Des.* **2005**, *5*, 1013-1021. (m) Fleischman, S. G.; Kuduva, S. S.; McMahon, J. A.; Moulton, B.; Walsh, R. D. B.; Rodríguez-Hornedo, N.; Zaworotko, M. J. Crystal Engineering of the Composition of Pharmaceutical Phases: Multiple-Component Crystalline Solids Involving Carbamazepine. *Cryst. Growth Des.* **2003**, *3*, 909-919. (n) Remenar, J. F.; Morissette, S. L.; Peterson, M. L.; Moulton, B.; Mac Phee, J. M.; Guzman, H. R.; Almarsson, O. Crystal Engineering of Novel Cocrystals of a Triazole Drug with 1,4-Dicarboxylic Acids. *J. Am. Chem. Soc.* **2003**, *125*, 8456-8457.

(5) (a) Aakero□y, C. B.; Forbes, S.; Desper, The Effect of Water Molecules in Stabilizing Co-crystals of Active Pharmaceutical Ingredients. *CrystEngComm* **2012**, *12*, 2435-2443. (b) Weyna, D. R.; Cheney, M. L.; Shan, N.; Hanna, M.; Zaworotko, M. J.; Sava, V.; Song, S.; Sanchez-Ramos, J. R. : Improving Solubility and Pharmacokinetics of Meloxicam via Multiple-Component Crystal Formation. *Mol. Pharmaceutics* **2012**, *9*, 2094-2102. (c) Smith, A. J.; Kavuru, P.; Wojtas, L.; Zaworotko, M. J.; Shytle, R. D. Cocrystals of Quercetin with Improved Solubility and Oral Bioavailability. *Mol. Pharmaceutics* **2011**, *8*, 1867−1876. (d) Sanphui, P.; Goud, N. R.; Khandavilli, U. B. R.; Nangia, A. Fast Dissolving Curcumin Cocrystals. *Cryst. Growth Des.* **2011**, *11*, 4135−4145. (e) Cheney, M. L.; Weyna, D. R.; Shan, N.; Hanna, M.; Wojtas, L.; Zaworotko, M. J. Coformer Selection in Pharmaceutical Cocrystal Development: A Case Study of a Meloxicam Aspirin Cocrystal That Exhibits Enhanced Solubility and Pharmacokinetics. *J. Pharm. Sci.* **2011**, *100*, 2172−2181. (f) Aakero□y, C. B.; Forbes, S.; Desper, J Beatty, A. M.; Helfrich, B. A. Using Cocrystals To Systematically Modulate Aqueous Solubility and Melting Behavior of an Anticancer Drug *J. Am. Chem. Soc.* **2009**, *13*, 17048-17049. (g) Banerjee, R.; Bhatt, P. M.; Desiraju, G. R. Solvates of Sildenafil Saccharinate. A New Host Material. *Cryst. Growth Des.* **2006**, *6*, 1468-1478. (h) Friščić, T.; Trask, A. V; Jones, W.;

Motherwell, W. D. S. Screening for Inclusion Compounds and Systematic Construction of Three-Component Solids by Liquid-Assisted Grinding. *Angew. Chem., Int. Ed.* **2006**, *45*, 7546-7550. (i) Reddy, L. S.; Babu, N. J.; Nangia, A. Carboxamide-Pyridine N-oxide Heterosynthon for Crystal Engineering and Pharmaceutical Cocrystals. *Chem. Commun.* **2006**, 1369-1371.

(6) http://www.drugbank.ca/

(7) (a) Guthrie, F. On The Iodide of Iodammonium. *J. Chem. Soc*. **1863**, *16*, 239-244. (b) Hassel, O.; Rømming, C. Direct Structural Evidence for Weak Charge-transfer Bonds in Solids Containing Chemically Saturated Molecules. *Quart. Rev. Chem. Soc*. **1962**, *16*, 1-18. (c) Legon, A.C. Prereactive Complexes of Dihalogens XY with Lewis Bases B in the Gas Phase: A Systematic Case for the Halogen Analogue B - XY of the Hydrogen Bond B – HX. *Angew. Chem. Int. Ed*. **1999**, *38*, 2686-2714. (d) Metrangolo, P.; Neukirch, H.; Pilati, T.; Resnati, G. Halogen Bonding Based Recognition Processes: A World Parallel to Hydrogen Bonding. *Acc. Chem. Res*. **2005**, *38*, 386-395. (e) Metrangolo, P.; Resnati, G. Halogen Bonding: A Paradigm in Supramolecular Chemistry. *Chem. Eur. J*. **2001**, *7*, 2511-2519. (f) Rissanen, K. Halogen Bonded Supramolecular Complexes and Networks. *CrystEngComm* **2008**, *10*, 1107-1113. (g) Pennington, W. T.; Hanks, T. W.; Arman, H. D. Halogen Bonding with Dihalogens and Interalogens. In *Halogen Bonding Fundamentals and Applications,* Metrangolo P. and Resnati G., Eds.; Structure and Bonding; Springer: Berlin 2008, *126*, pp. 65-104. (h) Formiguè, M.; Batail, P. Activation of Hydrogen- and Halogen-Bonding Interactions in Tetrathiafulvalene-Based Crystalline Molecular Conductors. *Chem. Rev.* **2004**, *104*, 5379-5418. (i) Crihfield, A.; Hartwell, J.; Phelps, D.; Walsh, R. B.; Harris, J. L.; Payne, J. F.; Pennington, W. T.; Hanks, T. W. Crystal Engineering Through Halogen Bonding. 2. Complexes of Diacetylene-Linked Heterocycles with Organic Iodides. *Cryst. Growth & Des.* **2003**, *3*, 313-320.

(8) (a) Clark, T.; Hennemann, M.; Murray, J. S.; Politzer, P. Halogen Bonding: The Sigma-Hole. *J. Mol. Model.* **2007**, *13*, 291-296. (b) Riley, K. E.; Murray, J. S.; Concha, M. C.; Hobza, P.; Politzer, P. Br···O Complexes as Probes of Factors Affecting Halogen Bonding: Interactions of Bromobenzenes and Bromopyrimidines with Acetone. *J. Chem. Theory Comput.* **2009**, 5, 155-163. (c) Politzer, P.; Murray, J. S.; Clark, T. Halogen Bonding: An Electrostatically-driven Highly Directional Noncovalent Interaction. *Phys. Chem. Chem. Phys.* **2010**, *12*, 7748-7757.

(9) (a) http://www.iupac.org/web/ins/2009-032-1-100 The definition given here should be taken as provisional. (b) http://blogs.rsc.org/ce/2010/11/02/defining-the-halogen-bond-iupac-task-group-need-your-input/; *Chemistry International* **2010**, *32*, 20;(c) http://www.halogenbonding.eu/

(10) (a) Aakero□y, C. B.; Rajbanshi, A.; Metrangolo, M.; Resnati, G.; Parisi, M. F.; Desper, J.; Pilati, T. The Quest for a Molecular Capsule Assembled Via Halogen Bonds. *CrystEngComm* **2012**, *14*, 6366-6368. (b) Nayak, S. N.; Terraneo, G.; Forni, A.; Metrangolo, M.; Resnati, G. C-Br···O Supramolecular Synthon: In Situ Cryocrystallography of Low Melting Halogen-Bonded Complexes. *CrystEngComm* **2012**, *14*, 4259-4261. (c) Metrangolo, P.; Murray, J. S.; Pilati, T.; Politzer, P. Resnati, G.; Terraneo, G. The Fluorine Atom as a Halogen Bond Donor, *viz.* a Positive Site. *CrystEngComm* **2011**, *13*, 6593-6596. (d) Lemouchi, C.; Vogelsberg, C. S.; Zorina, L.; Simonov, S.; Batail, P.; Brown, S.; Garcia-Garibay, M. A. Ultra-fast Rotors for Molecular Machines and Functional Materials via Halogen Bonding: Crystals of 1,4-Bis(iodoethynyl)bicyclo[2.2.2]octane with Distinct Gigahertz Rotation at Two Sites. *J. Am. Chem. Soc.* **2011**, *133*, 6371-6379. (d) Abate, A.; Brischetto, M.; Cavallo, G.; Lahtinen, M.; Metrangolo, P.; Pilati, T.; Radice, S.; Resnati, G.; Rissanen, K.; Terraneo, G. Dimensional encapsulation of $I^-\cdots I_2\cdots I^-$ in an organic salt crystal matrix. *Chem. Commun.* **2010**, 2724-2726.

(f) Abate, A.; Biella, S.; Cavallo, G.; Meyer, F.; Neukirch, H.; Metrangolo, P.; Pilati, T.; Resnati, G.; Terraneo, G. Halide Anion-templated Assembly of di- and Triiodoperfluorobenzenes into 2D and 3D Supramolecular Networks *J. Fluorine Chem.* **2010**, *130*, 1171-1177**. (g)** Gattuso, G.; Notti, A.; Pappalardo, S.; Parisi, M.; Pilati, T.; Resnati, G.; Terraneo G. Ion-pair Separation via Selective Inclusion/Segregation Processes. *CrystEngComm* **2009**, *11*, 1204-1206. (h) Biella, S.; Gattuso, G.; Notti, A.; Metrangolo, P.; Pappalardo, S.; Parisi, M. F.; Pilati, T.; Resnati, G.; Terraneo, G. Halogen Bonding-based Anion Coordination in Calixarene/Inorganic Halide/Diiodoperfluorocarbon Assemblies. *Supramol. Chem.* **2009**, *21*, 149-156.

(11) Hardegger, L. A.; Kuhn, B.; Spinnler, B.; Anselm, L.; Ecabert, R.; Stihle, M.; Gsell, B.; Thoma, R.; Diez, J.; Benz, J.; Plancher, J.-M.; Hartmann, G.; Banner, D. W.; Haap, W.; Diederich. F. Systematic Investigation of Halogen Bonding in Protein–Ligand Interactions. *Angew. Chem. Int. Ed.* **2011**, *50*, 314-318.

(12) (a) See Cambridge Structure Database Analysis Section in SI. (b) Perkins, C.; Libri, S.; Adams, H.; Brammer, L. Diiodoacetylene: Compact, Strong Ditopic Halogen Bond Donor. *CrystEngComm* **2012**, *14*, 3033-3038. (c) Stang, P. J. Alkynyl- and Alkenyl(phenyl)iodonium Compounds. New Synthetic Methods. *Angew. Chem. Int. Ed.* **1992**, *31*, 274-285.

(13) Lutz, P. J.; Borokhov, O.; Ban, S. A. "Preservative blends containing iodine containing compounds", US6946427B2.

(14) Avtomonov, E. V.; Gruning, R.; Lorberth, J. Crystal and Molecular Structure of 3-Iodo-2-propynyl-N-butylcarbamate. *Z. Naturforsch.,B:Chem.Sci.***1997**, *52*, 256 (CSD code: TOYPUS)

(15) We define 'normalized contact', the ratio Nc = Dij/(rvdWi + rvdWj), whereDij is the distance between the atomsi and j and rvdWi and rvdWj are the van der Waals radii for

atomsiand j, respectively. If the electron donor j is an anionic atom, rvdWj is substituted by rPj , the Pauling ionic radius of anion atom j. van der Waals radii and Pauling ionic radii were obtained from web of element (http://www.webelements.com/).

(16) (a) Priimagi, A.; Cavallo, G.; Forni, A.; Gorynsztejn-Leben, M.; Kaivola, M.; Metrangolo, M.; Milani, R.; Shishido, A.; Pilati, T.; Resnati, G.; Terraneo, G. Halogen Bonding versus Hydrogen Bonding in Driving Self-Assembly and Performance of Light-Responsive Supramolecular Polymers. *Adv. Functional Mat.* **2012**, *22*, 2572-2579. (b) Fox, D.; Metrangolo, P.; Pasini, D.; Pilati, T.; Resnati, G.; Terraneo G. Site-selective Supramolecular Synthesis of Halogen-bonded Cocrystals Incorporating the Photoactive Azo Group. *CrystEngComm* **2008**, *10*, 1132-1136. (17) Rege, P. D.; Malkina, O. L.; Goroff, N. S. *J. Am. Chem. Soc.* **2002**, *124*, 370-371. (b) Gao, K.; Goroff, N. S. Two New Iodine-Capped Carbon Rods. *J. Am. Chem. Soc.* **2000**, *122*, 9320-9321.

(18) Bouchmella, K.; Dutremez, S. G.; Alonso, B.; Mauri, F.; Gervais, C. ^{1}H, ^{13}C, and ^{15}N Solid-State NMR Studies of Imidazole- and Morpholine-Based Model Compounds Possessing Halogen and Hydrogen Bonding Capabilities. *Cryst. Growth Des.* **2008**, *8*, 3941-3950.

(19) Attrell, R. J.; Widdifield, C. M.; Korobkov, I.; Bryce, D. L. Weak Halogen Bonding in Solid Haloanilinium Halides Probed Directly via Chlorine-35, Bromine-81, and Iodine-127 NMR Spectroscopy. *Cryst. Growth Des*. **2012**, *12*, 1641-1653.

(20) The cocrystal **4** is hydrated as deducted from the presence of an intense and narrow resonance at 4.88 ppm (about 3 water molecules from signal integration which agrees with elemental analysis data, see Experimental Section).

(21) Owing to the broadening effect of the 2nd-order dipolar coupling to the quadrupolar iodine-27 nucleus and the large distance from hydrogen atoms, very long contact times (>7 ms) were required in the cross-polarization and in the NQS experiments for increasing the C3 signal intensity. NQS spectra (Figure 8) were fundamental for resolving overlapped C3 resonances.

(22) Viger-Gravel, J.; Korobkov, I.; Bryce, D. L. Multinuclear Solid-State Magnetic Resonance and X-ray Diffraction Study of Some Thiocyanate and Selenocyanate Complexes Exhibiting Halogen Bonding. *Cryst. Growth Des.* **2011**, *11*, 4984-4995.

(23) As in previous applications of ^{1}H CRAMPS experiments, it is clear that the resolution provided by the *w*PMLG5 method is much superior as compared to fast-MAS experiments. While a resolution improvement is observed for all signals, we focus our discussion herein mainly on signals of hydrogen atoms involved in HB.

(24) Barrtko, J. P. Free-flowing composition of a biocide and a processing additive therewith for incorporation into a polymer or plastic matrix product. US 2006/0229381 A1

(25) (a) European Pharmacopoeia 7th ed. **2010**; 2.9.36, 308–311. (b) Darshak, A. B.; Trivedi, R..; Dastidar, P.; Ghosh, P. K.; Pramanik, A.; Kumar, V. G. A practical approach to produce near-spherical common salt crystals with better flow characteristics *Cryst. Growth Des.* **2006**, *6*, 1591-1594.

(26) Baldrighi, M.; Metrangolo, P.; Resnati, G.; Terraneo, G. "3-iodo-2-propynyl-*N*-butylcarbamate cocrystals" patent application MI2012A000586.

(27) (a) Sheldrick, G. M. SADABS, empirical absorption correction program, University of Gottingen; based upon the method of Blessing, R. H. 25b. (b) Blessing, R. H. An Empirical

Correction for Absorption Anisotropy. *ActaCrystallogr., Sect. A: Found. Crystallogr.* **1995**, *51*, 33-38.

(28) Sheldrick, G. M. A Short History of SHELX. *Acta Crystallogr., Sect. A.* **2008**, *64*, 112-122.

(29) Farrugia, L. J. WinGX Suite for Small-molecule Single-crystal Crystallography. *J. Appl. Crystallogr.*, **1999**, *32*, 837-383.

(30) Macrae, C. F.; Bruno, I. J.; Chisholm, J.A.; Edgington, P. R.; McCabe, P.; Pidcock, E.; Rodriguez-Monge, L.; Taylor, R.; van de Streek J.; Wood, P. A. Mercury CSD 2.0 - New Features for the Visualization and Investigation of Crystal Structures. *J. Appl. Cryst.* **2008**, *41*, 466-470, http://www.ccdc.cam.ac.uk/mercury.

(31) Vinogradov, E.; Madhu, P. K.; Vega, S. High-resolution Proton Solid-state NMR Spectroscopy by Phase-modulated Lee-Goldburg Experiment. *Chem. Phys. Lett.* **1999**, *314*, 443-450.

Halogen bonding and pharmaceutical cocrystals: The case of a widely used preservative

Michele Baldrighi,[†] Gabriella Cavallo,[†] Michele R. Chierotti,[‡] Roberto Gobetto,[‡] Pierangelo Metrangolo,[†,#] Tullio Pilati,[†] Giuseppe Resnati,*[†,#] and Giancarlo Terraneo[†,#]*

[†]NFMLab, Department of Chemistry, Materials, and Chemical Engineering ‘‘Giulio Natta’’, Politecnico di Milano, Via L. Mancinelli 7, 20131 Milan, Italy;

[‡]Department of Chemistry, University of Torino, V. P. Giuria 7, 10125 Turin, Italy;

[#]Center for Nano Science and Technology@PolimMi, Istituto Italiano di Tecnologia, Via Pascoli 70/3, 20133 Milan, Italy

Contents

SI 1. Cambridge Structure Database Analysis.

Figure SI 1.1 Scatterplot of short contacts given by 1-iodoalkynes with different electron donor sites.

Figure SI 1.2 Total number of short intermolecular contacts and XB contacts occurring in CSD between 1-iodoalkynes and selected XB acceptors.

Figure SI 1.3 Scatterplot of short contacts given by 1-iodoalkynes with halogenated anions as electron donor sites.

Figure SI 1.4 Scatterplot of short contacts given by 1-iodoalkynes with nitrogen atoms as electron donor sites.

Figure SI 1.5 Scatterplot of short contacts given by 1-iodoalkynes with oxygen atoms as electron donor sites.

Figure SI 1.6 Scatterplot of short contacts (reported as normalized contact) given by 1-iodoalkynes with different electron donor sites.

Figure SI 1.7 Scatterplot of short contacts given by 1-iodoalkynes with different electron donor sites when XB classification criterion is applied (C-I···D angle in between 140° and 180°).

Figure SI 1.8 Scatterplot of short contacts given by 1-iodoalkynes with hydrogen atoms as electron acceptor sites.

SI 2. InfraredSpectroscopy (FT-IR).

Figure SI 2.1 (ATR)-IR spectrumcocrystal**IPBC**

Figure SI 2.2 (ATR)-IR spectrum cocrystal **1**

Figure SI 2.3 (ATR)-IR spectrum cocrystal **2**

Figure SI 2.4 (ATR)-IR spectrum cocrystal **3**

Figure SI 2.5 (ATR)-IR spectrum cocrystal **4**

SI 3. Differential Scanning Calorimetry (DSC).

Figure SI 3.1 Left: DSC thermogram of **1**. Right: DSC thermogram of **2**.

Figure SI 3.2 Left: DSC thermogram of **3**. Right: DSC thermogram of **4**.

SI 4. Powder X-ray Diffraction (PXRD).

Figure SI 4.1PXRD pattern of **IPBC**.

Figure SI 4.2 PXRD pattern of **BiPyEt**.

Figure SI 4.3 PXRD pattern of **BiPy**.

Figure SI 4.4 PXRD pattern of **TBAI**.

Figure SI 4.5 PXRD pattern of **$CaCl_2$**.

Figure SI 4.6 PXRD pattern of cocrystal**1**.

Figure SI 4.7PXRD patterns of cocrystal**1**, **BiPyEt** and **IPBC**.

Figure SI 4.8 Superimposed PXRD pattern of cocrystal**1** and simulated from single crystal.

Figure SI 4.9 PXRD pattern of cocrystal**2**.

Figure SI 4.10PXRD patterns of cocrystal**1**, **BiPy**and **IPBC**.

Figure SI 4.11 Superimposed PXRD patterns of cocrystal**2** and simulated from single crystal.

Figure SI 4.12PXRD pattern of cocrystal**3**.

Figure SI 4.13PXRD patterns of cocrystal**3**, **TBAI** and **IPBC**.

Figure SI 4.14 Superimposed PXRD patterns of cocrystal**3** and simulated from single crystal.

Figure SI 4.15 PXRD pattern of cocrystal**4**.

Figure SI 4.16PXRD patterns of cocrystal**4**, **$CaCl_2$** and **IPBC**.

SI 5. ^{1}H and ^{13}C Nuclear Magnetic Resonance (NMR).

Scheme SI 5.1 Hydrogen and **c**arbon atoms labeling in **IPBC**.

Figure SI 5.1^{1}H NMR spectrum in $CDCl_3$ of **IPBC**.

Figure SI 5.2^{1}H NMR spectrum in $CDCl_3$ of cocrystal**1**.

Figure SI 5.3 ^{1}H NMR spectrum in $CDCl_3$ of cocrystal**2**.

Figure SI 5.4 ^{1}H NMR spectrum in $CDCl_3$ of cocrystal**3**.

Figure SI 5.5 ^{13}C NMR spectrum in $CDCl_3$ of pure **IPBC**.

Figure SI 5.6 ^{13}C NMR spectrum in $CDCl_3$ of cocrystal**1** with different **BiPyEt**equivalents.

Figure SI 5.7 ^{13}C NMR spectrum in $CDCl_3$ of cocrystal**2** with different **BiPy** equivalents.

Figure SI 5.8 ^{13}C NMR spectrum in $CDCl_3$ of cocrystal**3** with different **TBAI** equivalents.

Figure SI 5.9 ^{13}C NMR spectrum in methanol-d_4 of **IPBC** and cocrystal**4**.

SI. 6. Solid-state NMR.

Figure SI 6.1NH region of the ^{15}N (40 MHz) CPMAS spectra of pure **IPBC** (a), **1** (b), **2**, (c), **3** (d),and **4** (e) recorded at 9 kHz.

SI. 7. Powder flow propertiesmeasurement.

Table SI 7.1 Values of angle of repose for cocrystal**4.**

Figure SI 7.1. Pictures of cones of **IPBC** (left) and cocrystal**4** (right) powders, taken after flowing the powders through the funnel from 25mm height.

Figure SI 7.2. Pictures of cones of **IPBC** (left) and cocrystal**4** (right) powders, taken after flowing the powders through the funnel from 50 mm height.

SI. 8. Crystal structure figures and check-cif.

Figure SI 8.1 Halogen bonded trimer present in cocrystal **1.**

Figure SI 8.2 Halogen bonded trimer present in cocrystal **2.**

Figure SI 8.3 Crystal packing of cocrystal **3.**

Check cif SI 8.4 Print screen of check cif for cocrystal **1.**

Check cif SI 8.5 Print screen of check cif for cocrystal **2.**

Check cif SI 8.6 Print screen of check cif for cocrystal **3.**

SI. 9. References

SI 1. Cambridge Structure Database Analysis.

All the five halogens can work as XB donor sites. Iodine is usually a better donor than bromine, chlorine, and fluorine as the heavier the halogens the more positive the σ-hole and the more asymmetric the distribution of the electron density. For a given halogen atom, its XB donor ability increases with the electron withdrawing ability of the moiety it is bound to and in organohalogen derivatives this ability increases moving from haloalkanes to haloalkenes to haloalkynes. We thus identified 1-iodoalkyne derivatives as ideal candidates to test the potential of XB in the formation of pharmaceutical cocrystals. A search in the Cambridge Structural Database (CSD) (see below criteria used for the CSD query) for supports our choice.

Most of the structures containing the 1-iodoalkyne group show short contacts with electron donors of pharmaceutical relevance (66 structures of 1-iodoalkenes are reported in the CSD and 56 of them show short contacts with oxygen and nitrogen atoms(neutral electron donor sites) or halogenated anions (charged electron donor sites). The median values of C-I···D (D is an electron donor atom) distances and angles (Figure SI 1.1) are 3.13 Å and 174.2°, respectively. These values are consistent with the presence of a remarkably positive σ-hole on the iodine atom and confirmthat 1-iodoalkynes are reliable XB donors. The asymmetric distribution of the electron density around the iodine atom,resulting in a negative belt orthogonal to the C-I bond, is confirmed by the angular distribution of short C-I···H HBs, the median value of the interaction being 88.2°.

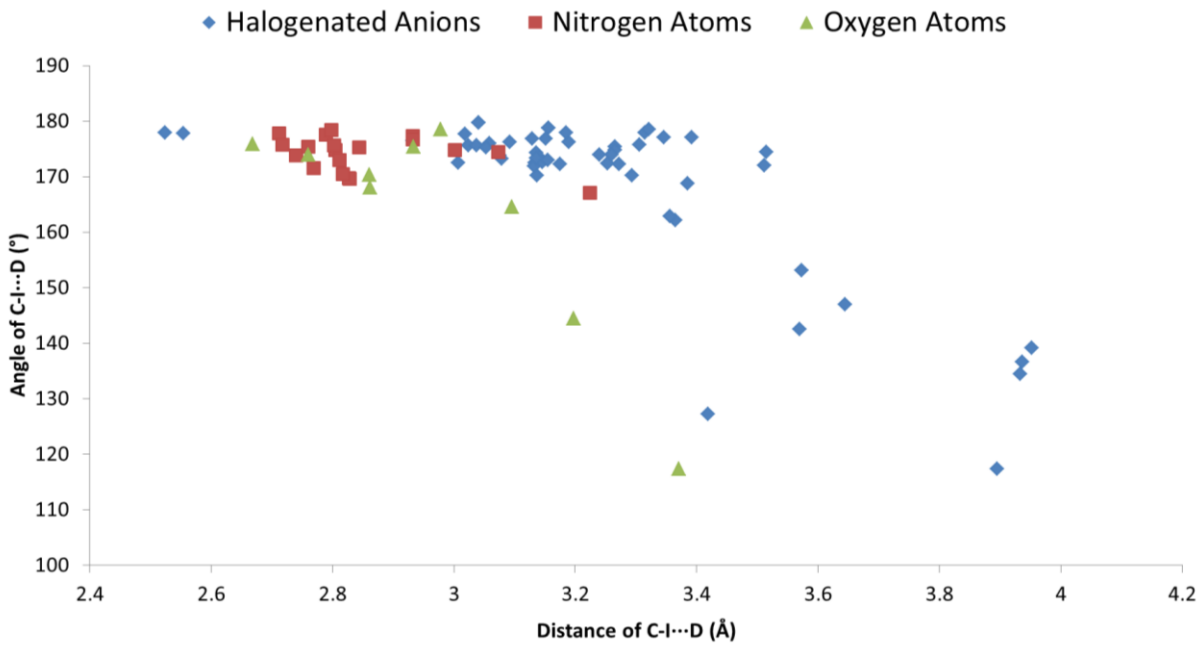

Figure SI 1.1. Scatterplot of short contacts given by 1-iodoalkynes with different electron donor sites. Blue rhombi: halogenated anions; Brown square: nitrogen atoms; Light green triangles : oxygen atoms. Angles are in deg (°). Distances are in Å.

An analysis of structures in CSD has been helpful also in identifying CCFs candidates. Black bars in Figure SI 1.2 represent all the "short intermolecular contacts" (as identified by ConQuest 1.14) between 1-iodoalkynyl moieties and three classes of electron density donors of pharmacological relevance. Gray bars represent those contacts that can be classified as XBs (if a C-I···D angle in between 140° and 180° is chosen as classification criterion). Nitrogen, oxygen atoms and halogenated anions give the smaller reductions in the contact number, if any, when applying the XB classification criterion. They are therefore the first choice when trying to elicit the XB donor potential of an 1-iodoalkynyl moiety. Moreover, an ideal XB acceptor must be: I) sterically accessible, II) not involved in self-aggregation processes and III) free from other competing XB donor or acceptor sites. We thus selected as CCFs two pyridyl derivatives (*i.d.***BiPyEt** and **BiPy**) and two halide anions (*i.e.***TBAI** and **$CaCl_2$**). Pyridine nitrogen typically works as monodentate XB

acceptors [1][i] while halide anions work as mono-, bi-, tri-, or tetradentate acceptors as a function of the structure of the XB donor and of the overall crystal packing requirements. [2][ii]

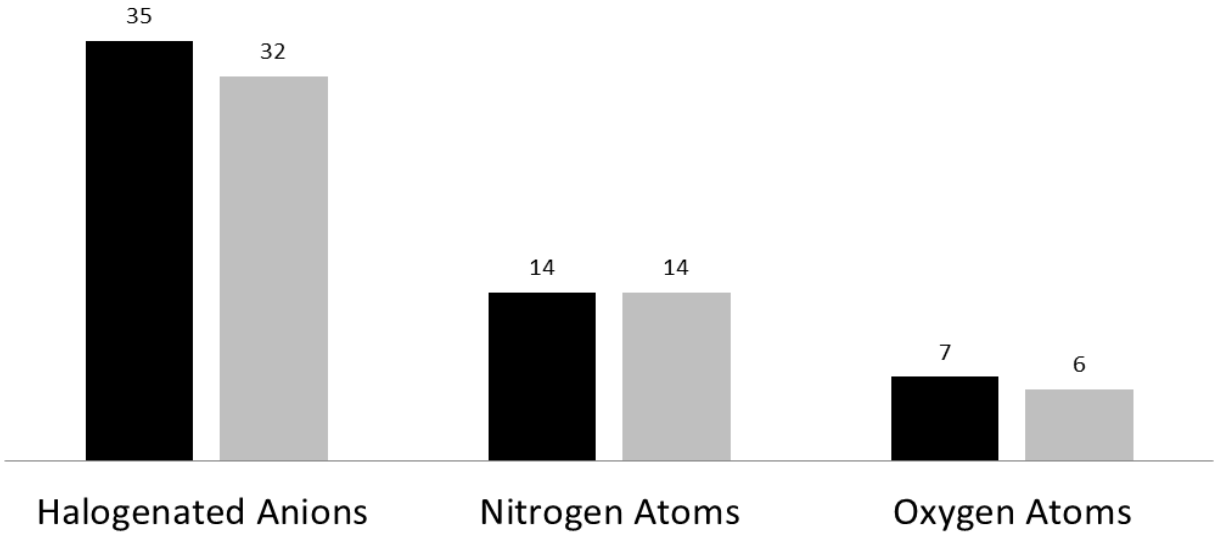

Figure SI 1.2. Total number of short intermolecular contacts (black bars) and XB contacts (gray bars) occurring in CSD between 1-iodoalkynes and selected XB acceptors.

Cambridge Structural Database (Version 5.33, 1 update Nov. 2011). Research performed using ConQuest (Version 1.14). Criteria used for the query: (I) iodine atom is bound to C≡C; (II) iodine atom interacts (via contact keyword) with halogenated anion, nitrogen atom and oxygen atoms; (III) the charge on iodine atom is set equal to zero; (IV) No filters were applied during the search.

Nc is 'normalized contact'. We define 'normalized contact', the ratio Nc = Dij/(rvdWi + rvdWj), whereDij is the distance between the atomsi and j and rvdWi and rvdWj are the van der Waals radii for atomsiand j, respectively. If the electron donor j is an anionic atom, rvdWj is substituted by rPj , the Pauling ionic radius of anion atom j. van der Waals radii and Pauling ionic radii were obtained from web of element (http://www.webelements.com/).

Pauling ionic: F-: 1.36 Å; Cl-: 1.81 Å; Br-: 1.95 Å; I-: 2.16 Å.

Van der Waals radii. I: 1.98 Å; N: 1.55 Å; O: 1.52 Å.

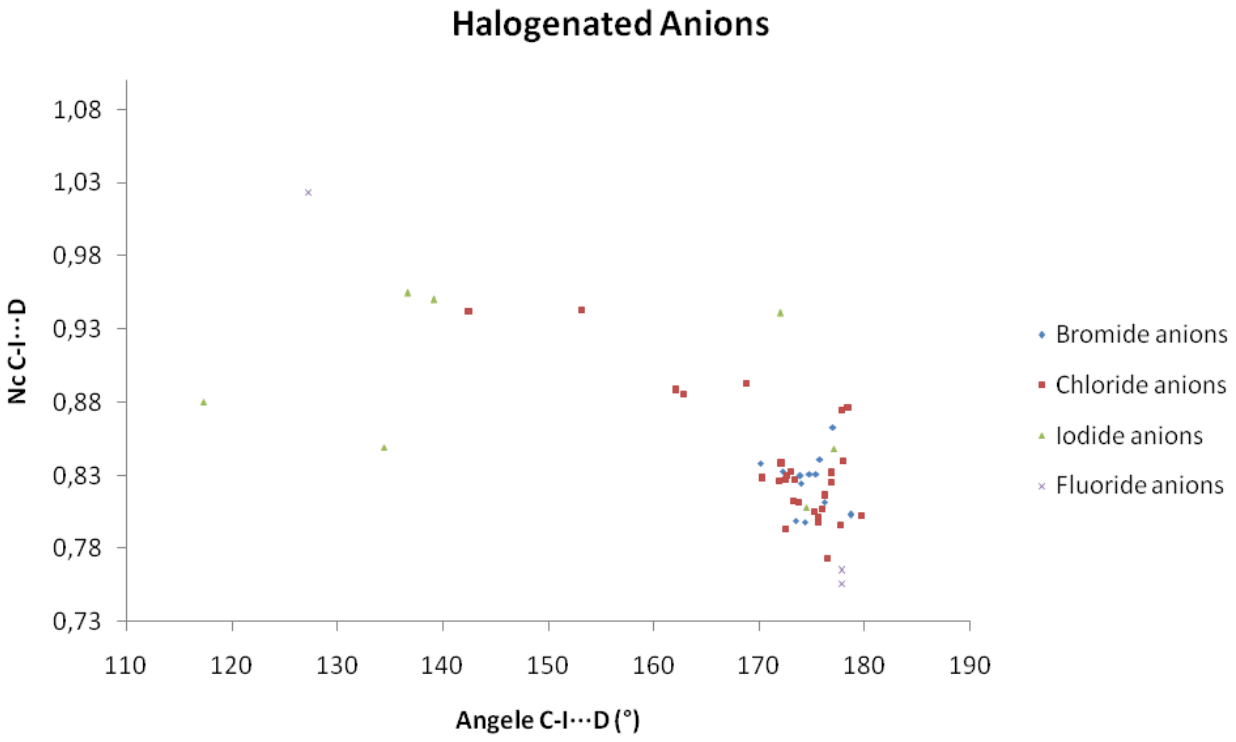

Figure SI 1.3. Scatterplot of short contacts given by 1-iodoalkynes with halogenated anions as electron donor sites (C-I···D). Angles are in deg (°). Normalized contact (Nc).

The median values of C-I···D (D is halogenated anions) distances and angles are 3.18 Å and 174°, respectively. Number of entry for Fluoride anions: 2; Chloride anions: 20; Bromide anions: 10; Iodide anions: 3.

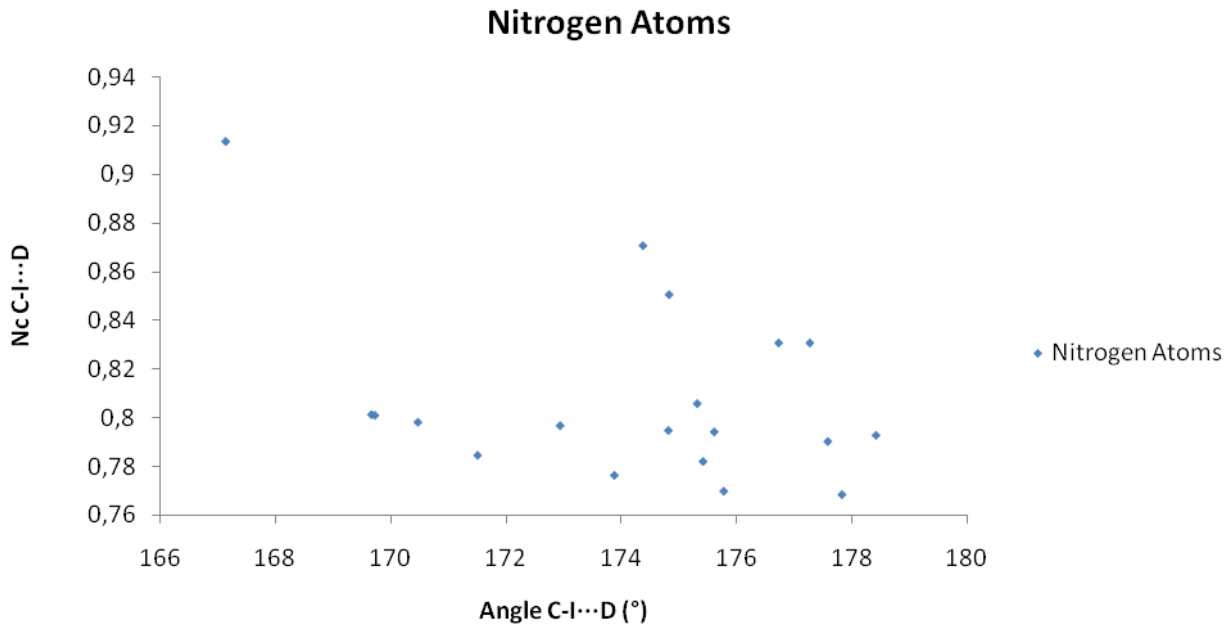

Figure SI 1.4. Scatterplot of short contacts given by 1-iodoalkynes with nitrogen atoms as electron donor sites (C-I···D). Angles are in deg (°). Normalized contact (Nc).

The median values of C-I···D (D is nitrogen atoms) distances and angles are 2.81 Å and 174.8°, respectively.

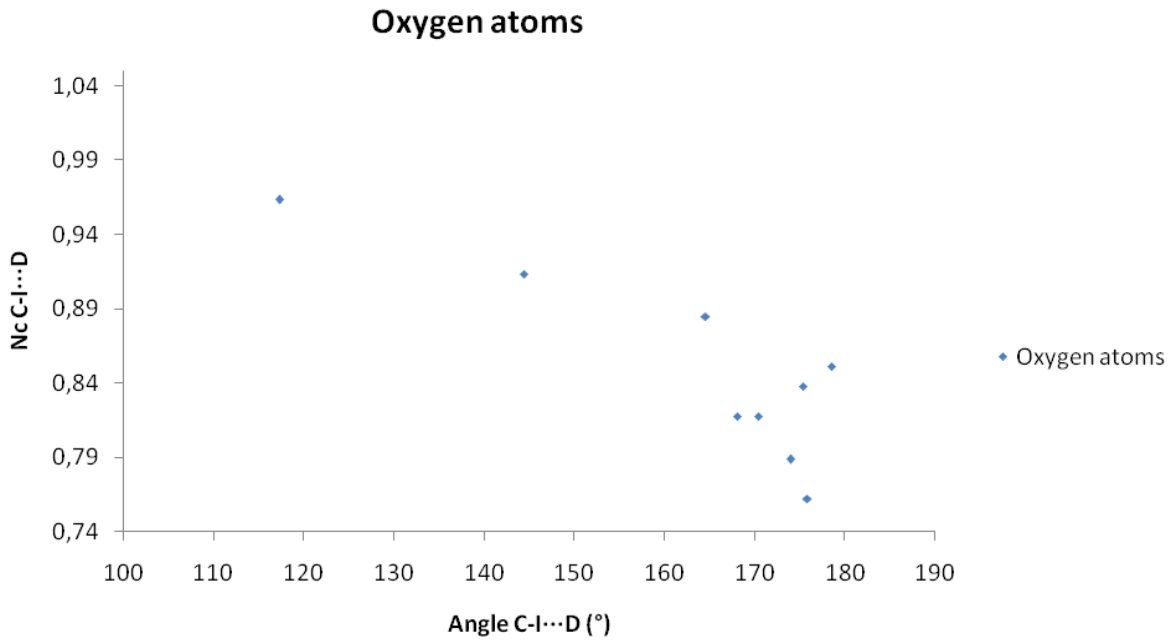

Figure SI 1.5. Scatterplot of short contacts given by 1-iodoalkynes with oxygen atoms as electron donor sites (C-I···D). Angles are in deg (°). Normalized contact (Nc).

The median values of C-I···D (D is oxygen atoms) distances and angles are 2.93 Å and 170.4°, respectively.

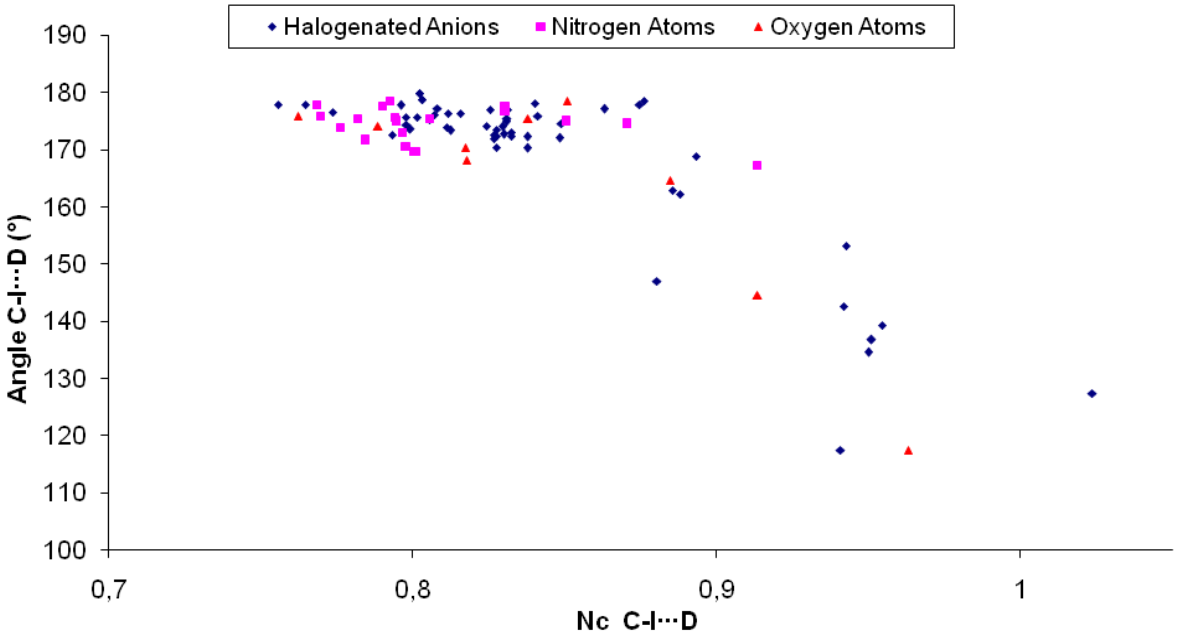

Figure SI 1.6. Scatterplot of short contacts given by 1-iodoalkynes with different electron donor sites. Blue rhombi: halogenated anions; Pink square: nitrogen atoms; Red triangles: oxygen atoms. Angles are in deg (°). Normalized contact (Nc).

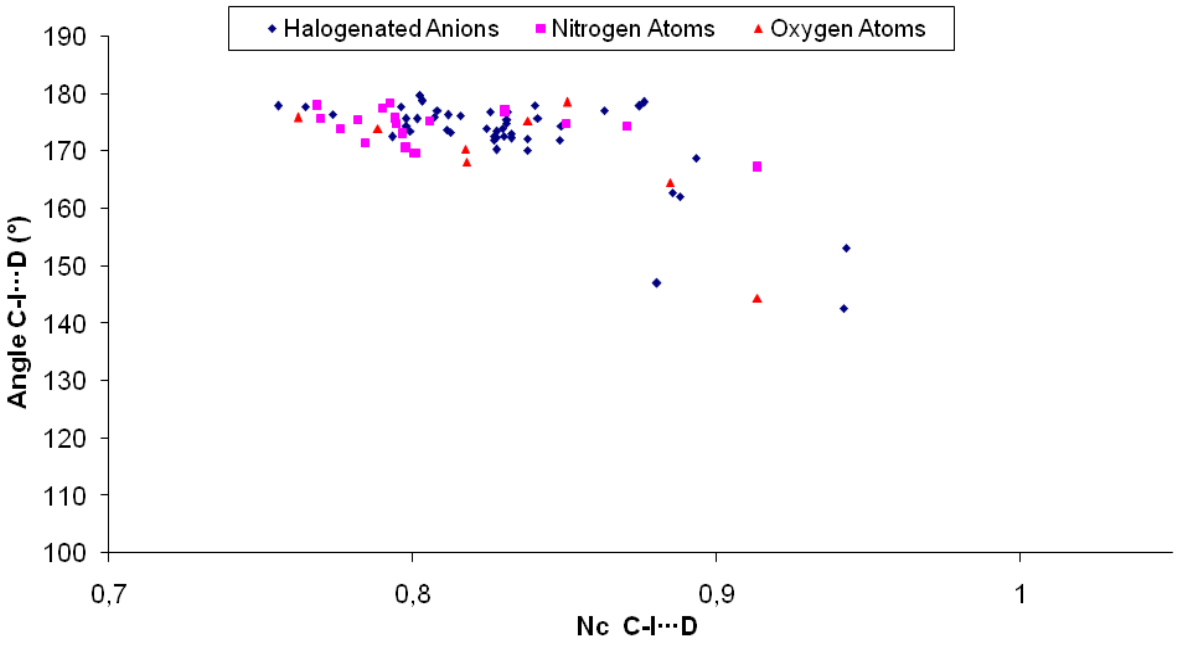

Figure SI 1.7. Scatterplot of short contacts given by 1-iodoalkynes with different electron donor sites when XB classification criterion is applied (C-I···D angle in between 140° and 180°). Blue rhombi: halogenated anions; Pink square: nitrogen atoms; Red triangles: oxygen atoms. Angles are in deg (°). Normalized contact (Nc).

The median values of C-I···D (D is an electron donor atom) distances and angles (using XB classification criterion) are 3.08 Å and 172.7°, respectively.

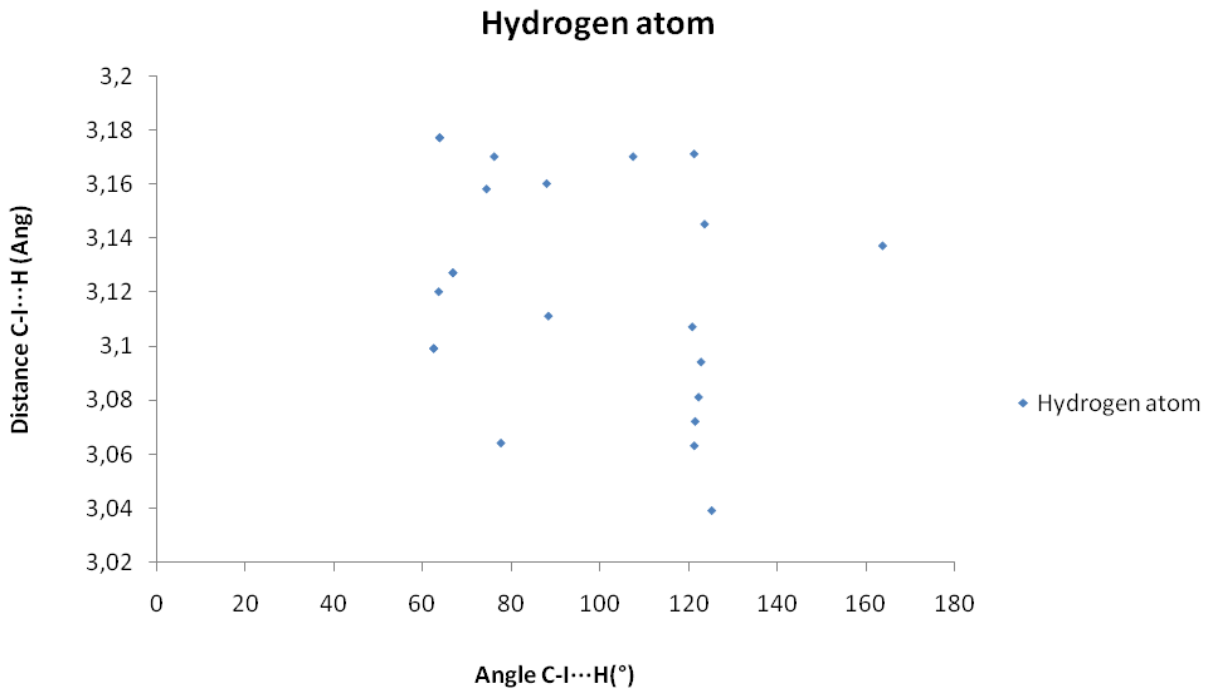

Figure SI 1.8. Scatterplot of short contacts given by 1-iodoalkynes with hydrogen atoms as electron acceptor sites (C-I···H). Angles are in deg (°). Distances I···H are in Å.

The median values of C-I···H distances and angles are 3.12 Å and 88.2°, respectively.

SI 2. Infrared Spectroscopy (FT-IR). The IR characterization of samples was performed on a Nicolet Nexus FTIR spectrometer equipped with Smart Endurance ATR-device. Spectra were measured over the range of 4000-550 cm^{-1} and analyzed using Omnic software v6.2. Peak values are given in wavenumbers and rounded to 1 cm^{-1} upon automatic assignment. The peak intensity is described as: strong (s); medium (m), weak (w) and broad (b).

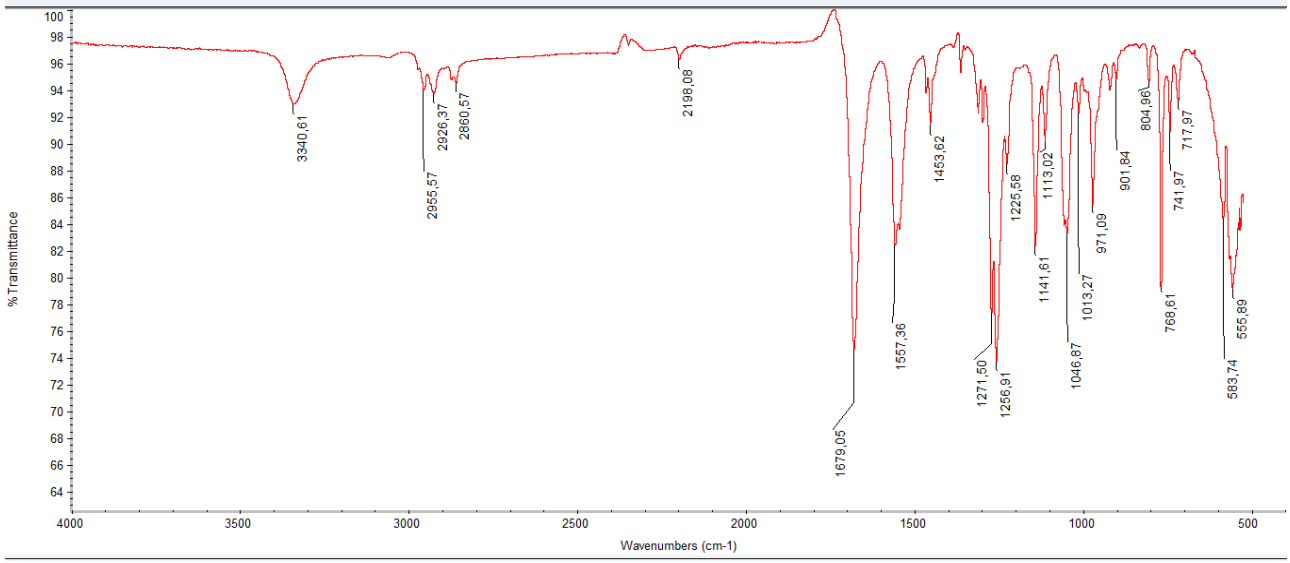

Figure SI 2.1. (ATR)-IR spectrum of crystalline**IPBC**.

(ATR)-FTIR ν: 3314 (w), 2955 (w), 2926 (w), 2860 (w), 2198 (w), 1679 (s), 1557 (m), 1454 (m), 1271 (s), 1257 (s), 1226 (m), 1141 (m), 1113 (w), 1047 (m), 1013 (m), 971 (w), 901 (w), 804 (s), 769 (s), 584 (s) cm^{-1}.

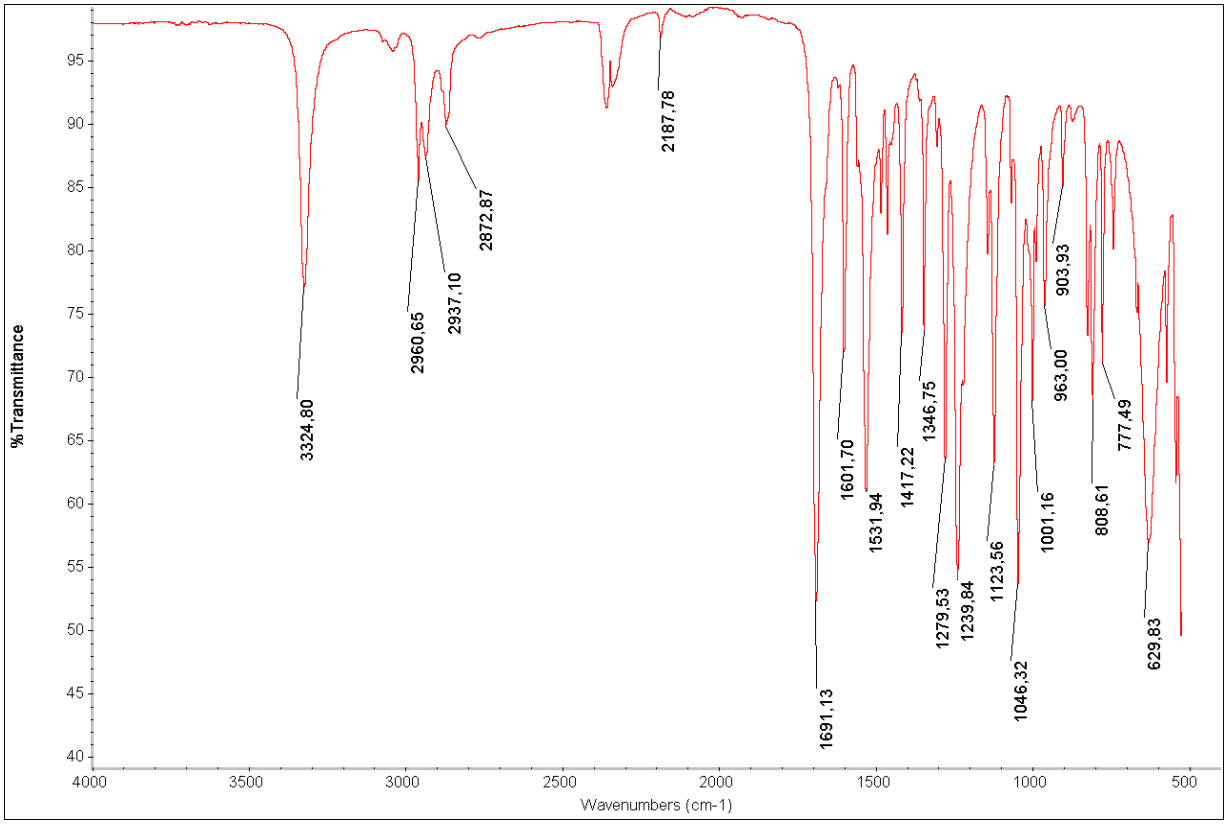
%Transmittance
Wavenumbers (cm-1)
3324,80
2960,65
2937,10
2872,87
2187,78
1691,13
1601,70
1531,94
1417,22
1346,75
1279,53
1239,84
1123,56
1046,32
1001,16
963,00
903,93
808,61
777,49
629,83

Figure SI 2.2. (ATR)-IR spectrum of cocrystal**1**.

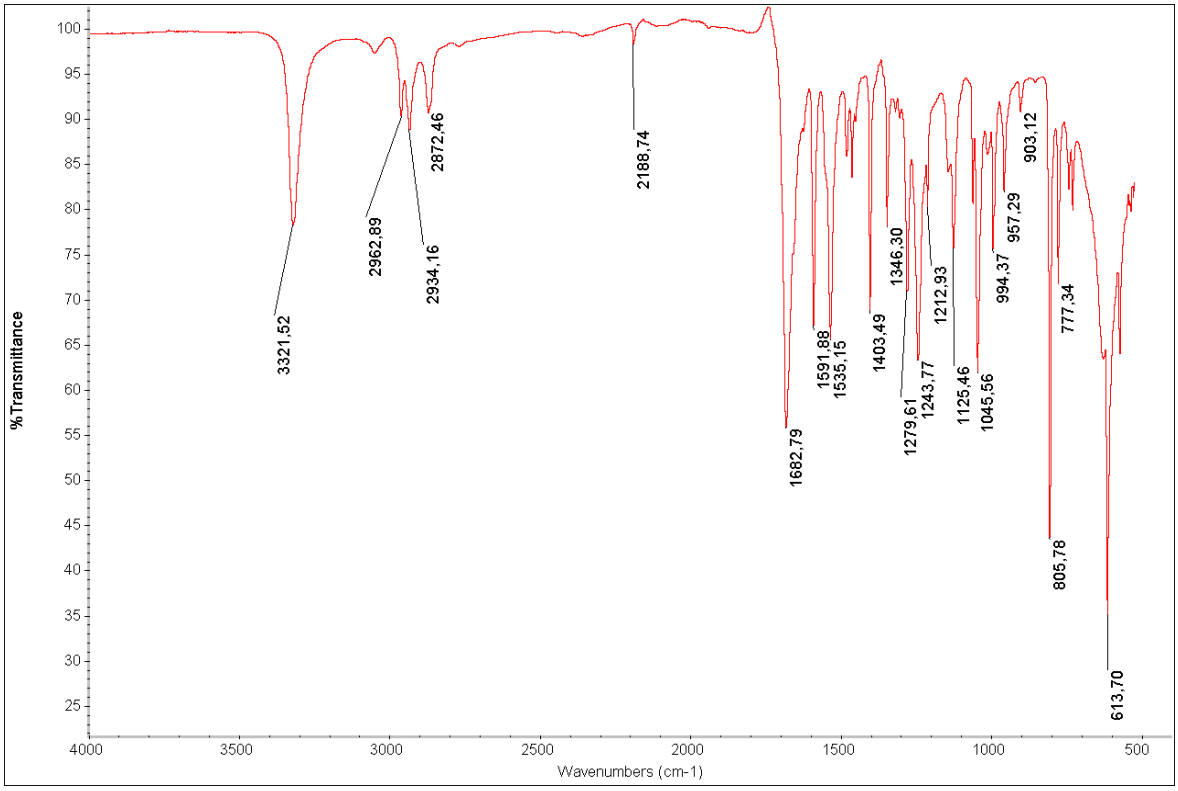

Figure SI 2.3. (ATR)-IR spectrum of cocrystal**2.**

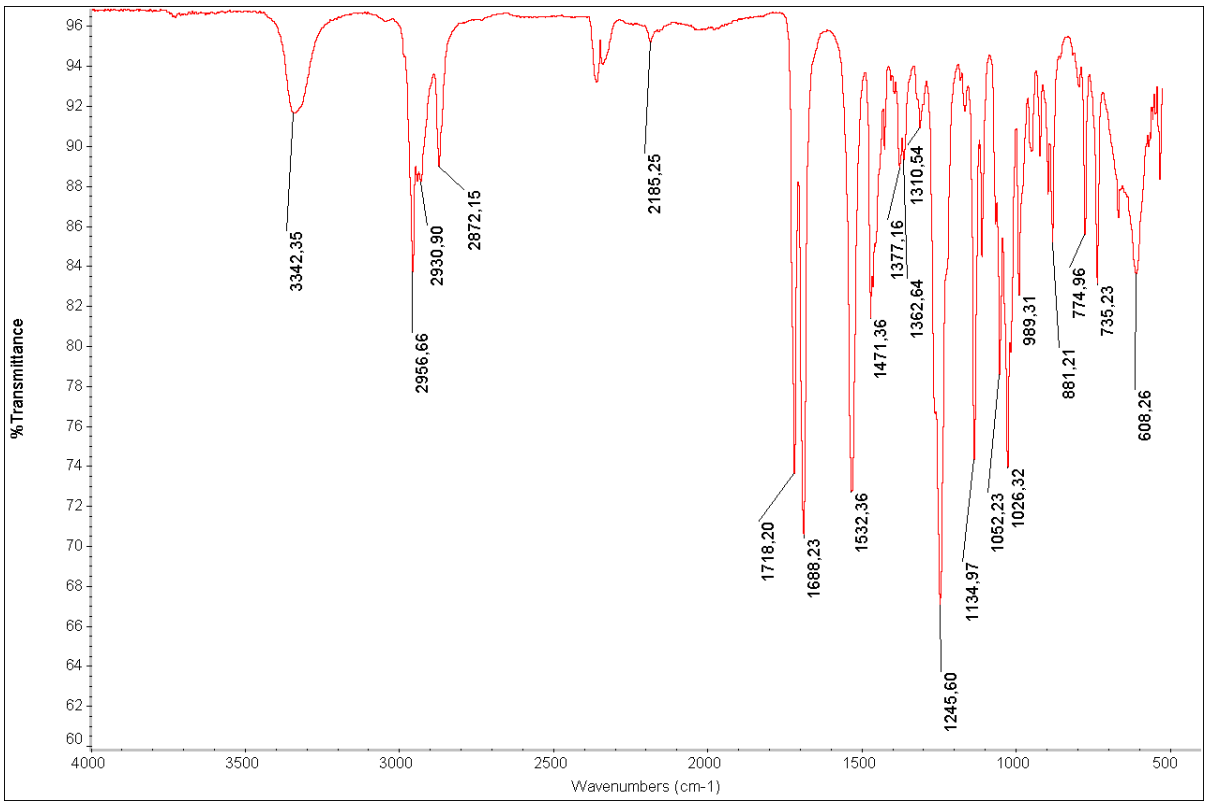

Figure SI 2.4. (ATR)-IR spectrum of cocrystal**3.**

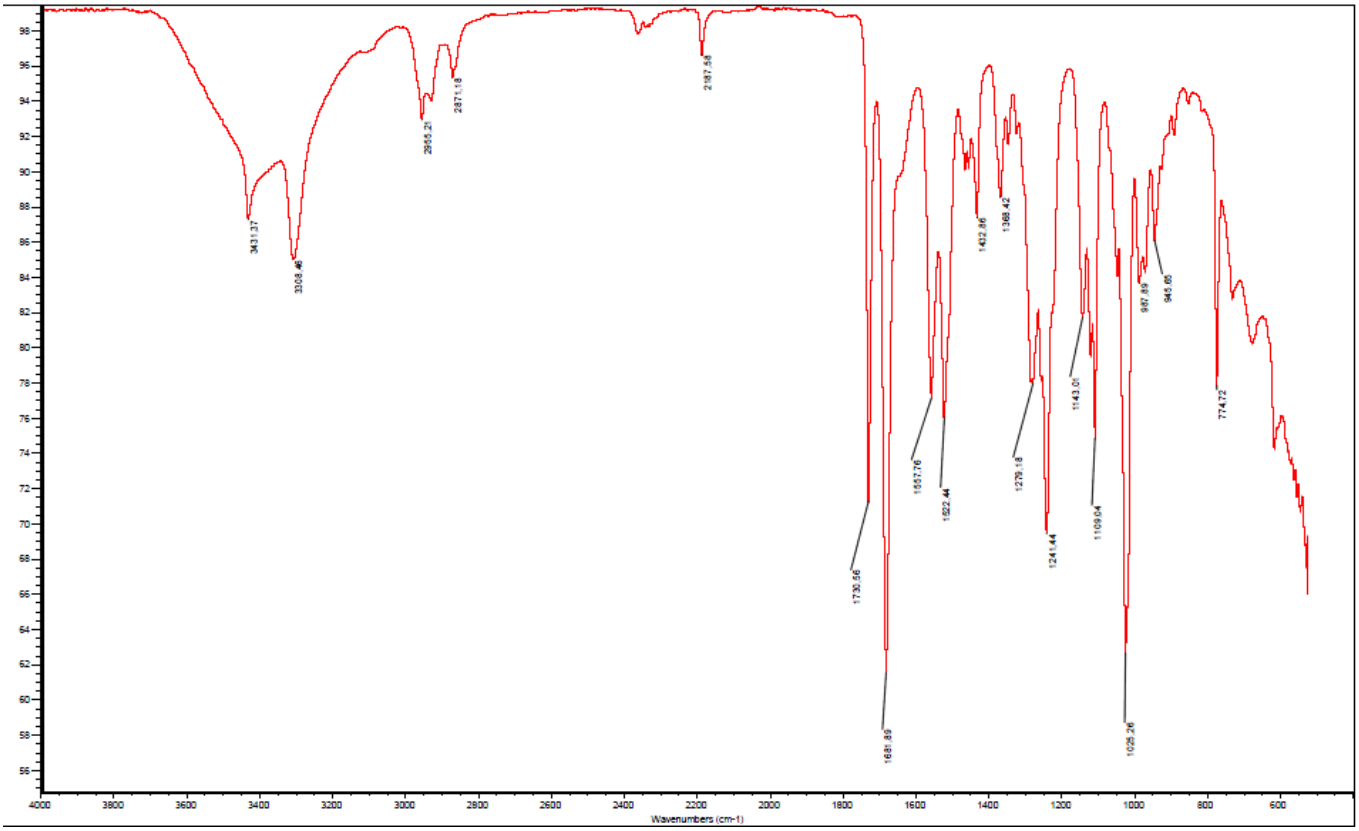

Figure SI 2.5. (ATR)-IR spectrum of cocrystal**4.**

SI 3. Differential Scanning Calorimetry (DSC). Thermal analysiswas performed on a Mettler Toledo DSC 823e differentialscanning calorimeter. Aluminum pans were used for all samples,and the instrument was calibrated using an indium standard. Forreference, an empty pan sealed in the same way as the sample wasused. The samples were heated inthe DSC cell from 25°C to the required temperature (meltingpoint of the cocrystal) at a rate of 10 °C/min.

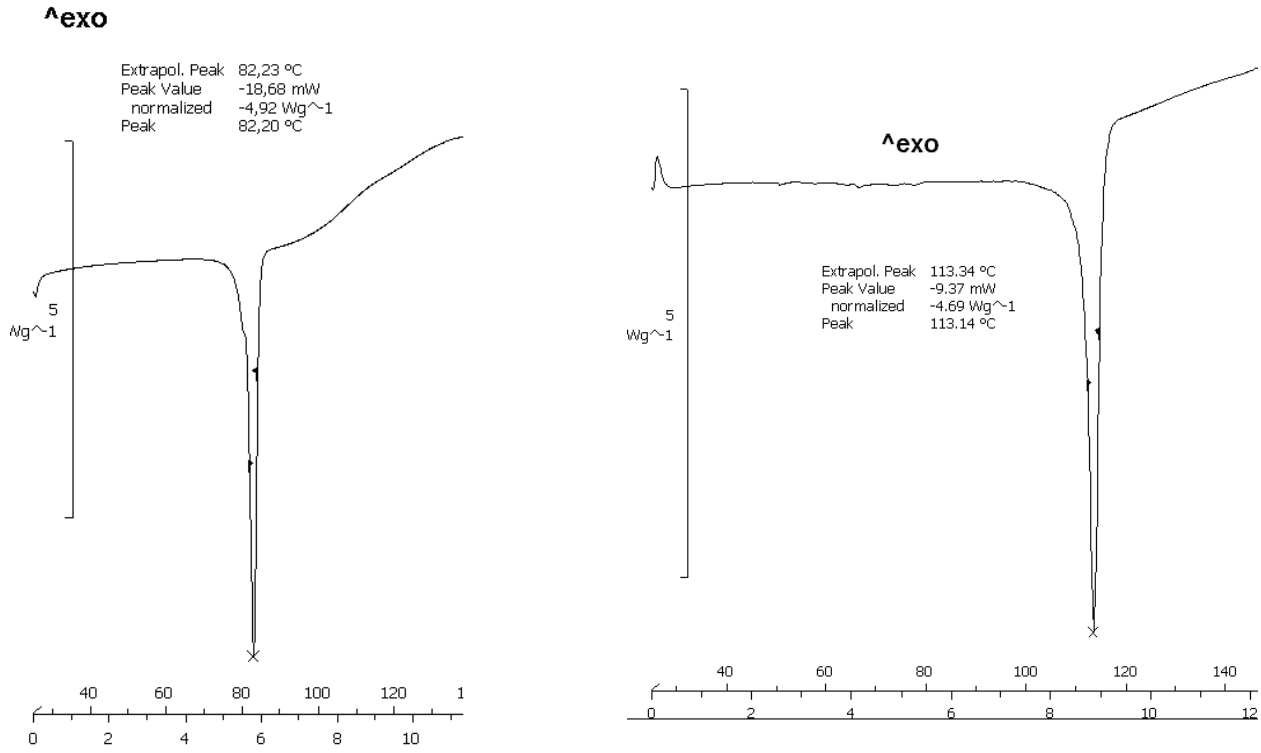

Figure SI 3.1. Left: DSC thermogram of cocrystal**1**. Right: DSC thermogram of cocrystal**2**.

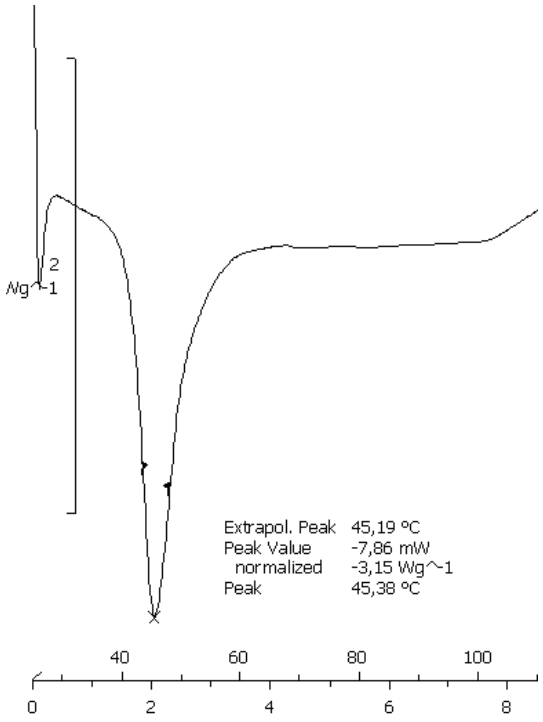
Wg^-1
2
1
Extrapol. Peak 45,19 °C
Peak Value -7,86 mW
normalized -3,15 Wg^-1
Peak 45,38 °C
40
60
80
100
0
2
4
6
8

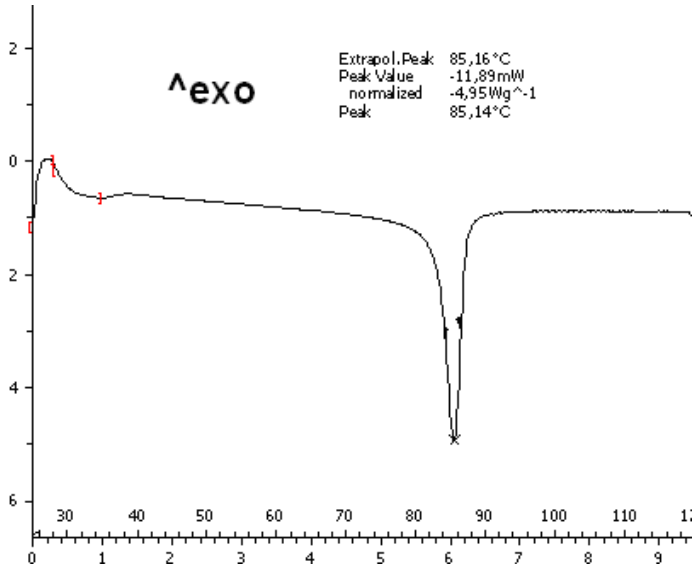
^exo
Extrapol.Peak 85,16 °C
Peak Value -11,89 mW
normalized -4,95 Wg^-1
Peak 85,14 °C
2
0
2
4
6
30
40
50
60
70
80
90
100
110
0
1
2
3
4
5
6
7
8
9

Figure SI 3.2. Left: DSC thermogram of cocrystal**3**. Right: DSC thermogram of cocrystal**4**.

SI 4. Powder X-ray Diffraction (PXRD). A Bruker AXS D8 powder diffractometer was used for all PXRD measurements with experimental parameters as follows: Cu-Kα radiation (λ= 1.54056Å). Scanning interval: 5-40°2θ. Step size 0.016°, exposure time 1.5 s per step. The experimental PXRD patterns and calculated PXRD patterns from single crystal structures were compared to confirm the composition of bulk materials.

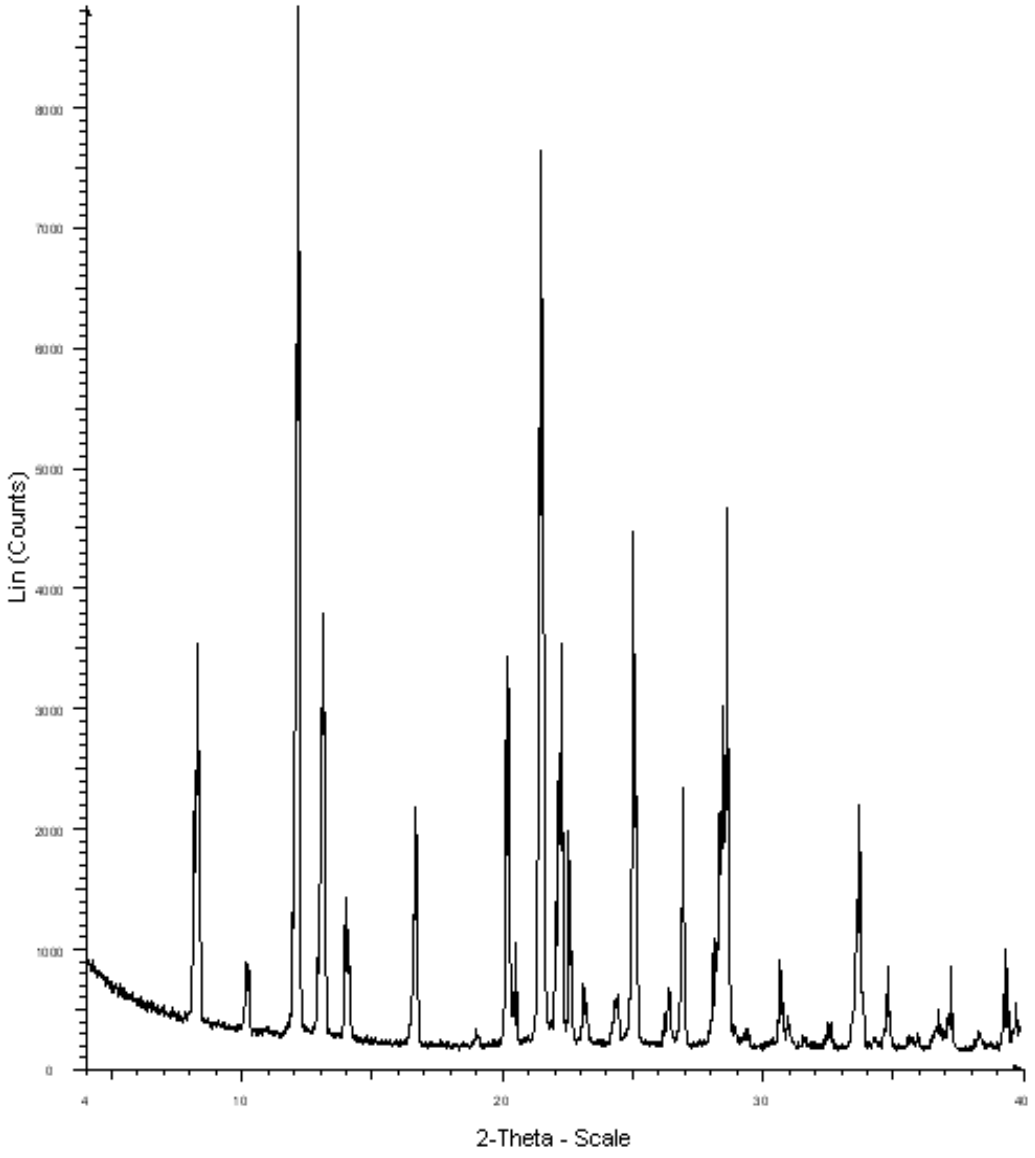

Figure SI 4.1. Experimental PXRDpattern of **IPBC**.

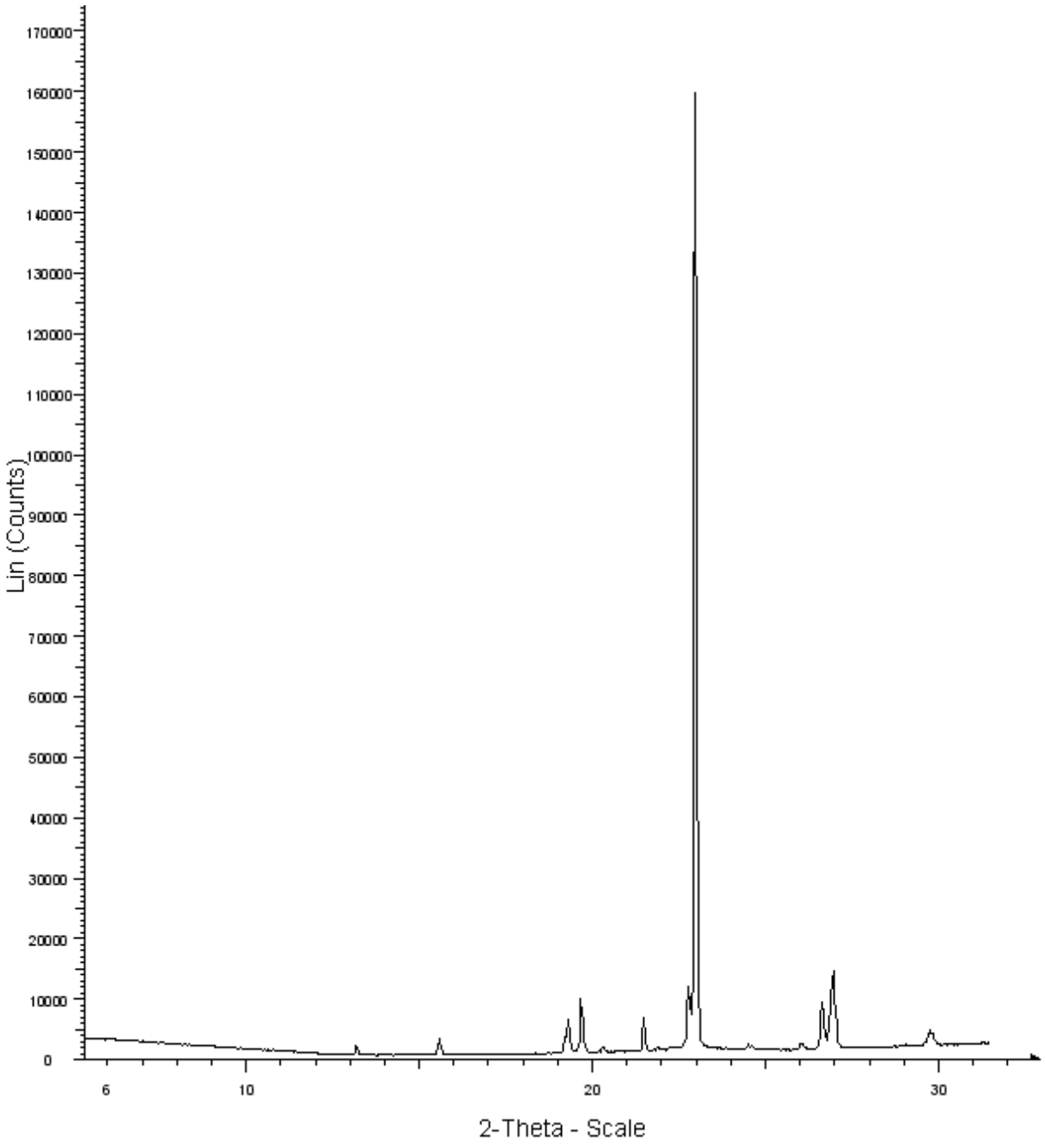

Figure SI 4.2. Experimental PXRD pattern of **BiPyEt**.

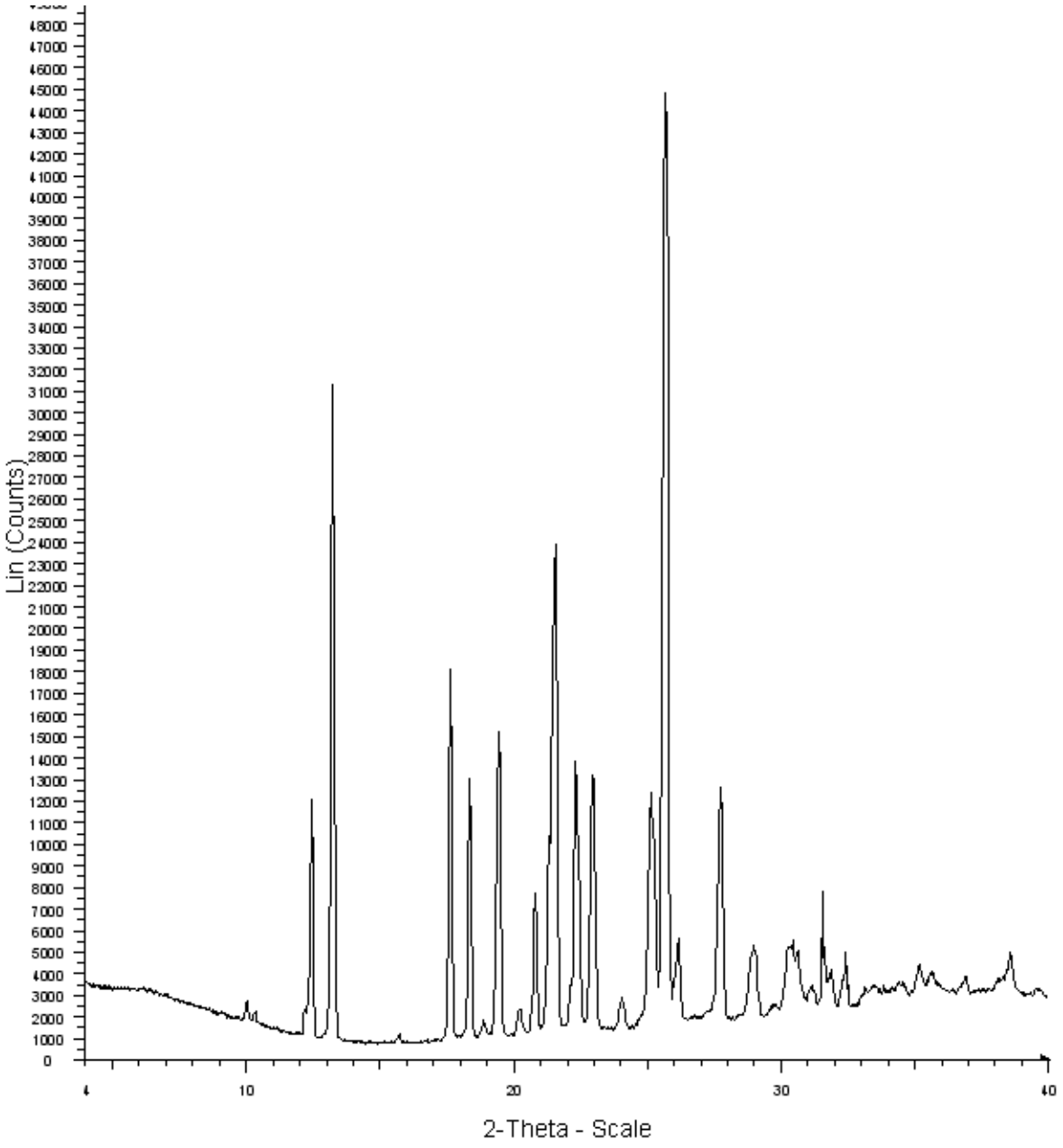

Figure SI 4.3. Experimental PXRD pattern of **BiPy**.

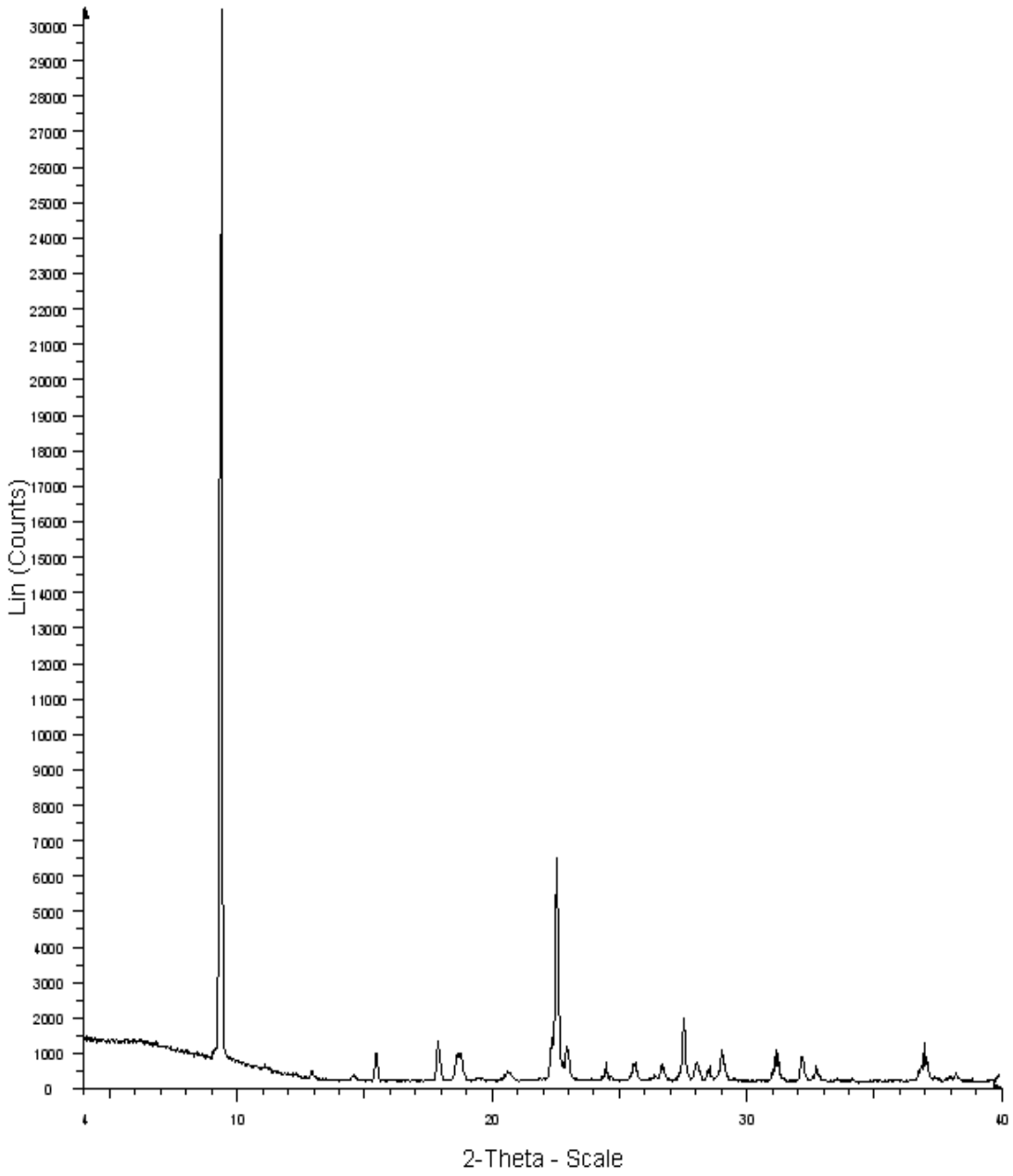

Figure SI 4.4. ExperimentalPXRD pattern of **TBAI**.

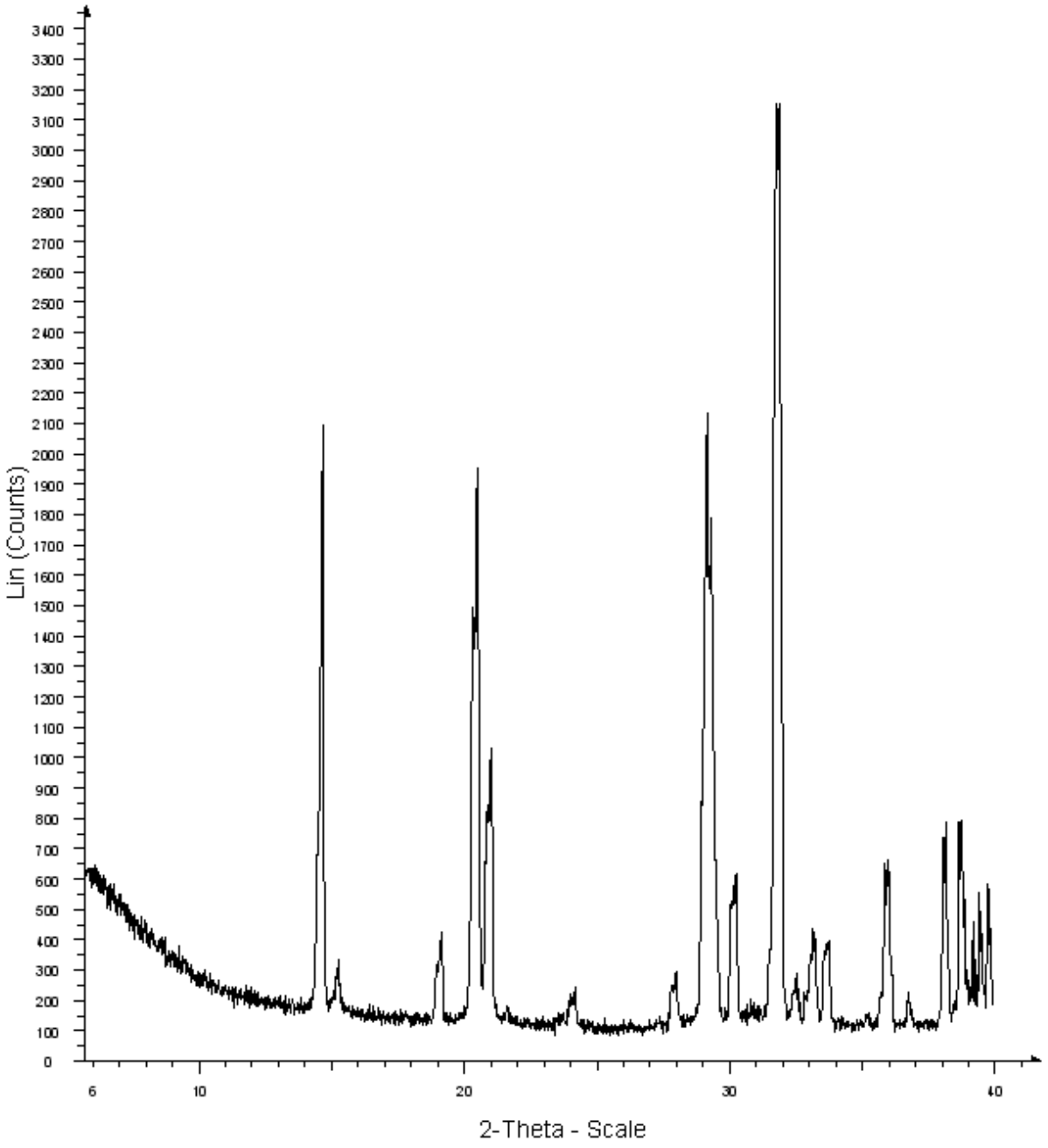

Figure SI 4.5. Experimental PXRD pattern of **$CaCl_2$**.

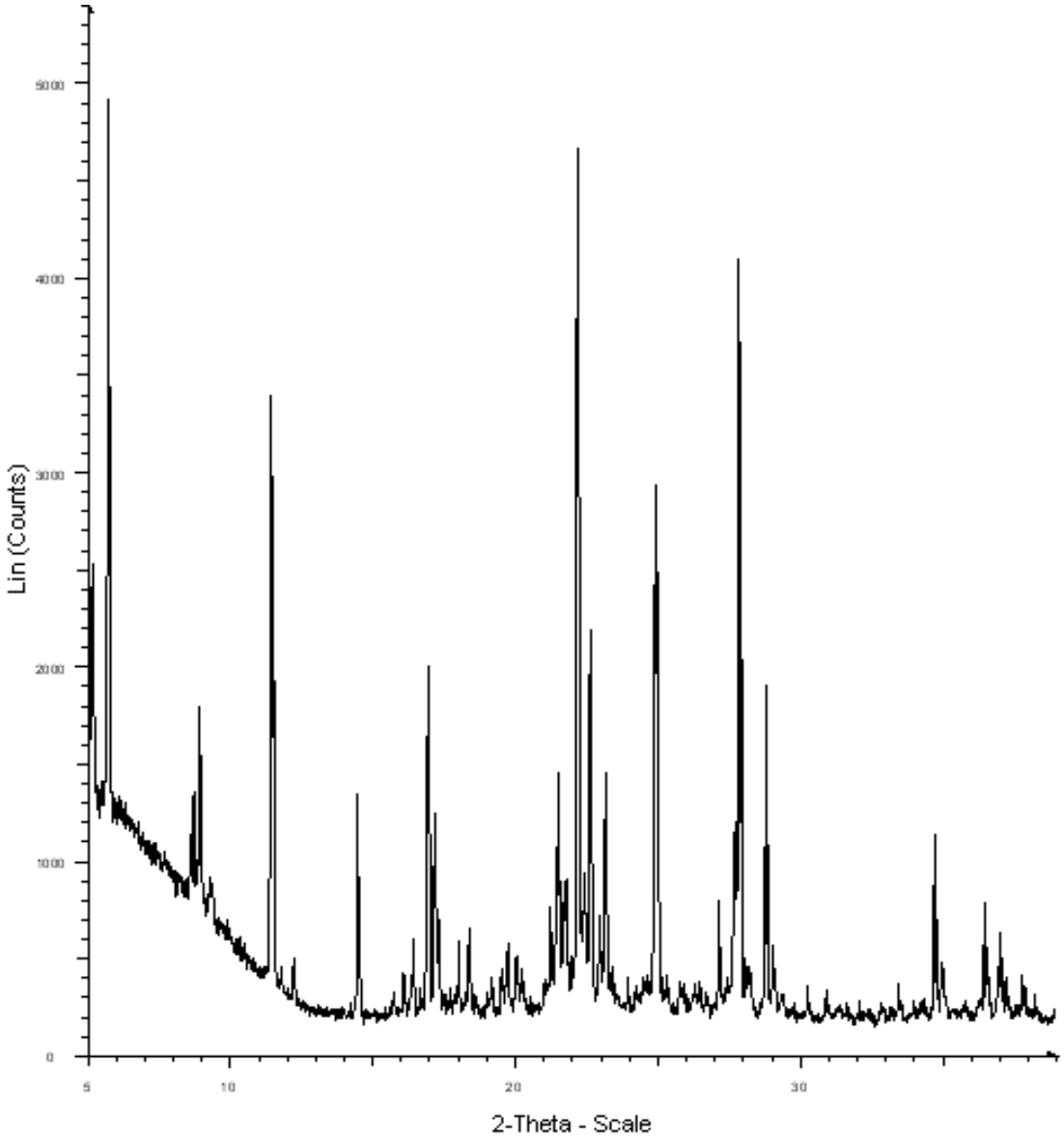

Figure SI 4.6. Experimental PXRD pattern of cocrystal**1**.

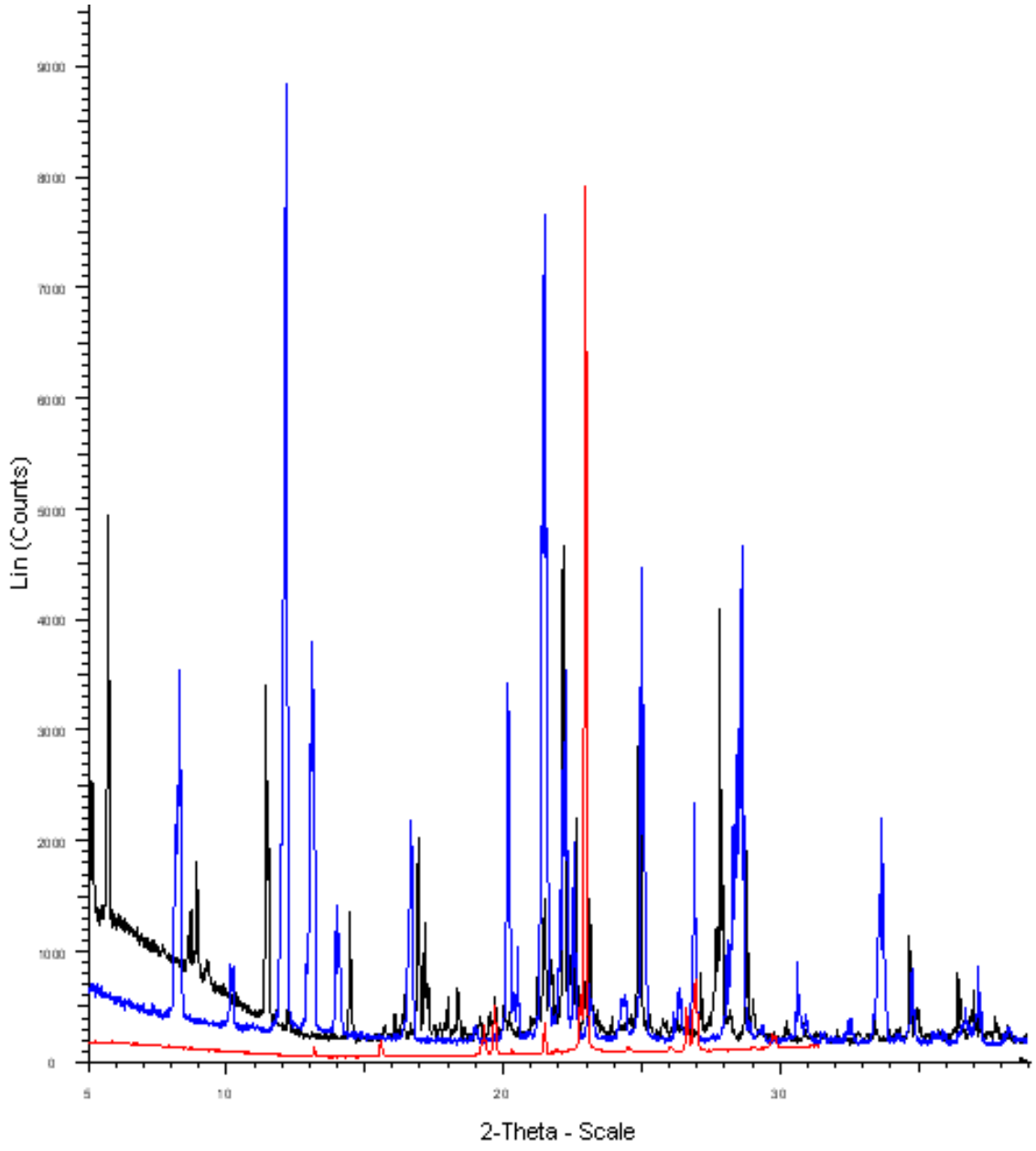

Figure SI 4.7. Experimental PXRD patterns of cocrystal**1** (black line), **BiPyEt** (red line) and **IPBC** (blue line).

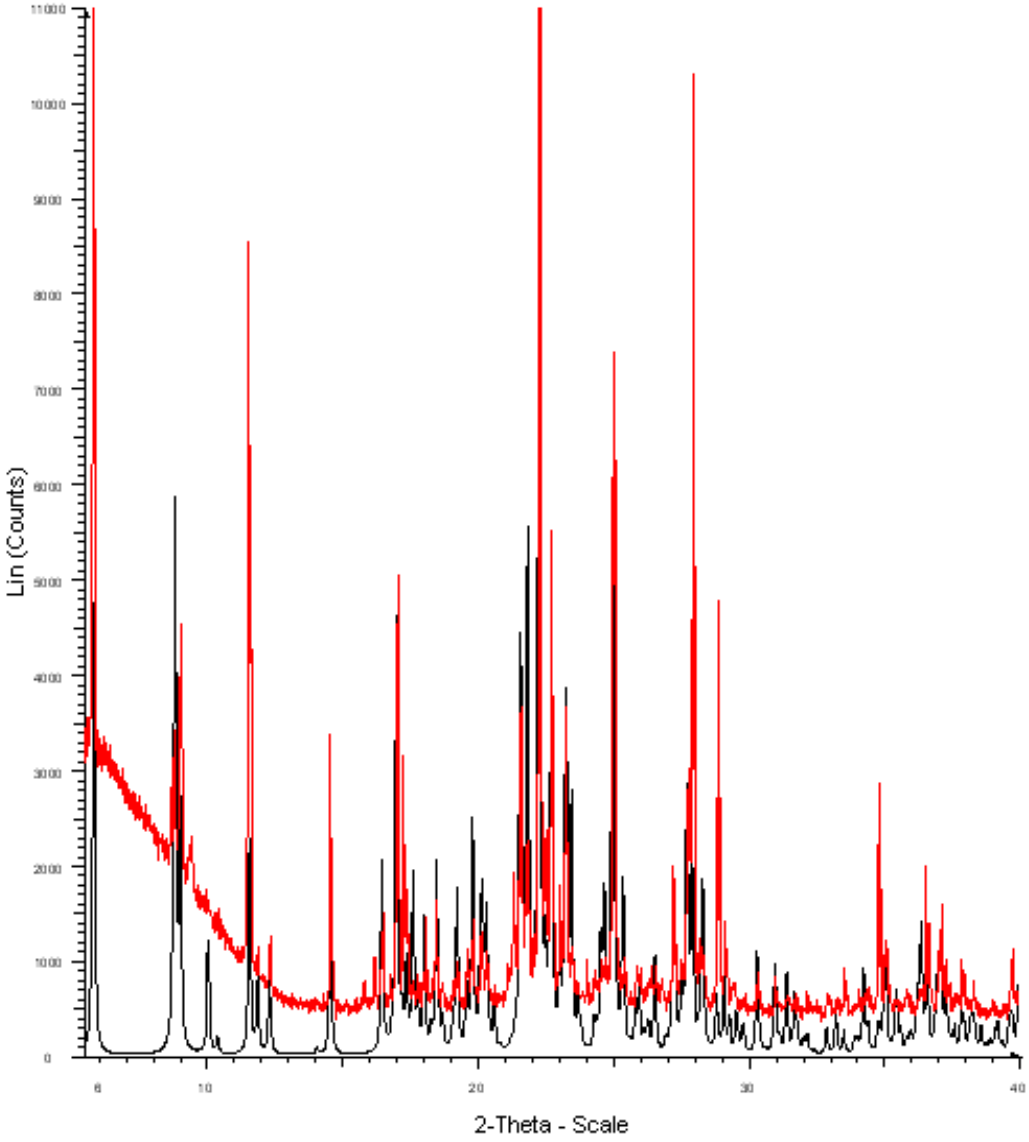

Figure SI 4.8. Superimposed PXRD patterns of cocrystal**1:** Experimental (red line) and simulated from single crystal (black line).

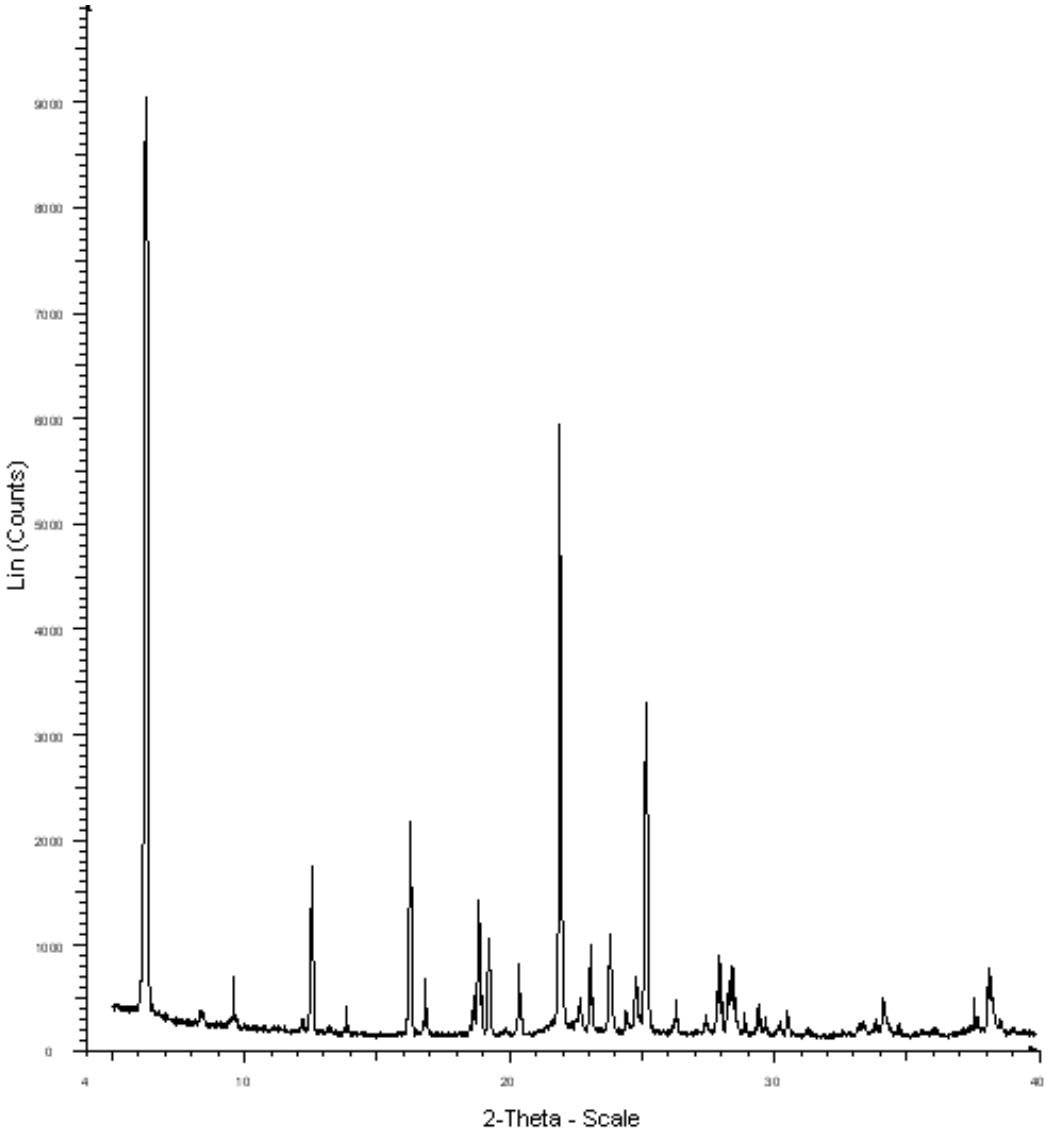

Figure SI 4.9. Experimental PXRD pattern of cocrystal**2**.

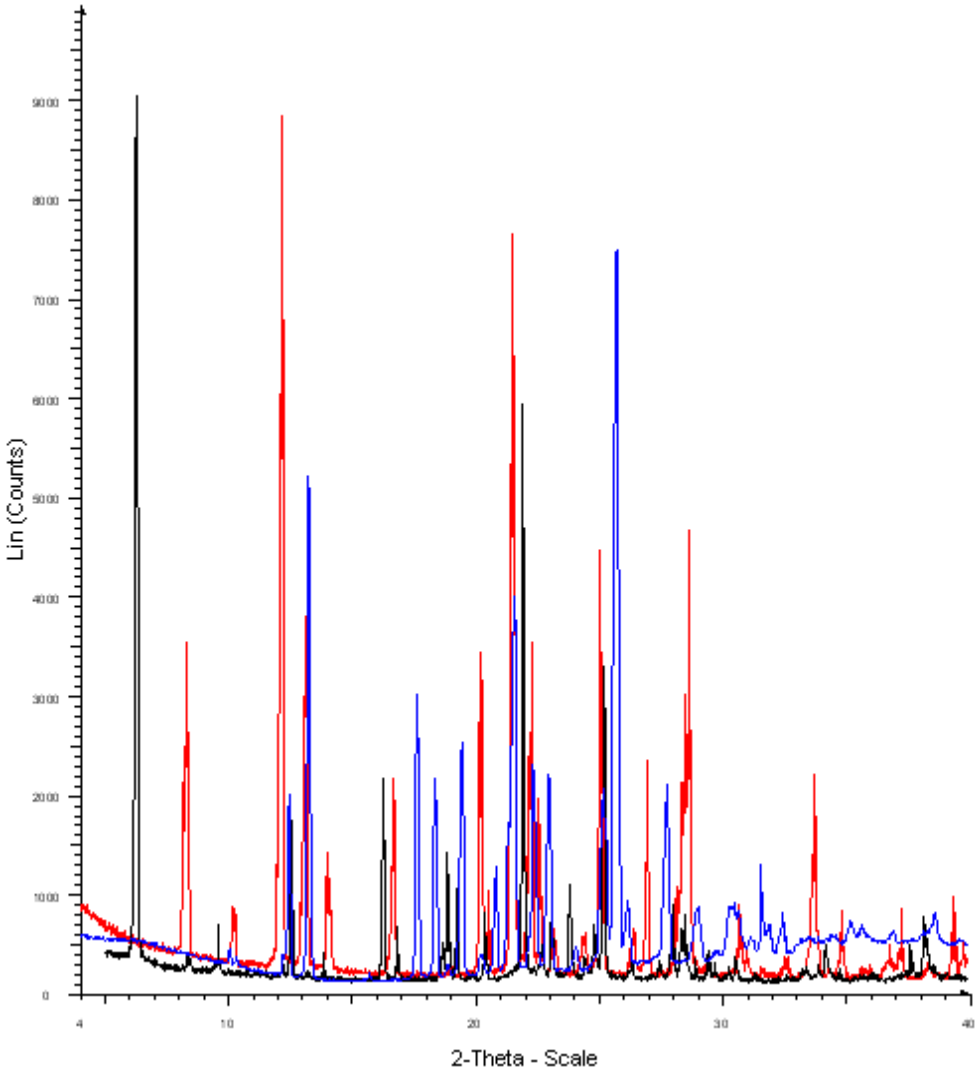

Figure SI 4.10. Experimental PXRD patterns of cocrystal**1** (black line), **DIPY** (blue line) and **IPBC** (red line).

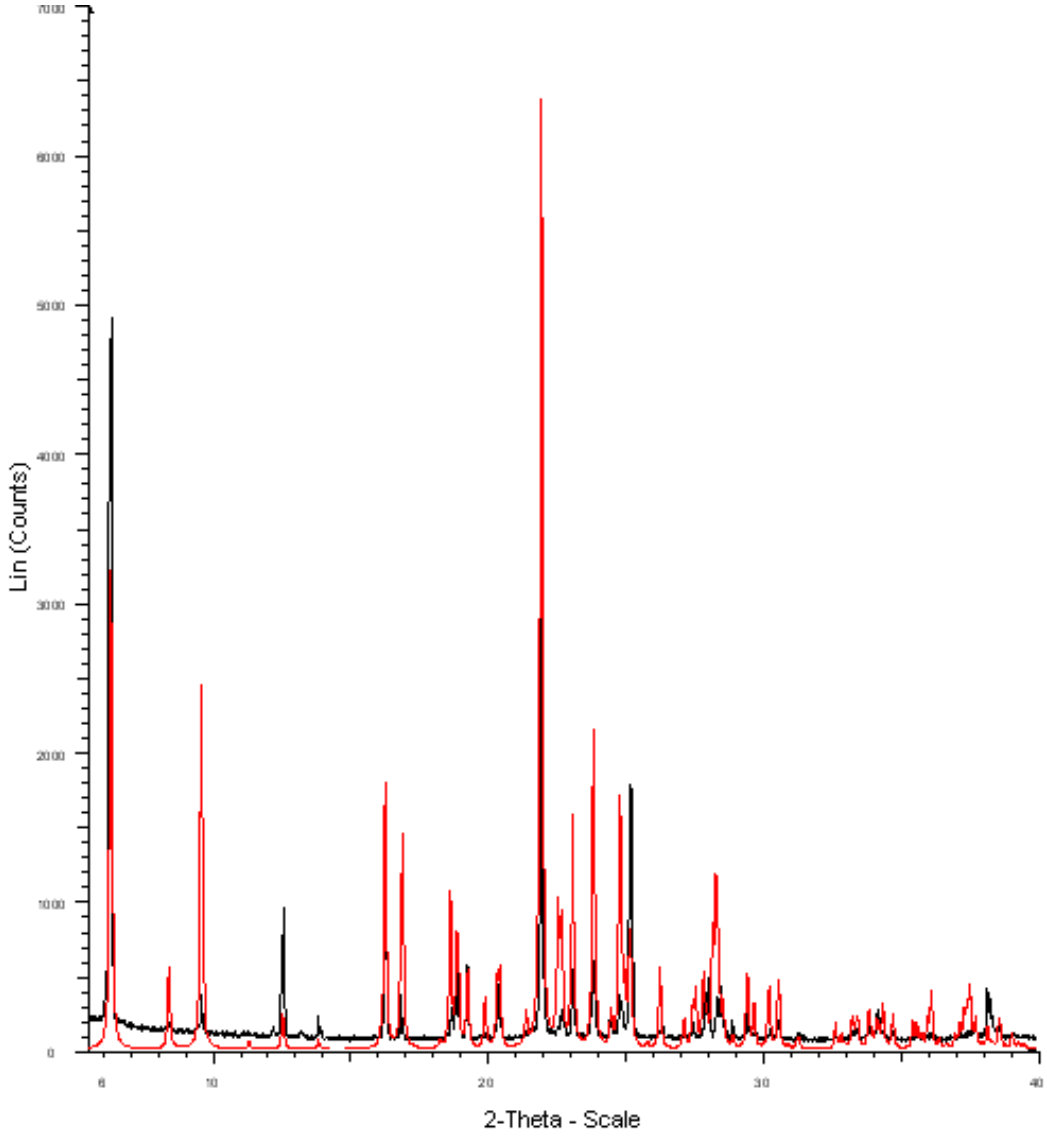
Lin (Counts)
7000
6000
5000
4000
3000
2000
1000
0
6
10
20
30
40
2-Theta - Scale

Figure SI 4.11. Superimposed PXRD patterns of cocrystal**2**: Experimental (black line) and simulated from single crystal (red line).

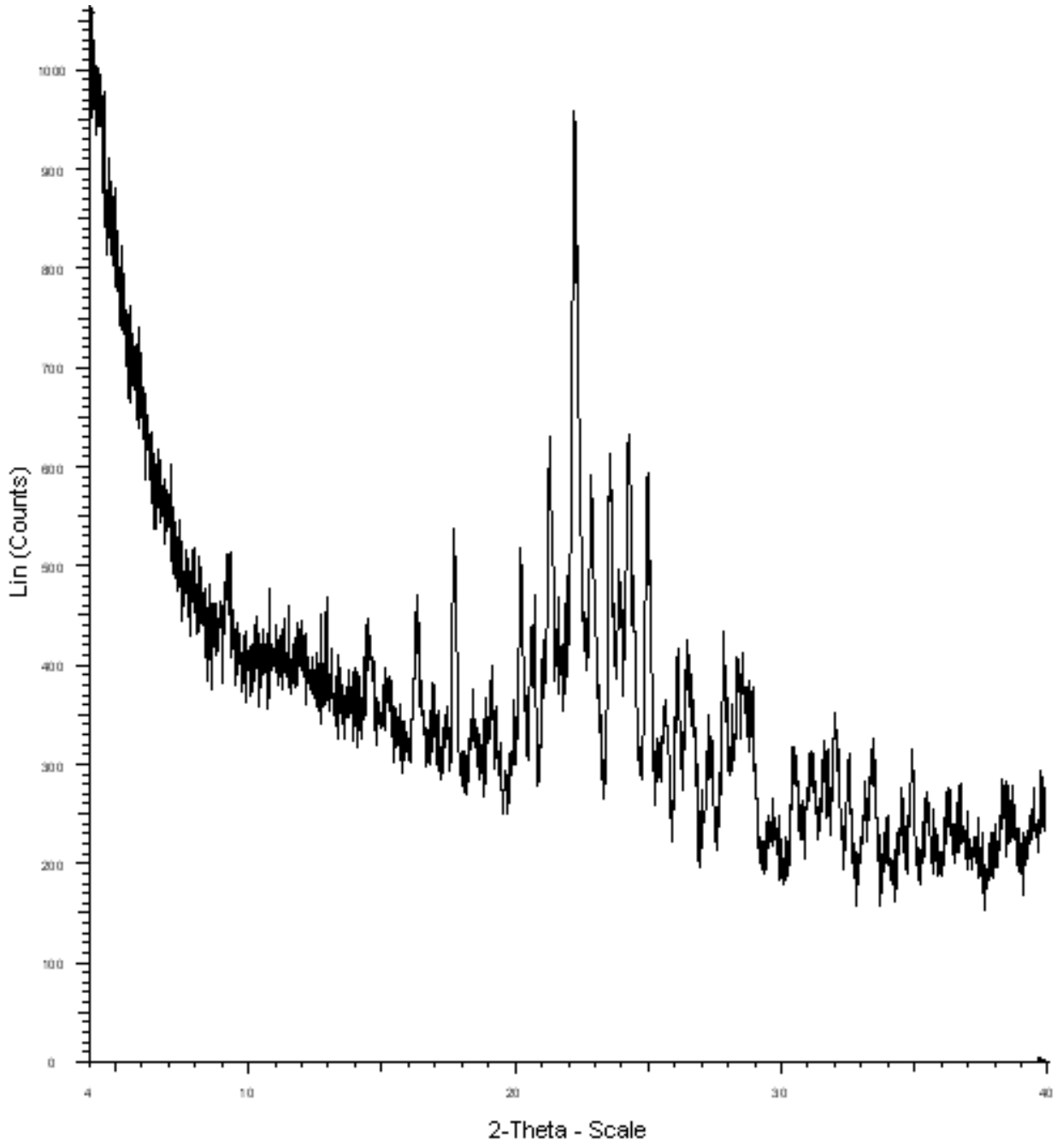

Figure SI 4.12. Experimental PXRD pattern of cocrystal**3**. The cocrystal**3** shows a very poor crystallinity.

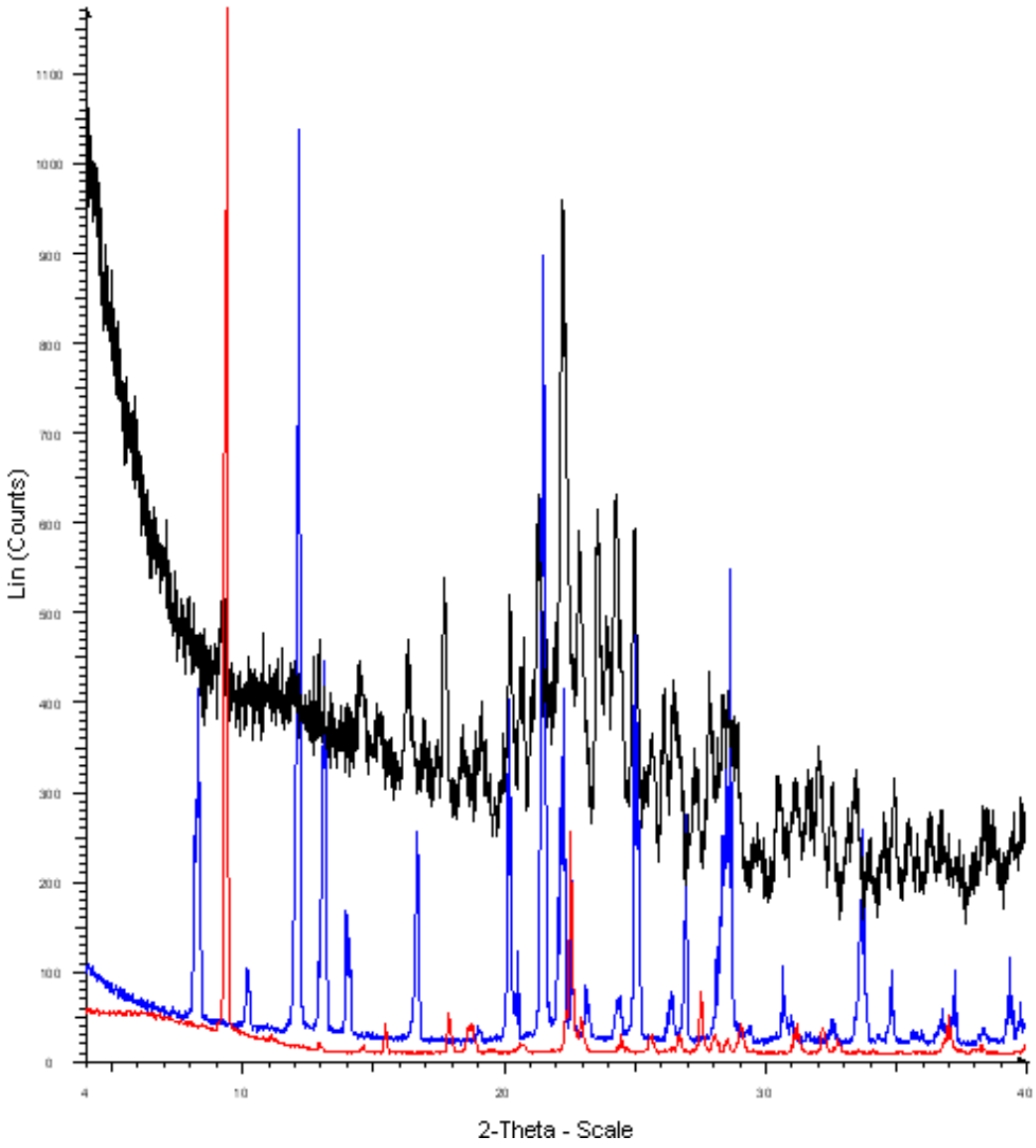

Figure SI 4.13. Experimental PXRD patterns of cocrystal**3** (black line), **TBAI** (red line) and **IPBC** (blue line).

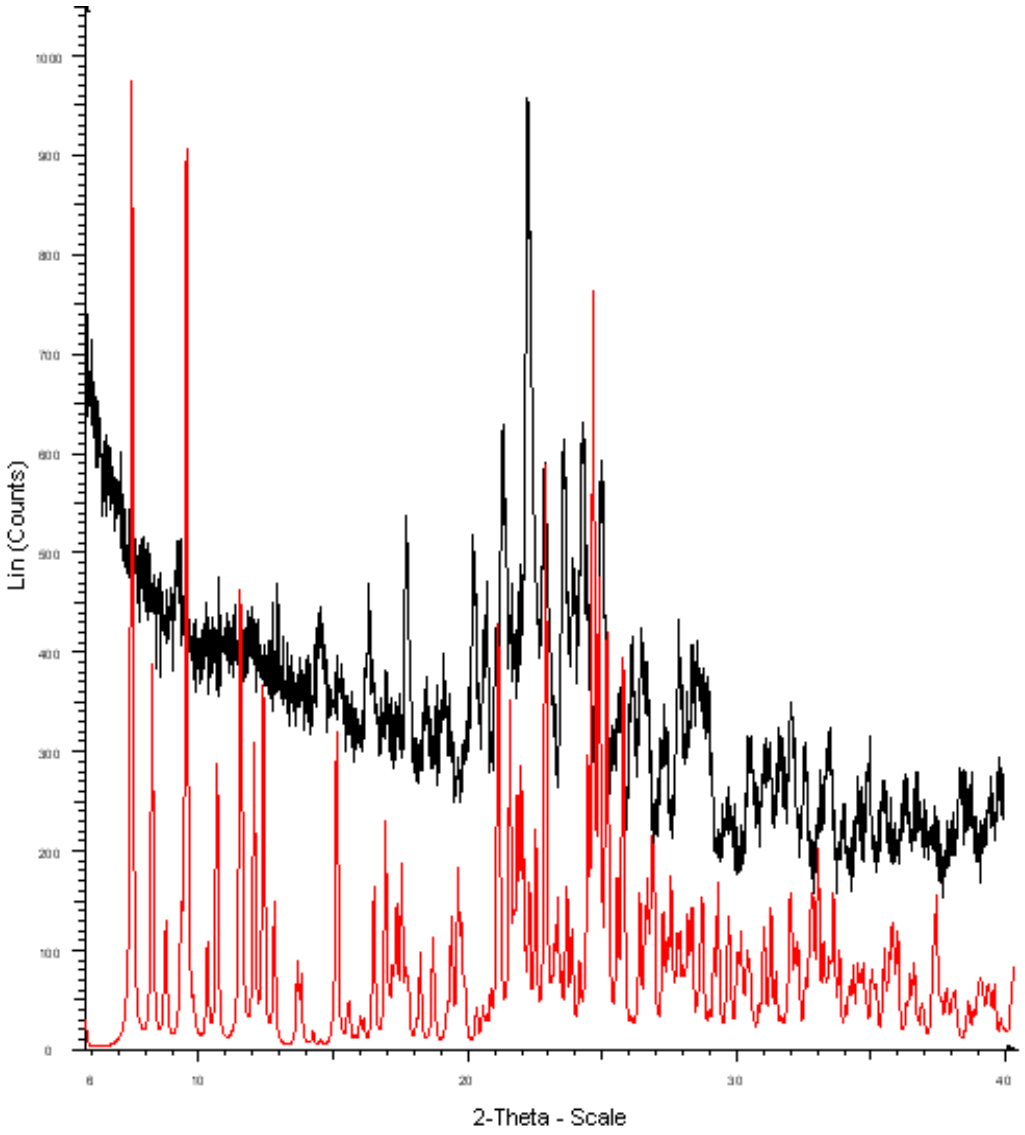

Figure SI 4.14. Superimposed PXRD patterns of cocrystal**3**: Experimental (black line) and simulated from single crystal (red line). Small differences in simulated from single crystal and bulk sample are due to poor crystallinity of cocrystal**3**. The PXRD was collected at room temperature (297 k) while the single crystal data were collected a 103 K.

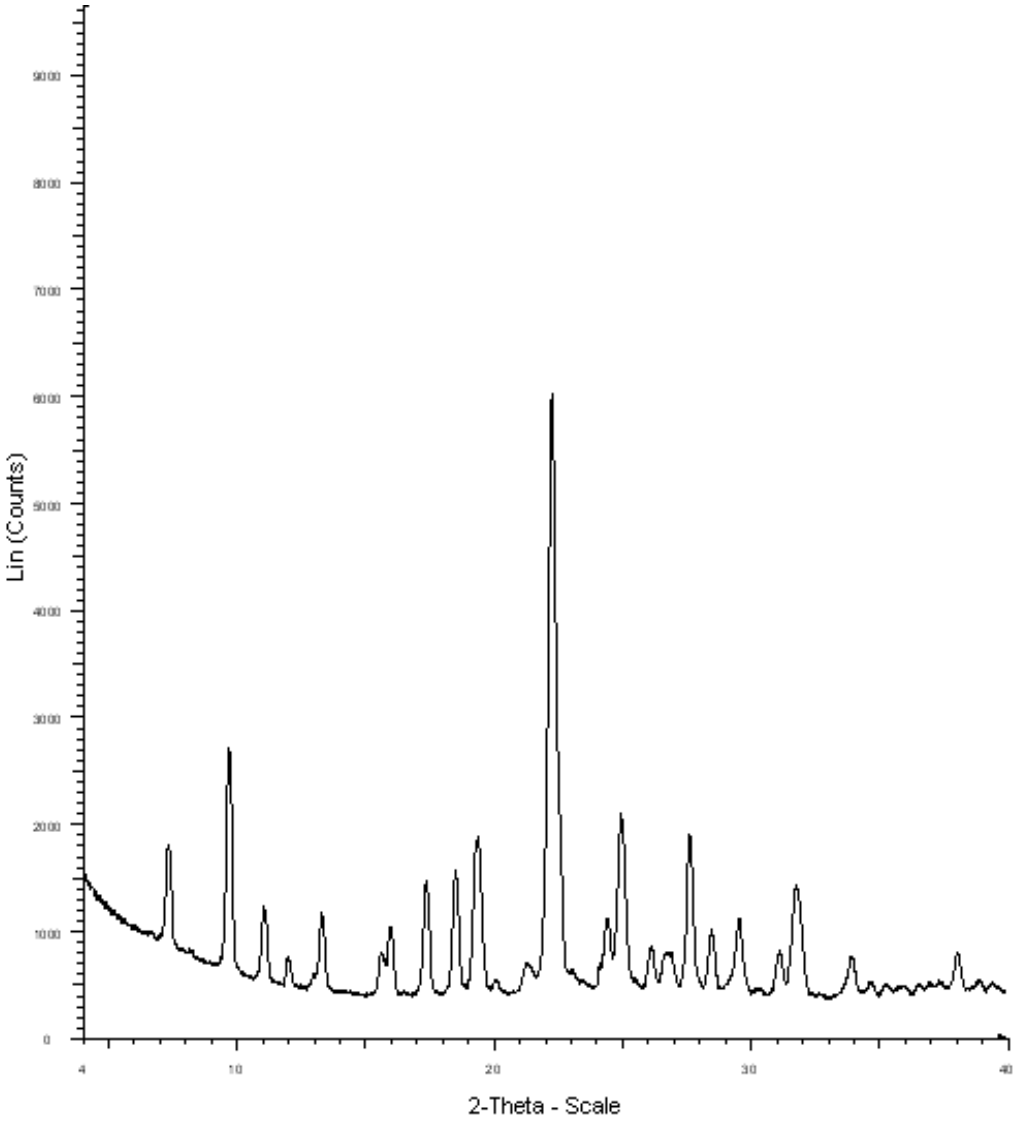

Figure SI 4.15. Experimental PXRD pattern of cocrystal**4**.

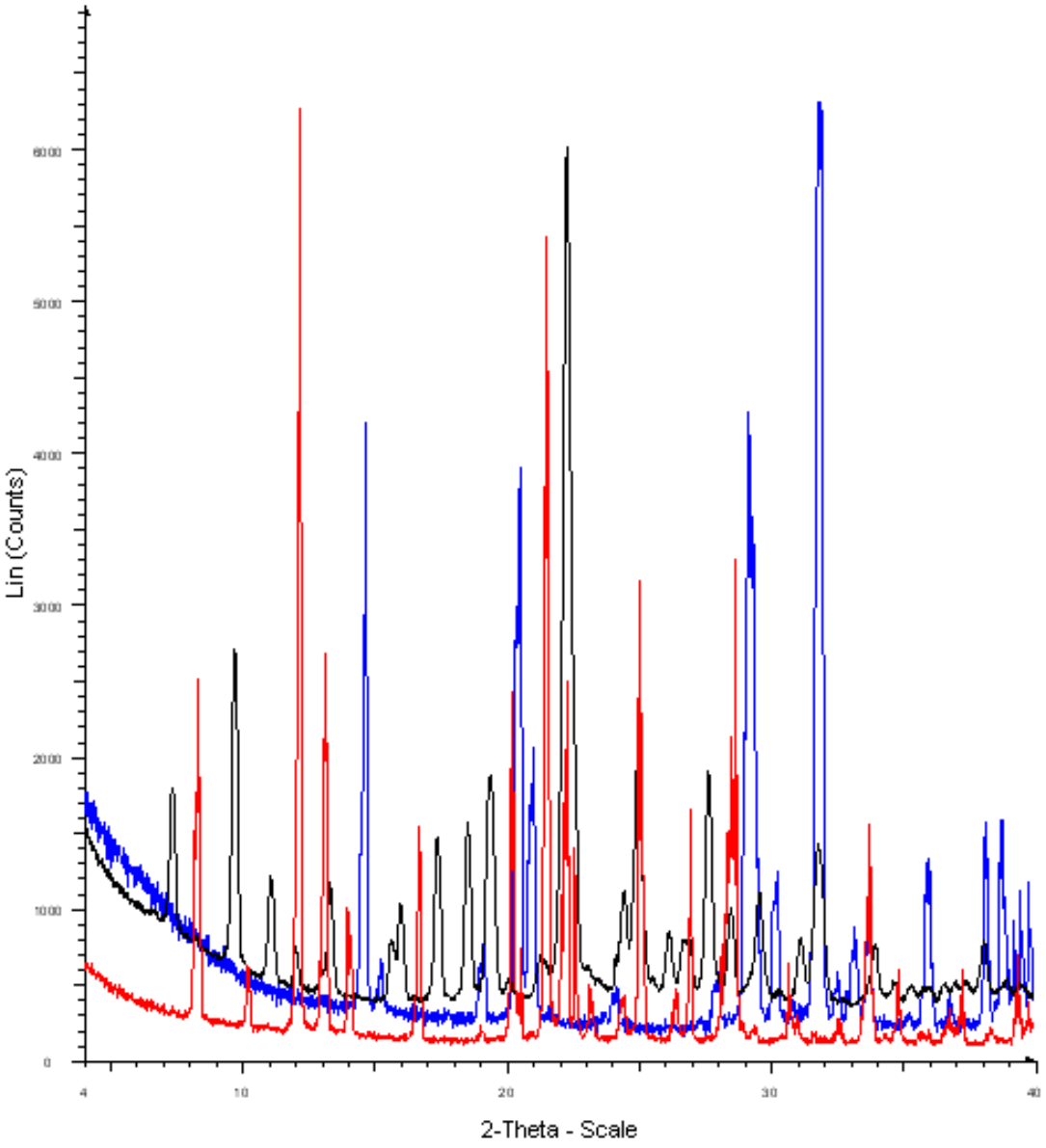

Figure SI 4.16. Experimental PXRD patterns of cocrystal**4** (black line), **$CaCl_2$** (blue line) and **IPBC** (red line).

SI 5.^{1}H and^{13}C Nuclear Magnetic Resonance. ^{1}H and^{13}C NMR spectra were recorded at ambient temperature on a Bruker AV400 or 250 MHz spectrometer. The experiments were carried out in different solvents as such $CDCl_3$and methanol-d_4.

SI Scheme 5.1. Hydrogen and **c**arbon atoms labeling in **IPBC**.

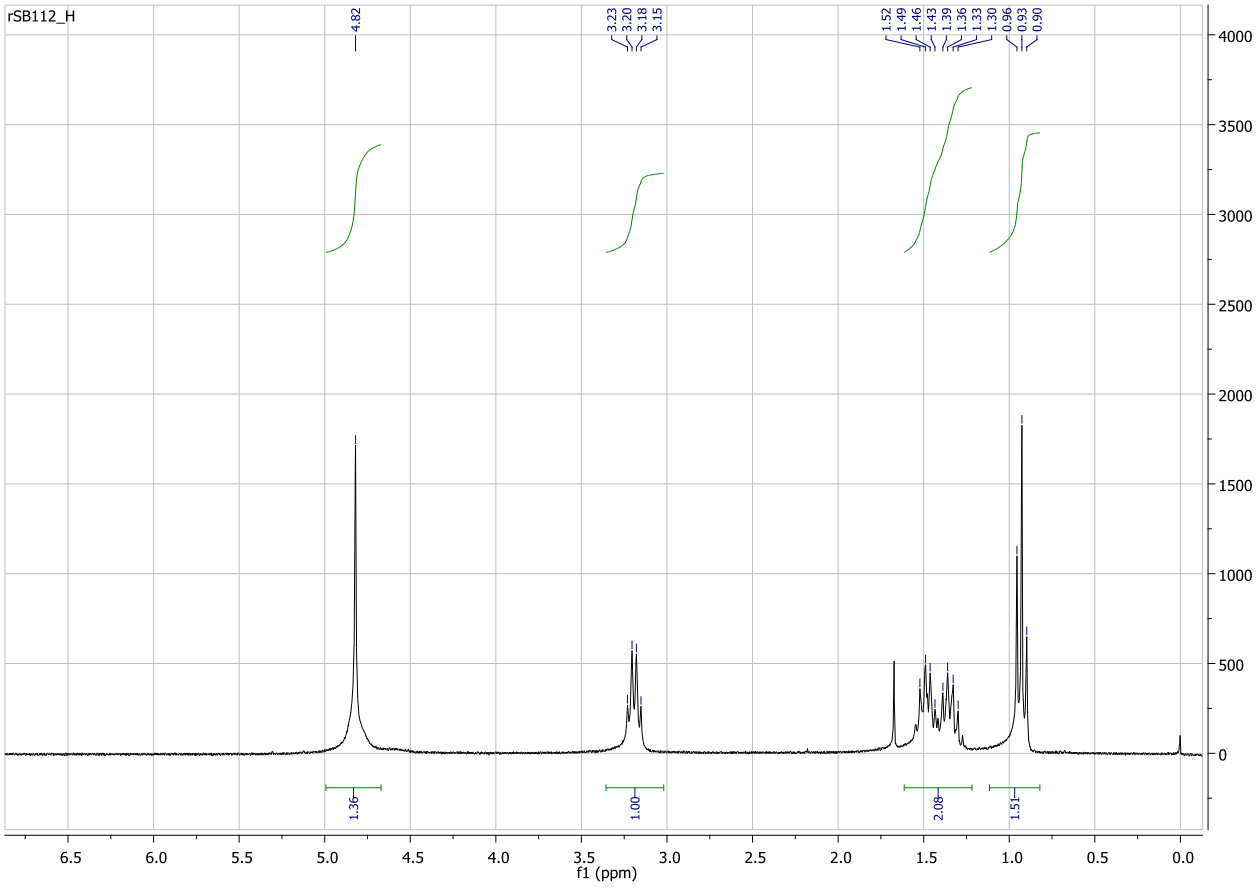

Figure SI 5.1.^{1}H NMR spectrum in $CDCl_3$ of **IPBC**.

^{1}H NMR (250 MHz, $CDCl_3$) δ: 4.82 (s, 3H, H1 overlap with NH hydrogen), 3.19 (dd, 2H, J = 13.0, 6.7 Hz, H5), 1.52 – 1.30 (m, 4H, H6 and H7), 0.93 (t, 3H, J = 7.2 Hz, H8).

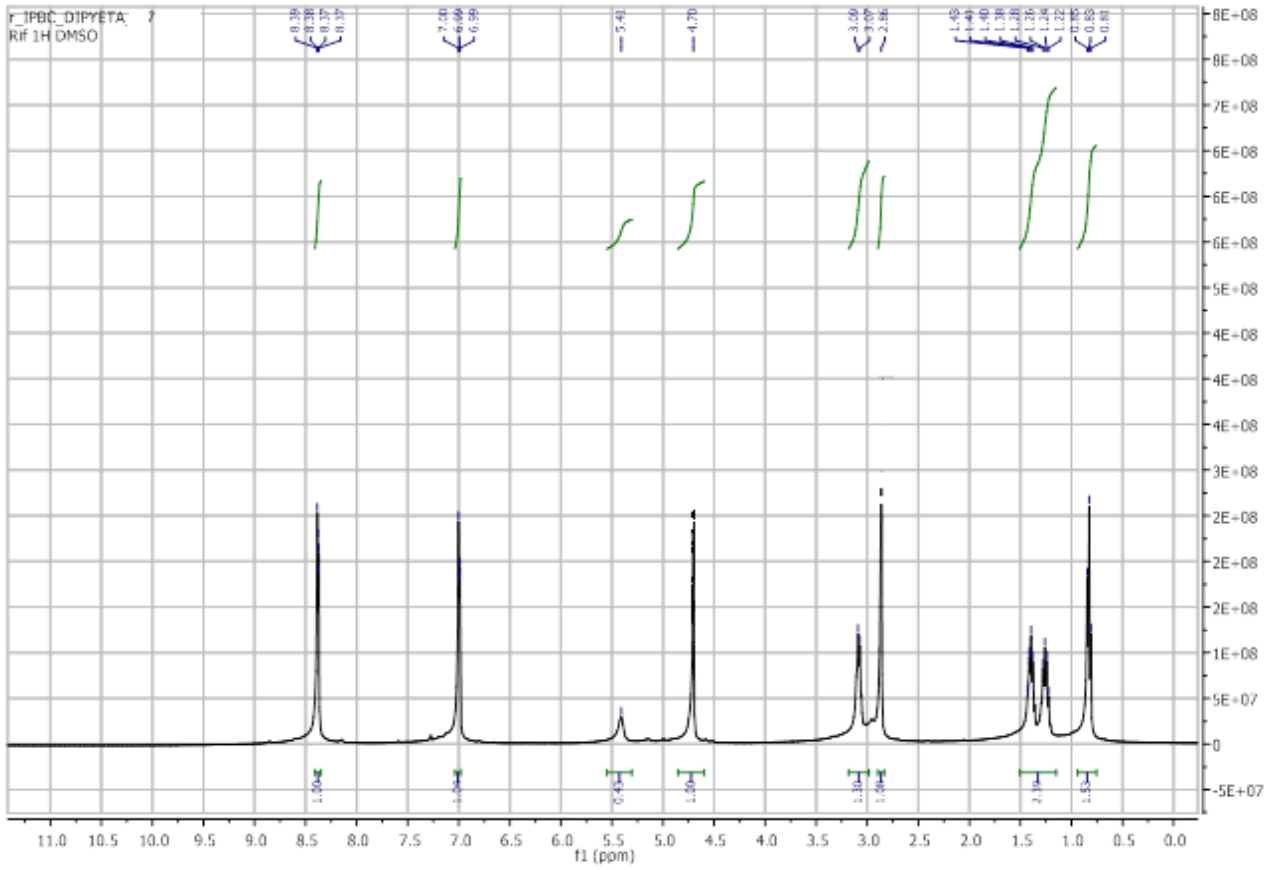

Figure SI 5.2. ^{1}H NMR spectrum in $CDCl_3$ of cocrystal **1**.

^{1}H NMR (400 MHz, $CDCl_3$) δ: 8.38 (dd, 4H, J = 4.5, 1.4 Hz, H_{py}), 7.04 - 6.98 (m, 4H, H_{py}), 5.41 (bs, 2H, NH), 4.70 (s, 4H, H1), 3.11 - 3.01 (m, 4H, H5), 2.86 (s, 4H, $H_{CH2BiPyEt}$), 1.47 - 1.37 (m, 4H, H6), 1.33 - 1.21 (m, 4H, H7), 0.83 (t, 6H, J = 7.3 Hz, H8).

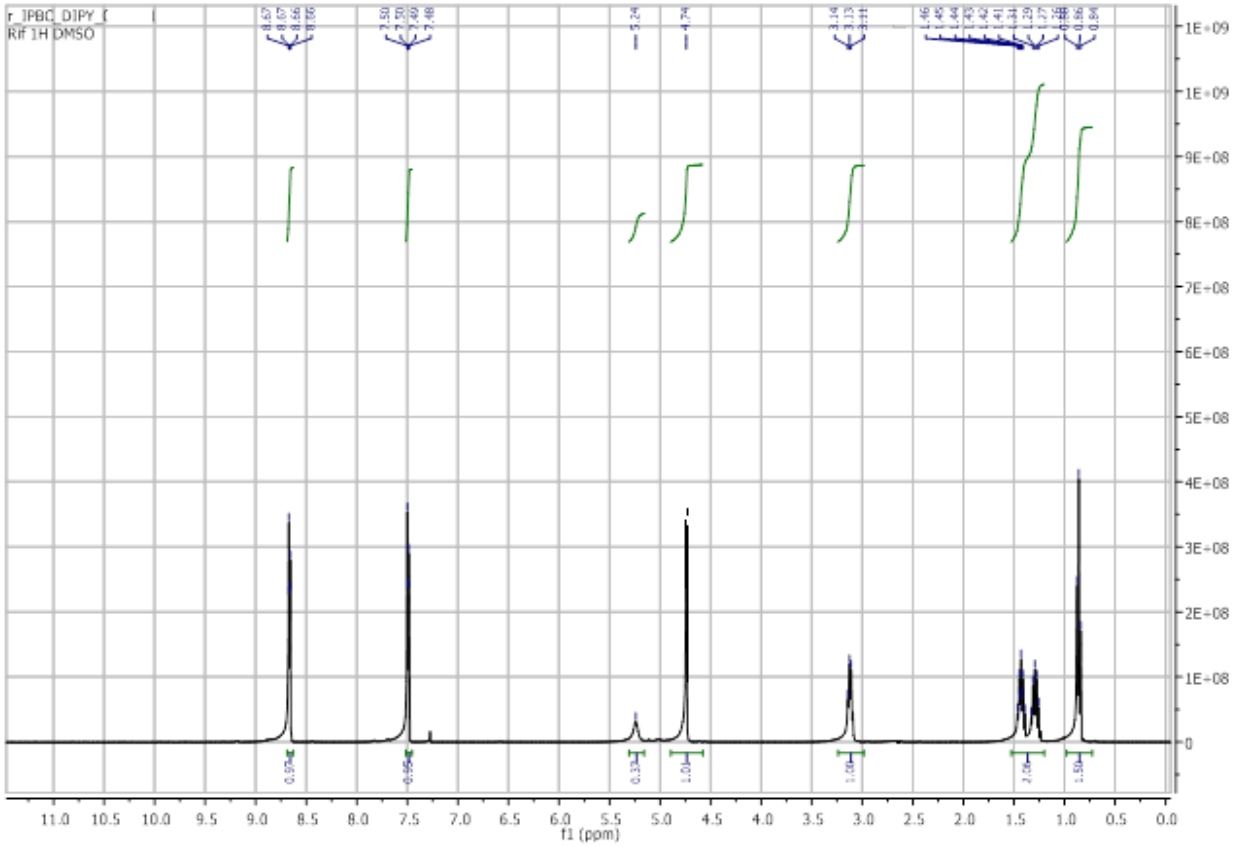

Figure SI 5.3. ^{1}H NMR spectrum in $CDCl_3$ of cocrystal **2**.

^{1}H NMR (400 MHz, $CDCl_3$) δ: 8.66 (dd, 4H,*J* = 4.5, 1.7 Hz,H_{py}), 7.49 (dd, 4H, *J* = 4.5, 1.7 Hz, H_{py}), 5.24 (bs, 2H, NH), 4.74 (s, 4H, H1), 3.24 – 2.99 (m, 4H, H5), 1.46 - 1.39 (m, 4H, H6), 1.33 - 1.23 (m, 4H, H7), 0.86 (t, 6H, *J* = 7.3 Hz, H8).

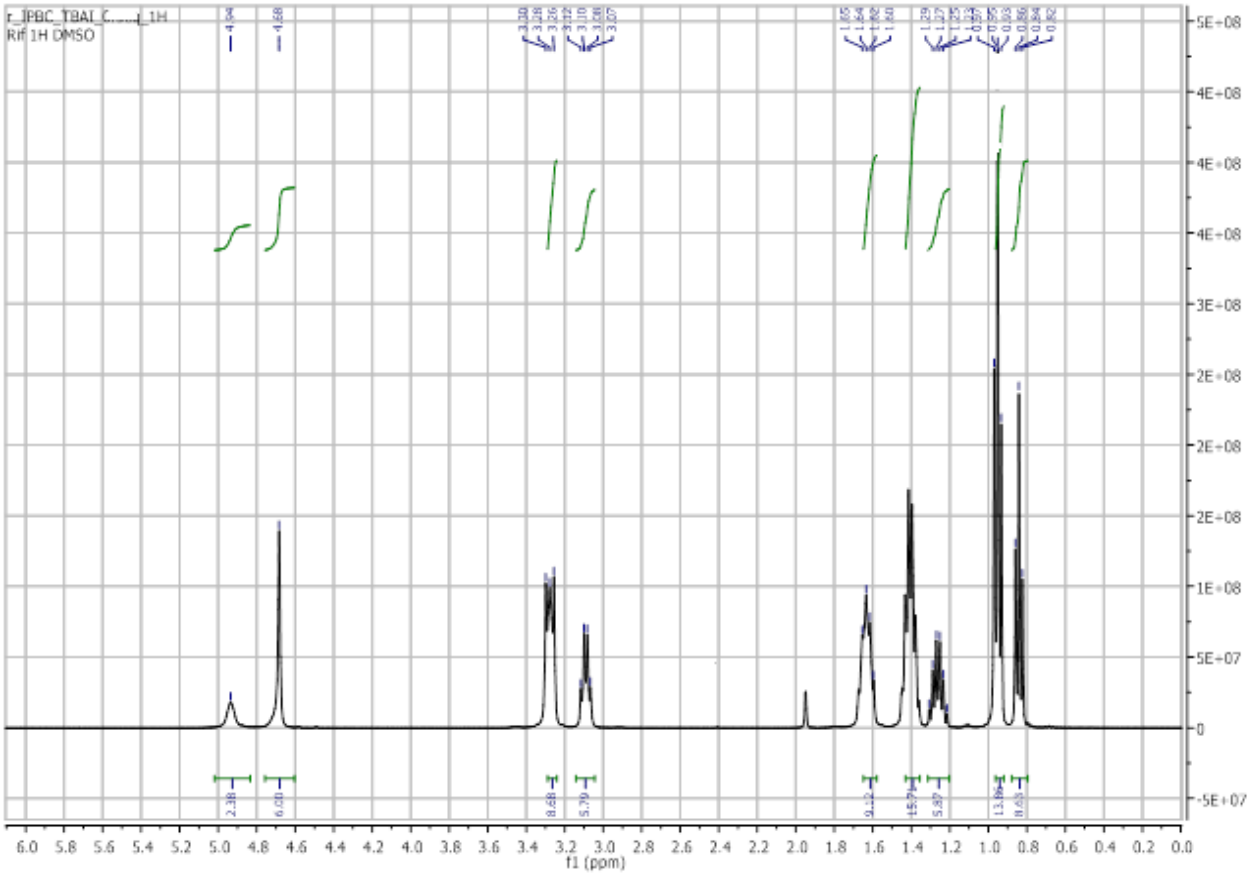

Figure SI 5.4. ^{1}H NMR spectrum in $CDCl_3$ of cocrystal **3**.

^{1}H NMR (400 MHz, $CDCl_3$) δ: 4.94 (bs, 3H, NH), 4.68 (s, 6H, H1), 3.35 - 3.22 (m, 8H, H_{TBAI}), 3.09 (dd, 6H,*J* = 13.3 and 6.7 Hz, H5), 1.72 - 1.56 (m, 8H, H_{TBAI}), 1.47 -1.34 (m, 14H, H6 and H_{TBAI}), 1.31 - 1.22 (m, 6H, H7), 0.95 (t, 12H, *J* = 7.3 Hz, H_{TBAI}), 0.84 (t, 9H, *J* = 7.3 Hz, H8).

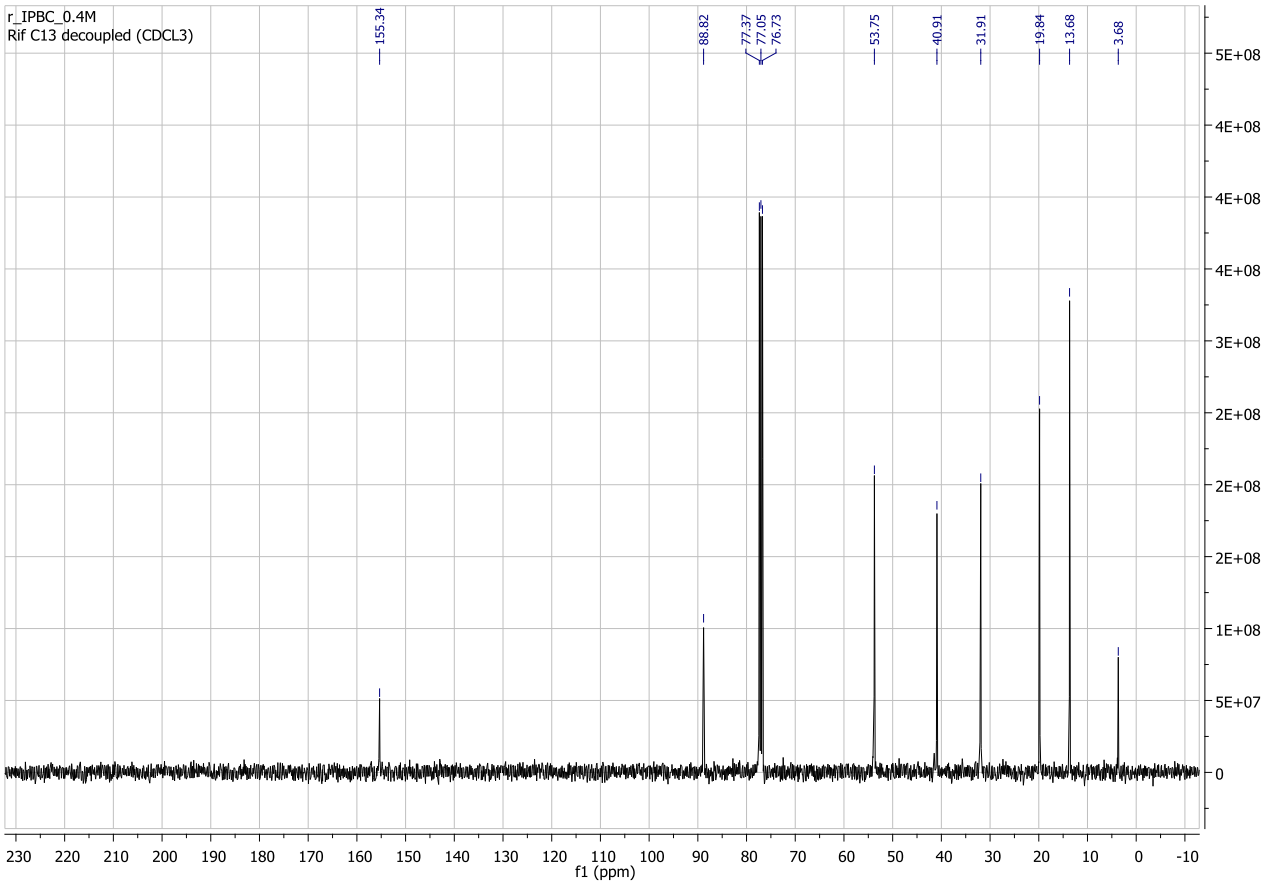

Figure SI 5.5. ^{13}C NMR spectrum in $CDCl_3$ of pure 3-iodo-2-propynyl-*N*-butylcarbamate **(IPBC**, 0.4 M**):** (101 MHz, $CDCl_3$) δ: 155.34 (C4), 88.82 (C2), 53.75 (C1), 40.91 (C5), 31.91 (C6), 19.84 (C7), 13.68 (C8), 3.68 (C3) ppm.

3-Iodo-2-propynyl-*N*-butylcarbamate (**IPBC**) and adducts **1**, **2** and **3** were dissolved in $CDCl_3$. 0.4 M concentration respects to **IPBC** was used in all the experiments. Incremental amount of XB acceptor has been added in order to evaluate the chemical shift variation of the carbon bound to iodine (Scheme 1)^{13}C NMR spectrum of cocrystal**4** was recorded in methanol-d_4.

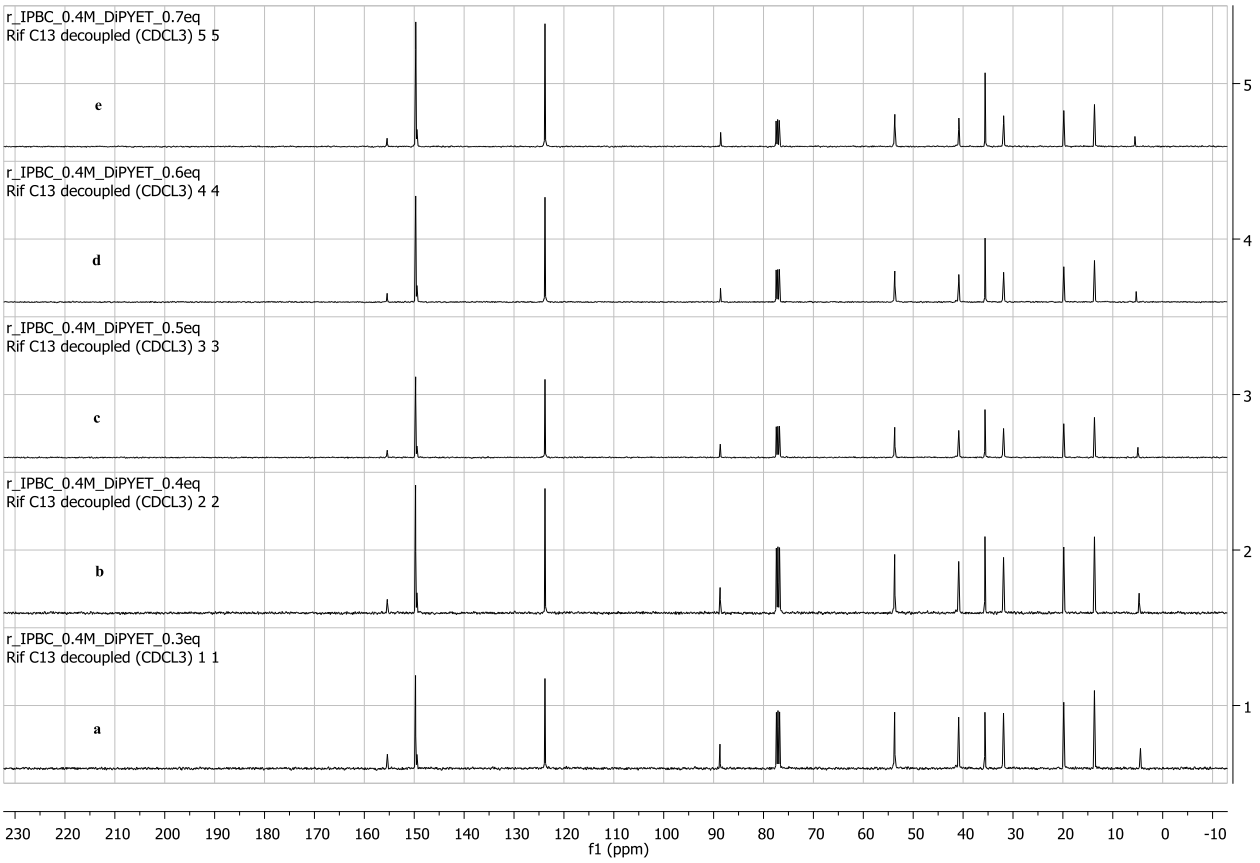

Figure SI 5.6. ^{13}C NMR spectrum in $CDCl_3$ of cocrystal **1** with different **BiPyEt** equivalent (0.3, 0.4, 0.5, 0.6 and 0.7 eq)**.**

(a)^{13}C NMR (0.3 eq of **BiPyEt**),(101 MHz, $CDCl_3$) δ: 155.38, 149.74, 149.48, 123.80, 119.51, 88.73, 77.41, 77.10, 76.78, 53.72, 40.89, 35.62, 31.90, 19.83, 13.67, 4.45 ppm.**(b)**^{13}C NMR (0.4 eq of **BiPyEt**), (101 MHz, $CDCl_3$) δ: 155.40, 149.73, 149.48, 123.80, 88.70, 77.43, 77.11, 76.79, 53.71, 40.88, 35.61, 31.89, 19.83, 13.67, 4.71 ppm. **(c)**^{13}C NMR (0.5 eq of **BiPyEt**),(101 MHz, $CDCl_3$) δ: 155.41, 149.72, 149.48, 123.80, 88.67, 77.44, 77.13, 76.81, 75.31, 53.70, 40.87, 35.61,

31.89, 19.82, 13.67, 4.96 ppm. **(d)** ^{13}C NMR (0.6 eq of **BiPyEt**),(101 MHz, $CDCl_3$) δ: 155.43, 149.71, 149.48, 123.79, 88.62, 77.46, 77.15, 76.83, 53.69, 41.45, 40.86, 35.59, 31.88, 19.82, 13.67, 5.31 ppm. **(e)** ^{13}C NMR (0.7eq of **BiPyEt**),(101 MHz, $CDCl_3$) δ: 155.44, 149.69, 149.48, 123.79, 88.59, 77.48, 77.16, 76.85, 53.68, 40.85, 35.58, 31.87, 19.82, 13.67, 5.56 ppm.

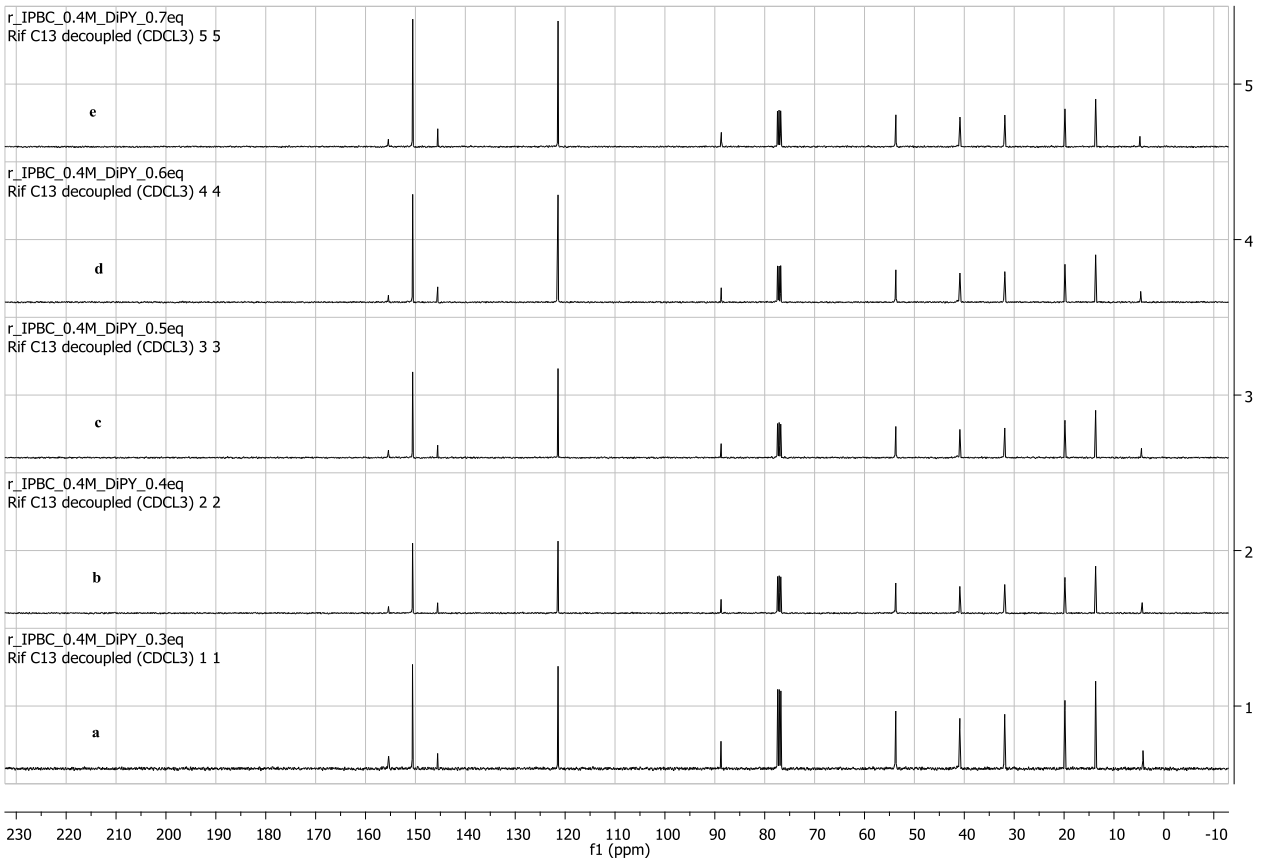

Figure SI 5.7. ^{13}C NMR spectrum in $CDCl_3$ of cocrystal **2** with different **BiPy** equivalent (0.3, 0.4, 0.5, 0.6 and 0.7 eq)**.**

(a) ^{13}C NMR (0.3 eq of **BiPy**),(101 MHz, $CDCl_3$) δ: 155.38, 150.58, 145.55, 121.42, 88.76, 77.40, 77.08, 76.76, 53.73, 40.89, 31.90, 19.83, 13.67, 4.18 ppm.**(b)** ^{13}C NMR (0.4 eq of **BiPy**),(101 MHz, $CDCl_3$) δ: 155.39, 150.57, 145.55, 121.42, 88.74, 77.41, 77.10, 76.78, 53.73, 40.89, 31.89, 19.83, 13.67, 4.35 ppm.**(c)** ^{13}C NMR (0.5 eq of **BiPy**), (101 MHz, $CDCl_3$)δ: 155.40, 150.56, 145.54, 121.42, 88.73, 77.42, 77.11, 76.79, 53.73, 40.88, 31.89, 19.83, 13.67, 4.48 ppm.**(d)** ^{13}C NMR (0.6 eq of **BiPy**), (101 MHz, $CDCl_3$) δ: 155.41, 150.55, 145.54, 121.42, 88.71, 77.43, 77.12, 76.80, 53.72, 40.88, 31.88, 19.83, 13.67, 4.65 ppm.**(e)** ^{13}C NMR (0.7eq of **BiPy**), (101 MHz, $CDCl_3$) δ: 155.42, 150.54, 145.53, 121.42, 88.69, 77.44, 77.13, 76.81, 53.71, 40.87, 31.88, 19.82, 13.67, 4.80 ppm.

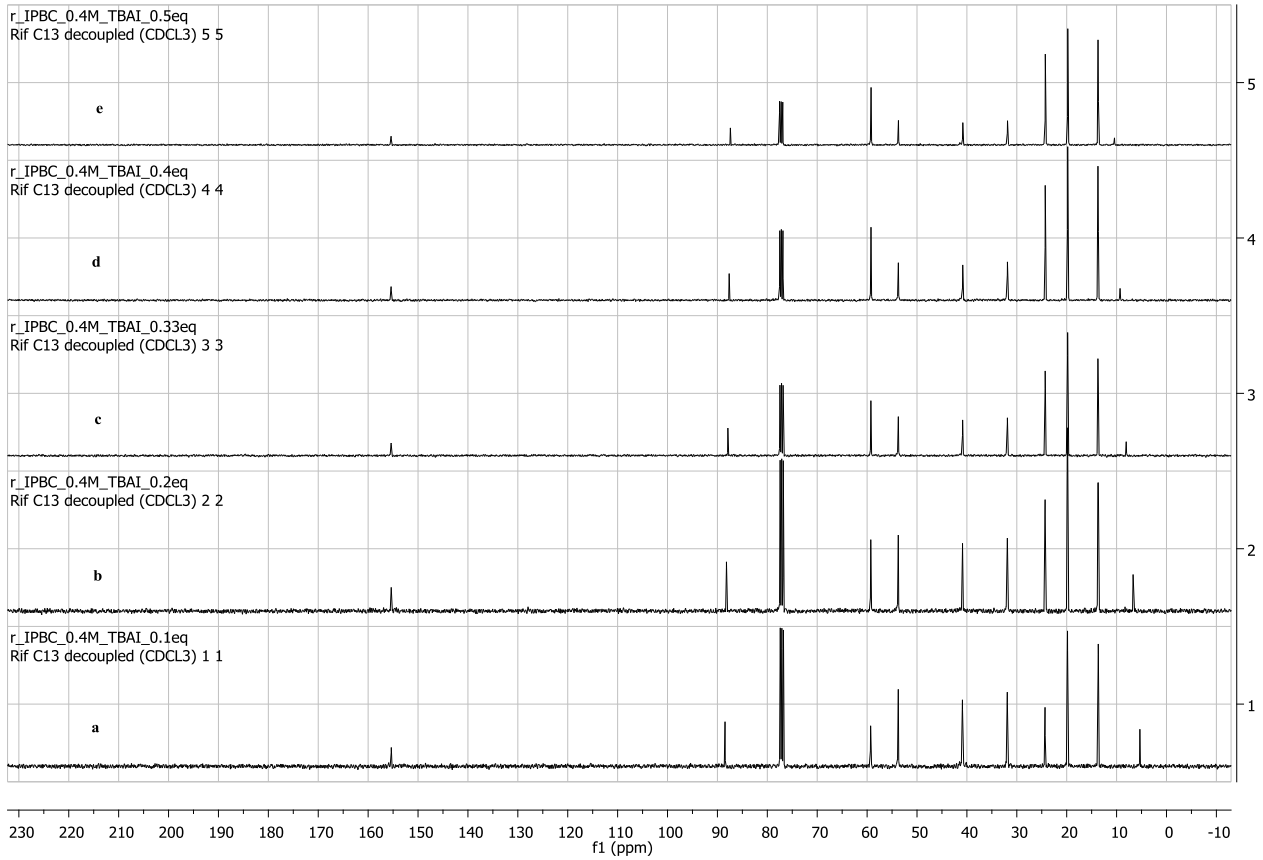

Figure SI 5.8.^{13}C NMR spectrum in $CDCl_3$ of cocrystal **3** with different **TBAI** equivalent (0.1, 0.2, 0.3, 0.4 and 0.5 eq)**.**

(a)^{13}C NMR (0.1 eq of **TBAI**),(101 MHz, $CDCl_3$) δ: 155.36, 88.47, 77.40, 77.08, 76.77, 59.29, 53.75, 40.89, 31.90, 24.34, 19.83, 13.75, 13.67, 5.33 ppm.**(b)**^{13}C NMR (0.2 eq of **TBAI**),(101 MHz, $CDCl_3$) δ: 155.37, 88.19, 77.43, 77.12, 76.80, 59.26, 53.75, 40.87, 31.89, 24.33, 19.83, 13.75, 13.66, 6.69 ppm.**(c)**^{13}C NMR (0.3 eq of **TBAI**),(101 MHz, $CDCl_3$) δ: 155.39, 87.90, 77.47, 77.15, 76.83, 59.24, 53.74, 40.86, 31.88, 24.31, 19.81, 13.75, 13.65, 8.07 ppm.**(d)**^{13}C NMR (0.4 eq of **TBAI**),(101 MHz, $CDCl_3$) δ: 155.39, 87.64, 77.50, 77.18, 76.87, 59.22, 53.73, 40.84, 31.87, 24.30, 19.80, 13.73, 13.65, 9.30 ppm.**(e)**^{13}C NMR (0.5 eq of **TBAI**),(101 MHz, $CDCl_3$) δ: 155.40, 87.40, 77.54, 77.22, 76.90, 59.20, 53.72, 40.82, 31.86, 24.29, 19.78, 13.72, 13.64, 10.42 ppm.

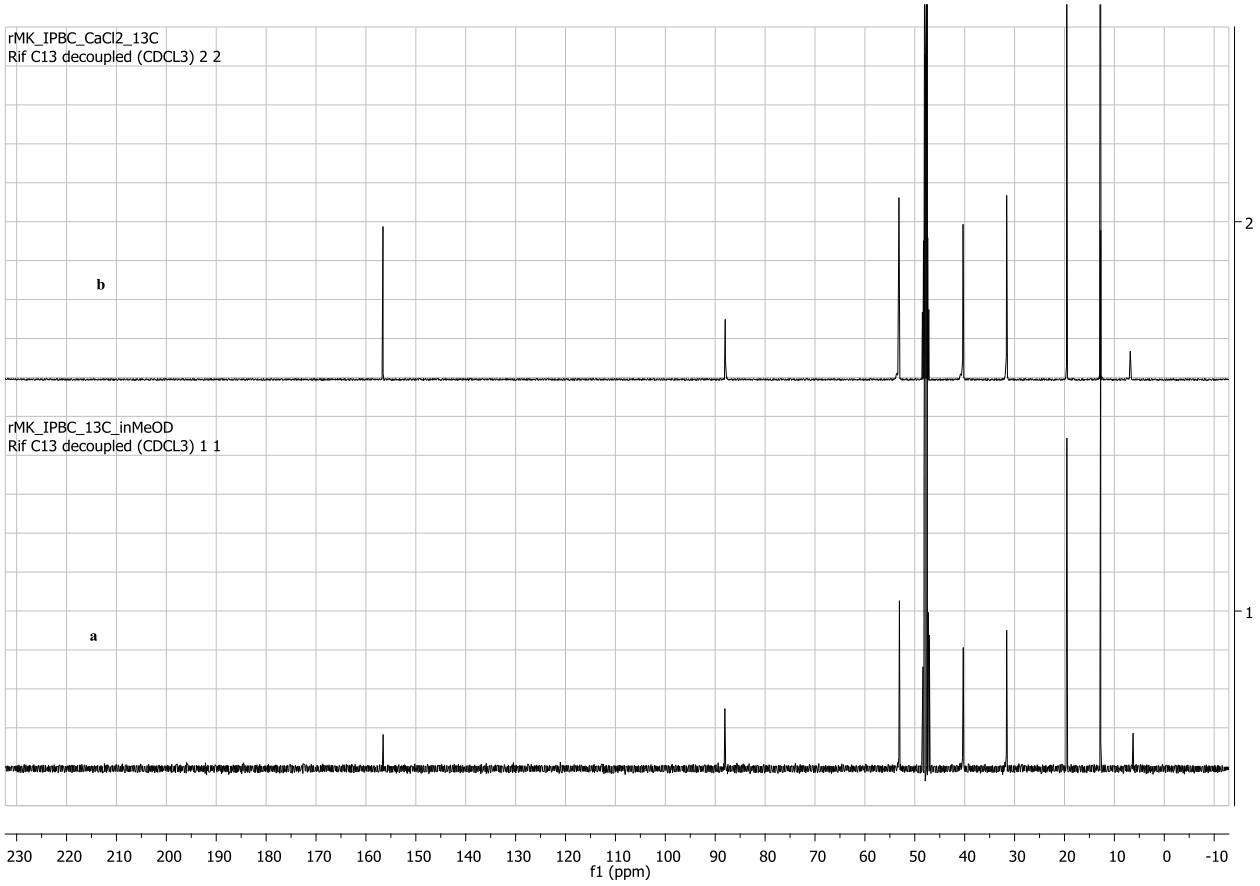

Figure SI 5.9. ^{13}C NMR spectrum in methanol-d_4 of **IPBC** (a) and cocrystal **4** (b)**.**

SI. 6. Solid-state NMR.

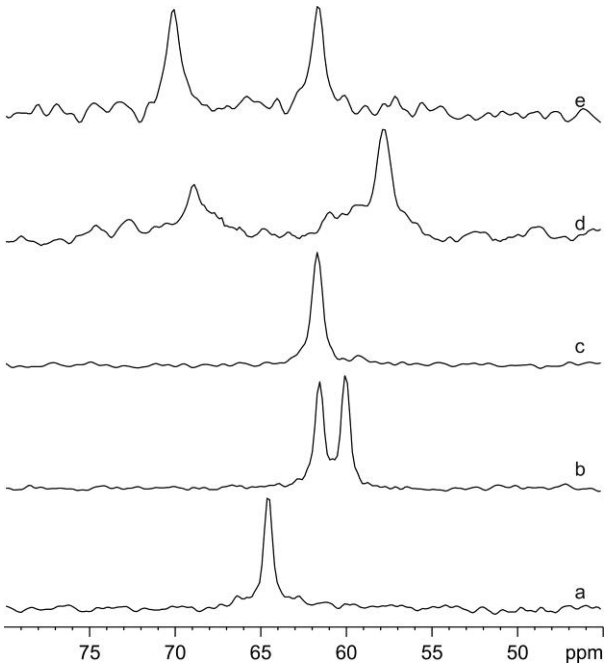

Figure SI 6.1.NH region of the ^{15}N (40 MHz) CPMAS spectra of pure **IPBC** (a), **1** (b), **2**, (c), **3** (d),and **4** (e) recorded at 9 kHz.

SI. 7. Powder flow propertiesmeasurement.

Table SI 7.1 Values of angle of repose for cocrystal **4.**

Funnel/flat surface distance:25mm

Measurement	L (pixel)	H (pixel)	Angle of repose (°)
01	624	149	25.5
02	779	128	18.2
03	709	113	17.7
04	638	128	21.9
05	553	113	22.2
06	1460	241	18.3
07	1176	225	20.9
08	1233	225	20.1
09	1290	227	19.4
10	1403	241	19.0

Average	**20.3±2.4**

Funnel/flat surface distance: 50mm

Measurement	L (pixel)	H (pixel)	Angle of repose (°)
11	1105	128	13.0
12	723	113	17.4
13	879	113	14.4
14	1049	92	9.9
15	921	128	15.5
16	1729	176	11.5
17	1772	170	10.9
18	1474	184	14.0

Average	**13.3±2.5**

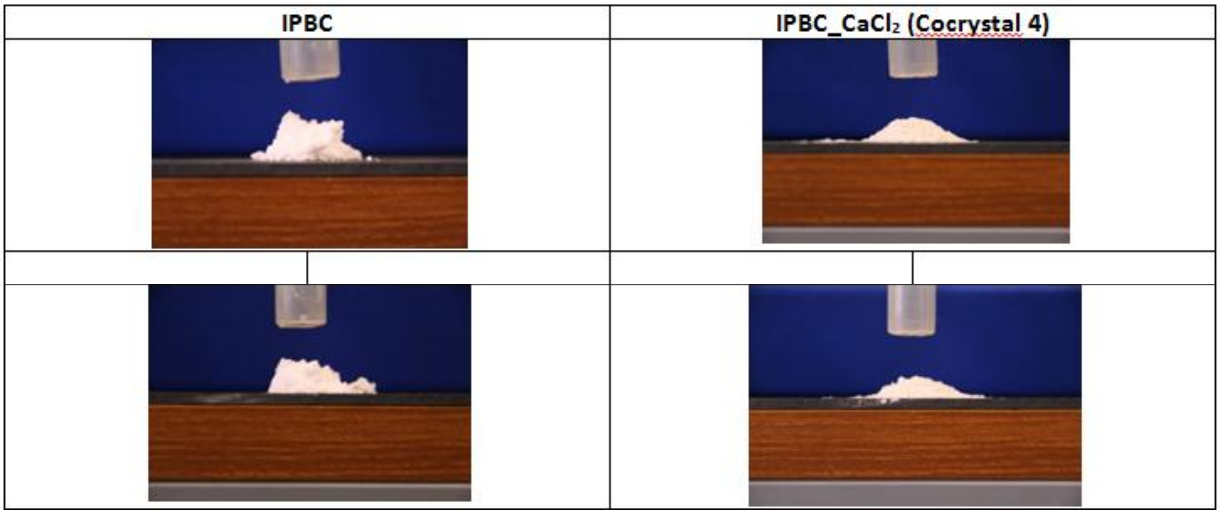

Figure SI 7.1. Pictures of cones of **IPBC** (left) and cocrystal **4** (right) powders, taken after flowing the powders through the funnel from 25mm height.

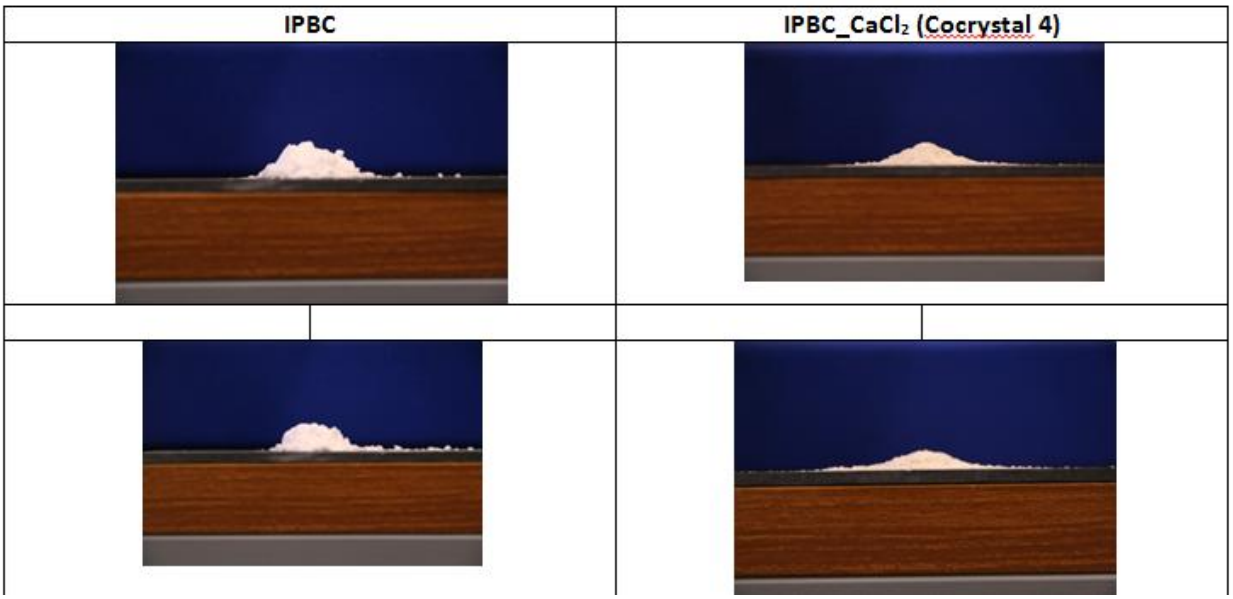

Figure SI 7.2. Pictures of cones of **IPBC** (left) and cocrystal **4** (right) powders, taken after flowing the powders through the funnel from 50 mm height.

SI 8. Crystal structure figures and check cif

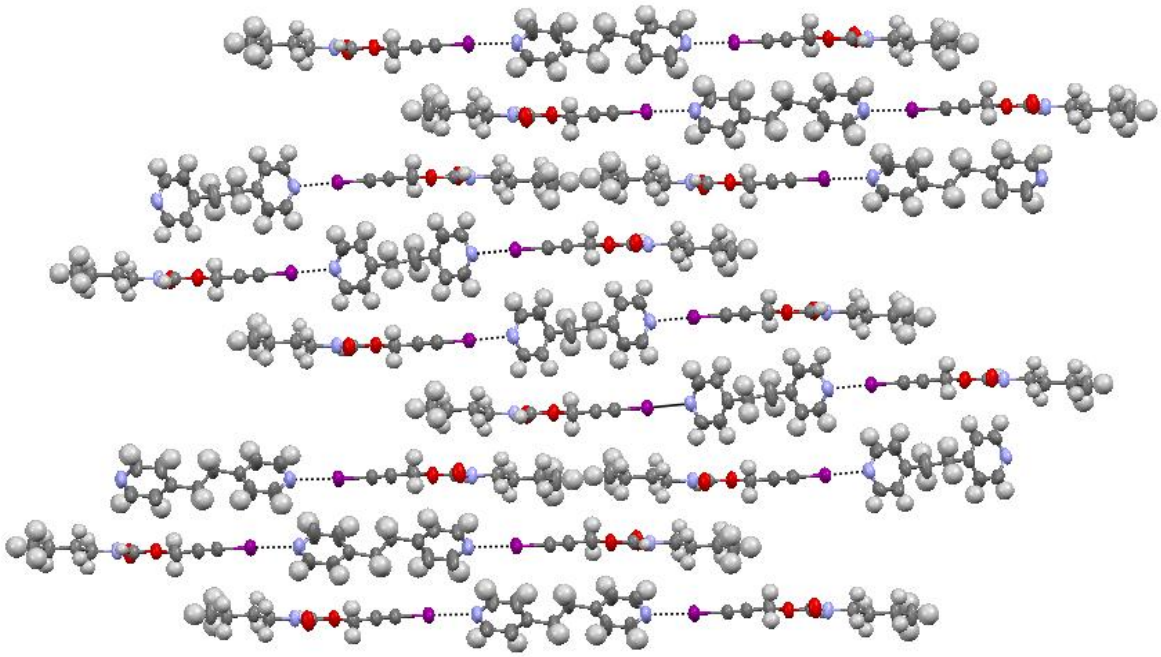

Figure SI 8.1. Halogen bonded trimer present in cocrystal **1.** View alog *b*-axies (+30° in *z*).Colour code: Gray: carbon; red: oxygen; Blue: nitrogen; Purple: iodine; Hydrogen: white. XBs are pictured as black dotted lines.

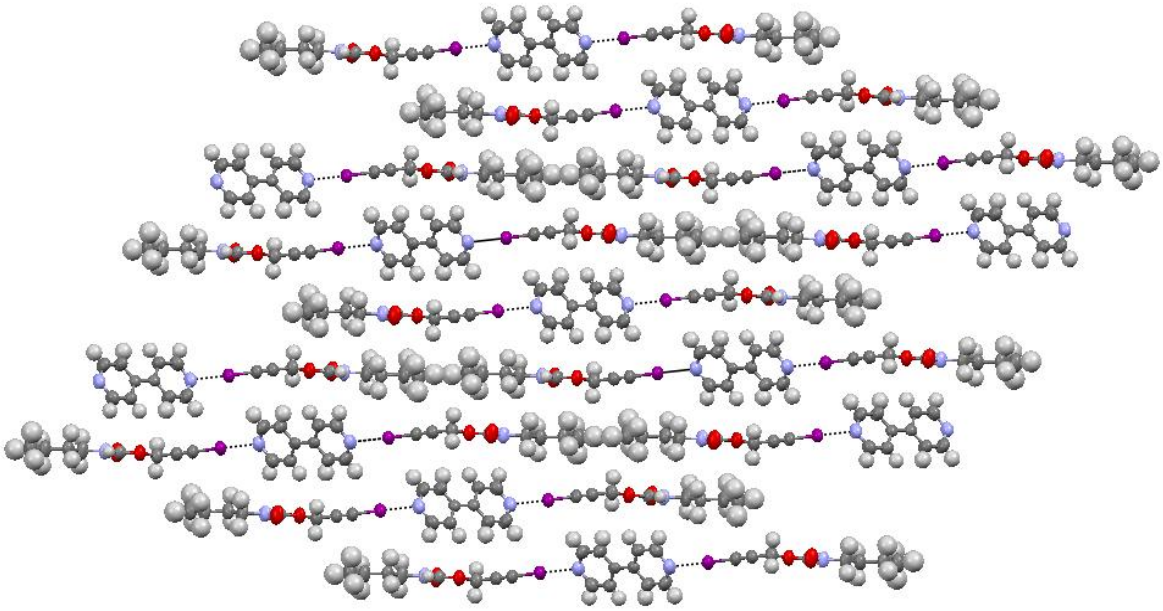

Figure SI 8.2. Halogen bonded trimer present in cocrystal **2.** View alog *b*-axies (-30° in z).Colour code as in Figure SI 7.1. XBs are pictured as black dotted lines.

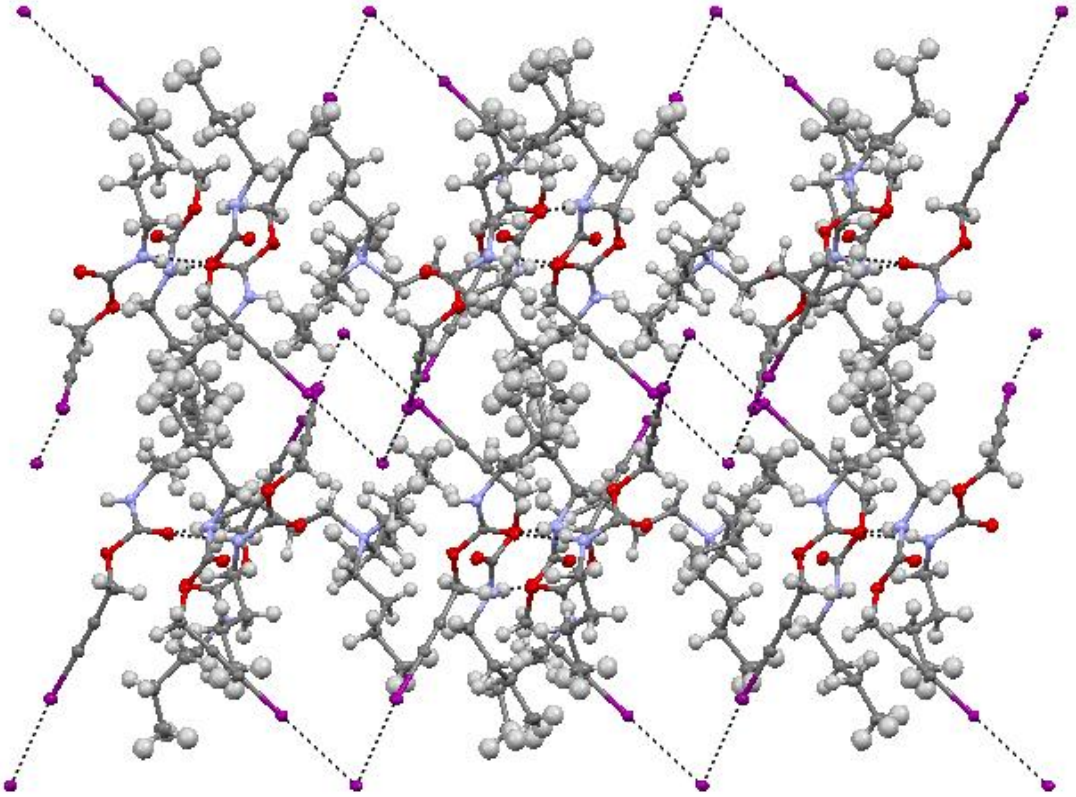

Figure SI 8.3. Crystal packing of cocrystal **3.** View alog *b*-axies.Colour code as in Figure SI 7.1. XBs and HBs are pictured as black dotted lines.

Check cif SI 8.4. Print screen of check cif for cocrystal **1.**

checkCIF/PLATON (standard)

Structure factors have been supplied for datablock(s) sb30

No syntax errors found. CIF dictionary
Please wait while processing .... Interpreting this report
Structure factor report

Datablock: sb30

Bond precision: C-C = 0.0073 A Wavelength=0.71073

Cell: a=30.666(3) b=4.9869(4) c=21.068(2)
alpha=90 beta=92.115(6) gamma=90

Temperature: 297 K

	Calculated	Reported
Volume	3219.7(5)	3219.7(5)
Space group	P 2/c	P 2/c
Hall group	-P 2yc	-P 2yc
Moiety formula	C12 H12 N2, 2(C8 H12 I N O2)	C12 H12 N2, 2(C8 H12 I N O2)
Sum formula	C28 H36 I2 N4 O4	C28 H36 I2 N4 O4
Mr	746.41	746.41
Dx,g cm-3	1.540	1.540
Z	4	4
Mu (mm-1)	1.989	1.989
F000	1480.0	1480.0
F000'	1476.73	
h,k,lmax	39,6,27	39,6,27
Nref	7427	7414
Tmin,Tmax	0.723,0.905	0.594,0.746
Tmin'	0.545	

Correction method= MULTI-SCAN

Data completeness= 0.998 Theta(max)= 27.500

R(reflections)= 0.0383(4592) wR2(reflections)= 0.1234(7414)

S = 1.077 Npar= 353

The following ALERTS were generated. Each ALERT has the format
test-name_ALERT_alert-type_alert-level.
Click on the hyperlinks for more details of the test.

Alert level B

PLAT919_ALERT_3_B Reflection # Likely Affected by the Beamstop ... 1
PLAT934_ALERT_3_B Number of (Iobs-Icalc)/SigmaW .gt. 10 Outliers . 2

Alert level C

PLAT241_ALERT_2_C Check High Ueq as Compared to Neighbors for C26
PLAT242_ALERT_2_C Check Low Ueq as Compared to Neighbors for C18
PLAT242_ALERT_2_C Check Low Ueq as Compared to Neighbors for N4
PLAT242_ALERT_2_C Check Low Ueq as Compared to Neighbors for C24
PLAT250_ALERT_2_C Large U3/U1 Ratio for Average U(i,j) Tensor 3.5
PLAT250_ALERT_2_C Large U3/U1 Ratio for Average U(i,j) Tensor 2.1
PLAT250_ALERT_2_C Large U3/U1 Ratio for Average U(i,j) Tensor 2.2
PLAT360_ALERT_2_C Short C(sp3)-C(sp3) Bond C17 - C17_a ... 1.43 Ang.
PLAT360_ALERT_2_C Short C(sp3)-C(sp3) Bond C23 - C23_b ... 1.36 Ang.
PLAT911_ALERT_3_C Missing # FCF Refl Between THmin & STh/L= 0.600 5
PLAT912_ALERT_4_C Missing # of FCF Reflections Above STh/L= 0.600 8
PLAT918_ALERT_3_C Reflection(s) # with I(obs) much smaller I(calc) 1
PLAT919_ALERT_3_C Large Value of Not (SHELXL) Weight Optimized S . 48.36

Alert level G

PLAT005_ALERT_5_G No _iucr_refine_instructions_details in CIF .... ?
PLAT431_ALERT_2_G Short Inter HL..A Contact I1 .. N3 . 2.81 Ang.
PLAT431_ALERT_2_G Short Inter HL..A Contact I2 .. N4 . 2.84 Ang.
PLAT790_ALERT_4_G Centre of Gravity not Within Unit Cell: Resd. # 2
C12 H12 N2

0 **ALERT level A** = Most likely a serious problem - resolve or explain
2 **ALERT level B** = A potentially serious problem, consider carefully
13 **ALERT level C** = Check. Ensure it is not caused by an omission or oversight
4 **ALERT level G** = General information/check it is not something unexpected

0 ALERT type 1 CIF construction/syntax error, inconsistent or missing data
11 ALERT type 2 Indicator that the structure model may be wrong or deficient
5 ALERT type 3 Indicator that the structure quality may be low
2 ALERT type 4 Improvement, methodology, query or suggestion
1 ALERT type 5 Informative message, check

It is advisable to attempt to resolve as many as possible of the alerts in all categories. Often the minor alerts point to easily fixed oversights, errors and omissions in your CIF or refinement strategy, so attention to these fine details can be worthwhile. In order to resolve some of the more serious problems it may be necessary to carry out additional measurements or structure refinements. However, the purpose of your study may justify the reported deviations and the more serious of these should normally be commented upon in the discussion or experimental section of a paper or in the "special_details" fields of the CIF. checkCIF was carefully designed to identify outliers and unusual parameters, but every test has its limitations and alerts that are not important in a particular case may appear. Conversely, the absence of alerts does not guarantee there are no aspects of the results needing attention. It is up to the individual to critically assess their own results and, if necessary, seek expert advice.

Check cif SI 8.5. Print screen of check cif for cocrystal **2.**

checkCIF/PLATON report

No syntax errors found. CIF dictionary
Please wait while processing .... Interpreting this report

Datablock: sb104_n

Bond precision: C-C = 0.0054 A Wavelength=0.71073
Cell: a=28.683(2) b=4.9270(4) c=21.429(2)
alpha=90 beta=99.92(2) gamma=90
Temperature: 296 K

	Calculated	Reported
Volume	2983.1(5)	2983.1(4)
Space group	C 2/c	C 2/c
Hall group	-C 2yc	-C 2yc
Moiety formula	C8 H12 I N O2, 0.5(C10 H8 N2)	C8 H12 I N O2, 0.5(C10 H8 N2)
Sum formula	C13 H16 I N2 O2	C13 H16 I N2 O2
Mr	359.18	359.18
Dx,g cm-3	1.599	1.599
Z	8	8
Mu (mm-1)	2.144	2.144
F000	1416.0	1416.0
F000'	1412.71	
h,k,lmax	38,6,29	38,6,29
Nref	3924	3916
Tmin,Tmax	0.391,0.807	0.444,0.541
Tmin'	0.344	

Correction method= MULTI-SCAN
Data completeness= 0.998 Theta(max)= 28.860
R(reflections)= 0.0302(2785) wR2(reflections)= 0.0859(3916)
S = 1.043 Npar= 227

The following ALERTS were generated. Each ALERT has the format
test-name_ALERT_alert-type_alert-level.
Click on the hyperlinks for more details of the test.

Alert level A

PLAT431_ALERT_2_A Short Inter HL..A Contact I1 .. N2 .. 2.82 Ang.

Alert level C

PLAT241_ALERT_2_C Check High Ueq as Compared to Neighbors for C5
PLAT242_ALERT_2_C Check Low Ueq as Compared to Neighbors for C4
PLAT242_ALERT_2_C Check Low Ueq as Compared to Neighbors for C11

Alert level G

PLAT860_ALERT_3_G Note: Number of Least-Squares Restraints 60
PLAT164_ALERT_4_G Nr. of Refined C-H H-Atoms in Heavy-Atom Struct. 15

1 ALERT level A = In general: serious problem
0 ALERT level B = Potentially serious problem
3 ALERT level C = Check and explain
2 ALERT level G = General alerts; check

0 ALERT type 1 CIF construction/syntax error, inconsistent or missing data
4 ALERT type 2 Indicator that the structure model may be wrong or deficient
1 ALERT type 3 Indicator that the structure quality may be low
1 ALERT type 4 Improvement, methodology, query or suggestion
0 ALERT type 5 Informative message, check

PLATON version of 13/08/2009; check.def file version of 12/08/2009

Datablock sb104_n - ellipsoid plot

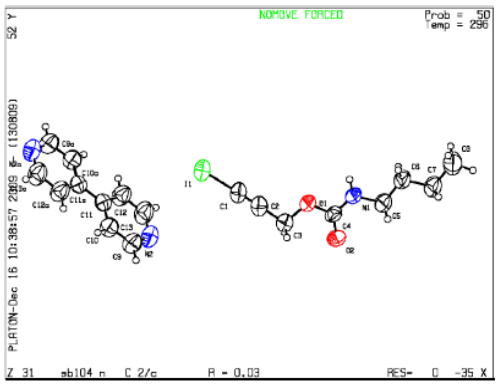

Check cif SI 8.6. Print screen of check cif for cocrystal **3.**

checkCIF/PLATON report

No syntax errors found. CIF dictionary
Please wait while processing .... Interpreting this report

Datablock: mk227

Bond precision: C-C = 0.0026 A Wavelength=0.71073
Cell: a=10.7688(9) b=20.204(2) c=23.735(2)
alpha=90 beta=94.778(2) gamma=90
Temperature: 103 K

	Calculated	Reported
Volume	5146.2(8)	5146.1(8)
Space group	P 21/c	P 21/c
Hall group	-P 2ybc	-P 2ybc
Moiety formula	C16 H36 N, 3(C8 H12 I N O2), I	C16 H36 N 1+, 3(C8 H12 N O2 I), I 1-
Sum formula	C40 H72 I4 N4 O6	C40 H72 I4 N4 O6
Mr	1212.62	1212.62
Dx,g cm-3	1.565	1.565
Z	4	4
Mu (mm-1)	2.464	2.464
F000	2400.0	2400.0
F000'	2393.24	
h,k,lmax	17,32,37	16,31,37
Nref	21739	19710
Tmin,Tmax	0.519,0.642	0.372,0.448
Tmin'	0.509	

Correction method= MULTI-SCAN
Data completeness= 0.907 Theta(max)= 34.450
R(reflections)= 0.0228(16146) wR2(reflections)= 0.0499(19710)
S = 1.050 Npar= 703

The following ALERTS were generated. Each ALERT has the format
test-name_ALERT_alert-type_alert-level.
Click on the hyperlinks for more details of the test.

Alert level B

PLAT230_ALERT_2_B Hirshfeld Test Diff for I3 -- C25 .. 7.49 su
PLAT431_ALERT_2_B Short Inter HL..A Contact I1 .. I4 .. 3.48 Ang.
PLAT431_ALERT_2_B Short Inter HL..A Contact I1 .. I3 .. 3.49 Ang.
PLAT431_ALERT_2_B Short Inter HL..A Contact I1 .. I2 .. 3.49 Ang.

Alert level C

PLAT042_ALERT_1_C Calc. and Reported MoietyFormula Strings Differ ?
PLAT731_ALERT_1_C Bond Calc 0.961(16), Rep 0.961(7) ..... 2.29 su-Ra
C3 -H3A 1.555 1.555 # 12
PLAT731_ALERT_1_C Bond Calc 0.960(17), Rep 0.959(8) ..... 2.13 su-Ra
C4 -H4A 1.555 1.555 # 14
PLAT731_ALERT_1_C Bond Calc 0.961(17), Rep 0.961(8) ..... 2.13 su-Ra
C4 -H4B 1.555 1.555 # 15
PLAT731_ALERT_1_C Bond Calc 0.965(15), Rep 0.964(7) ..... 2.14 su-Ra
C6 -H6B 1.555 1.555 # 22
PLAT731_ALERT_1_C Bond Calc 0.964(15), Rep 0.965(7) ..... 2.14 su-Ra
C7 -H7A 1.555 1.555 # 24
PLAT731_ALERT_1_C Bond Calc 0.963(17), Rep 0.963(7) ..... 2.43 su-Ra
C7 -H7B 1.555 1.555 # 25
PLAT731_ALERT_1_C Bond Calc 0.963(15), Rep 0.963(7) ..... 2.14 su-Ra
C13 -H13A 1.555 1.555 # 42
PLAT731_ALERT_1_C Bond Calc 0.963(16), Rep 0.964(7) ..... 2.29 su-Ra
C14 -H14B 1.555 1.555 # 46
PLAT731_ALERT_1_C Bond Calc 0.960(18), Rep 0.960(8) ..... 2.25 su-Ra
C16 -H16B 1.555 1.555 # 51
PLAT731_ALERT_1_C Bond Calc 0.966(17), Rep 0.965(8) ..... 2.13 su-Ra
C24 -H24B 1.555 1.555 # 74
PLAT731_ALERT_1_C Bond Calc 0.96(2), Rep 0.962(8) ..... 2.50 su-Ra
C24 -H24C 1.555 1.555 # 75
PLAT731_ALERT_1_C Bond Calc 0.963(18), Rep 0.961(8) ..... 2.25 su-Ra
C32 -H32B 1.555 1.555 # 97
PLAT731_ALERT_1_C Bond Calc 0.962(19), Rep 0.962(8) ..... 2.37 su-Ra
C32 -H32C 1.555 1.555 # 98
PLAT731_ALERT_1_C Bond Calc 0.96(2), Rep 0.960(8) ..... 2.50 su-Ra
C40 -H40B 1.555 1.555 # 120

Alert level G

PLAT860_ALERT_3_G Note: Number of Least-Squares Restraints 930
PLAT164_ALERT_4_G Nr. of Refined C-H H-Atoms in Heavy-Atom Struct. 69
PLAT710_ALERT_4_G Delete 1-2-3 or 2-3-4 Linear Torsion Angle ... # 21
I2 -C17 -C18 -C19 -98.00 6.00 1.555 1.555 1.555 1.555
PLAT710_ALERT_4_G Delete 1-2-3 or 2-3-4 Linear Torsion Angle ... # 23
C17 -C18 -C19 -O1 122.00 4.00 1.555 1.555 1.555 1.555
PLAT710_ALERT_4_G Delete 1-2-3 or 2-3-4 Linear Torsion Angle ... # 31
I3 -C25 -C26 -C27 93.00 15.00 1.555 1.555 1.555 1.555
PLAT710_ALERT_4_G Delete 1-2-3 or 2-3-4 Linear Torsion Angle ... # 33
C25 -C26 -C27 -O3 15.00 15.00 1.555 1.555 1.555 1.555
PLAT710_ALERT_4_G Delete 1-2-3 or 2-3-4 Linear Torsion Angle ... # 41
I4 -C33 -C34 -C35 -25.00 11.00 1.555 1.555 1.555 1.555
PLAT710_ALERT_4_G Delete 1-2-3 or 2-3-4 Linear Torsion Angle ... # 43
C33 -C34 -C35 -O5 -75.00 6.00 1.555 1.555 1.555 1.555

0 ALERT level A = In general: serious problem
4 ALERT level B = Potentially serious problem
15 ALERT level C = Check and explain
8 ALERT level G = General alerts; check

15 ALERT type 1 CIF construction/syntax error, inconsistent or missing data
4 ALERT type 2 Indicator that the structure model may be wrong or deficient
1 ALERT type 3 Indicator that the structure quality may be low
7 ALERT type 4 Improvement, methodology, query or suggestion
0 ALERT type 5 Informative message, check

SI. 9. References

[i](a) Bertani, R.; Metrangolo,P.; Moiana, A.; Perez, E.; Pilati, T.; Resnati, G.; Rico-Lattes,I.; Sassi, A.*Adv.Mater.***2002**, *14*, 1197-1201. (b) Metrangolo, P.; Meyer, F.; Pilati, T.; Proserpio,D.M.; Resnati, G.*Chem.-Eur.J.* **2007**, *13*, 5765-5772. (c) Lucassen, A. C. B.; Zubkov, T.; Shimon, L. J. W.; van der Boom, M. E. *CrystEngComm***2007**, *9*, 538-540. (d) Cincic, D.; Friščić,T.; Jones, W. *CrystEngComm***2011**, *13*, 3224-3231.(e) Aakeröy, C.B.; Schultheiss, N.C.; Rajbanshi, A.; Desper, J.; Moore, C. *Cryst.Growth Des* .**2009**, *9*, 432-441. (f) Prasang, C.; Whitwood, A.C.; Bruce, D.W. *Cryst.Growth Des.***2009**, *9*, 5319-5326. (g) Padgett, C.W.; Walsh, R.D.; Drake, G.W.; Hanks,T.W.; Pennington, W.T.*Cryst.GrowthDes.* **2005**, *5*, 745-753.

[ii] (a) Farina, A.; Meille, S.V.; Messina, M.T.; Metrangolo, P.; Resnati, G.; Vecchio, G. *Angew.Chem.,Int.Ed.* **1999**, *38*, 2433-2436. (b) Fox, D. B.; Liantonio, R.; Metrangolo, P.; Pilati,T.;Resnati, G.*J.FluorineChem.* .**2004**, *125*, 271-281.(c) Schoth, R.-M.; Lork, E.; Kolomeitsev, A. A.; Roschenthaler, G.-V. *J.FluorineChem.***1997**, *84*, 41-44 (d) Gattuso, G.; Pappalardo, A.; Parisi,M.F.; Pisagatti,I.; Crea, F.; Liantonio, R.; Metrangolo, P.; Navarrini, W.; Resnati, G.; Pilati,T.; Pappalardo, S.*Tetrahedron***2007**, *63*, 4951-4958. (e) Casnati, A.; Cavallo, G.; Metrangolo, P.; Resnati, G.; Ugozzoli, F.; Ungaro, R. *Chem.-Eur.J.***2009**, *15*, 7903-7912.